ANALYSIS OF SUBSYNCHRONOUS INTERACTION AND ITS MITIGATION FOR IMPROVING POWER SYSTEM PERFORMANCE

A Thesis Submitted
In Partial Fulfillment of the Requirements
for the Degree of

DOCTOR OF PHILOSOPHY

by

Neevatika Verma
(Roll No. 2K18/PHDEE/04)

Under the Supervision of
Prof. Narendra Kumar-I
Department of Electrical Engineering
Delhi Technological University, Delhi-110042

Department of Electrical Engineering

DELHI TECHNOLOGICAL UNIVERSITY
(Formerly Delhi College of Engineering)
Shahbad Daulatpur, Main Bawana Road, Delhi-110042. India

July, 2026

©Delhi Technological University – 2026 All rights reserved

DELHI TECHNOLOGICAL UNIVERSITY
(Formerly Delhi College of Engineering)
Shahbad Daulatpur, Main Bawana Road, Delhi-42

CANDIDATE'S DECLARATION

I **Neevatika Verma** hereby certify that the work which is being presented in the thesis entitled **"Analysis of Subsynchronous Interaction and its Mitigation for Improving Power System Performance"** in partial fulfillment of the requirements for the award of the Degree of Doctor of Philosophy, submitted in the Department of **Electrical Engineering**, Delhi Technological University is an authentic record of my own work carried out during the period from 2018 to 2025 under the supervision of **Prof. Narendra Kumar-I**.

The matter presented in the thesis has not been submitted by me for the award of any other degree of this or any other Institute.

Candidate's Signature

This is to certify that the candidate has incorporated all the corrections suggested by the examiner in the thesis and the statement made by the candidate is correct to the best of our knowledge.

Signature of Supervisor **Signature of External Examiner**

DELHI TECHNOLOGICAL UNIVERSITY

(Formerly Delhi College of Engineering)
Shahbad Daulatpur, Main Bawana Road, Delhi-42

CERTIFICATE BY THE SUPERVISOR

Certified that **Neevatika Verma** (2K18/PHDEE/04) has carried out their research work presented in this thesis entitled **"Analysis of Subsynchronous Interaction and its Mitigation for Improving Power System Performance "** for the award of **Doctor of Philosophy** from Department of Electrical Engineering, Delhi Technological University, Delhi, under my supervision. The thesis embodies results of original work, and studies are carried out by the student herself and the contents of the thesis do not form the basis for the award of any other degree to the candidate or to anybody else from this or any other University/Institution.

Prof. Narendra Kumar-I
Professor
Department of Electrical Engineering
Delhi Technological University
Shahbad Daulatpur, Main Bawana Road, Delhi-110042, India

Date:

Dedicated to my beloved father

Abstract

The global transition toward low-carbon and sustainable power systems has accelerated the large-scale integration of renewable energy sources, particularly Doubly-Fed Induction Generator (DFIG)-based wind farms. These systems are often connected to distant load centres through long transmission corridors equipped with fixed series compensation to enhance power transfer capability. While this configuration improves efficiency and reduces infrastructure costs, it has simultaneously introduced new dynamic stability challenges collectively termed Subsynchronous Interaction (SSI). SSI represents a broad class of oscillatory phenomena involving energy exchange between the electrical network and mechanical or control subsystems at frequencies below the fundamental grid frequency. Numerous historical disturbances in the U.S., China, and Europe have confirmed that SSI remains one of the most critical threats to modern power system security, often leading to shaft failures, equipment damage, forced wind farm outages, and severe power quality deterioration.

Despite widespread research on Sub-Synchronous Resonance (SSR) in conventional generator systems, the progression toward converter-dominated grids has revealed new SSI mechanisms—Sub-Synchronous Converter Control Interaction (SSCCI) and Sub-Synchronous Torsional Control Interaction (SSTCI)—that are not adequately captured by traditional IEEE classifications. A critical review of existing literature indicates that earlier studies commonly oversimplified DFIG behaviour by modeling rotor- and grid-side converters as ideal voltage sources, thereby neglecting essential controller dynamics that significantly influence SSI. Furthermore, mitigation strategies proposed in past studies relied heavily on FACTS devices, parameter tuning, or protection-based approaches, many of which are either economically impractical, sensitive to parameter variations, or insufficient under weak-grid and high-compensation conditions. This gap in modelling accuracy, classification clarity, and adaptive mitigation strategy motivates the present research.

This thesis develops a comprehensive framework that reclassifies SSI mechanisms, models the complete dynamics of DFIG-based wind power plants (WPPs), and

proposes a robust control-oriented mitigation solution. A new SSI taxonomy is established, categorizing phenomena into SSR, SSCCI, and SSTCI based on dominant interaction pathways. This classification fills the conceptual gap left by traditional IEEE standards and provides a clearer foundation for understanding modern converter-driven instabilities.

A high-fidelity mathematical model of a 100 MW aggregated DFIG-based WPP connected through a 161 kV series-compensated transmission line is then developed. Unlike simplified approaches, this model explicitly includes turbine aerodynamics, two-mass drive-train shaft dynamics, the sixth-order DFIG electrical model, Rotor-Side Converter (RSC) and Grid-Side Converter (GSC) controllers, DC-link dynamics, and the RLC behaviour of the compensated line. State-space equations for the complete system are derived to perform small-signal stability analysis. Eigenvalue analysis reveals the emergence of unstable subsynchronous modes—particularly a dominant SSR mode—whose severity increases with higher compensation levels and fluctuating wind speeds. Complementary time-domain simulations validate the predicted instability, confirming the accuracy of the developed model.

To address these stability concerns, a Battery Energy Storage System–based Damping Controller (BESDC) is proposed. Owing to its bidirectional active power capability and fast converter response, BESS is well-suited for providing supplemental damping to suppress oscillations. The BESDC is first designed using a classical lead–lag structure and integrated into the power electronic interface of the BESS. Simulation results demonstrate that the controller significantly enhances damping ratios, stabilizes critical subsynchronous modes, and mitigates oscillatory behaviour under varying wind speeds and partial compensation.

However, conventional fixed-parameter controllers exhibit performance degradation under off-nominal conditions, as real-world wind farms operate under wide variations in grid strength and wind profiles. To overcome this limitation, an advanced Upgraded Particle Swarm Optimization (UPSO)-based approach is introduced to optimally tune the BESDC parameters. UPSO integrates global and local search strategies, effectively resolving premature convergence issues associated with standard PSO and ensuring

fast, accurate parameter optimization. Comparative studies confirm that UPSO-based BESDC offers superior robustness, higher damping, and faster convergence across a broad operational spectrum.

Beyond electrical and mechanical interactions, the thesis also investigates transformer saturation during SSI events—a significantly underexplored phenomenon. Using a flux–voltage integral model, it is shown that subsynchronous components of voltage introduce deep flux excursions, accelerating core saturation even when the system operates within nominal limits. These flux distortions increase harmonic content, degrade power quality, elevate thermal stress, and compromise transformer lifespan. Findings emphasize that transformers, being indispensable grid interface components, must be included in SSI studies to avoid misinterpretation of system behaviour and underestimation of stability risks.

Overall, this research advances the state of the art by:

1. Proposing a modern SSI classification framework tailored to renewable-rich, converter-dominated networks.
2. Developing a detailed nonlinear model of DFIG-based WPPs including all critical dynamic subsystems.
3. Identifying SSR modes through small-signal and time-domain analysis using the IEEE First Benchmark Model.
4. Designing and validating a BESS-based damping controller capable of effectively mitigating SSR in wind-integrated systems.
5. Introducing a UPSO-based optimization strategy that delivers superior damping performance and robust stability.
6. Providing new insights into transformer saturation mechanisms induced by SSI.

The outcomes present a unified and practically deployable approach for enhancing SSI resilience in modern grids. The proposed UPSO-optimized BESS solution offers a scalable, fast-response, and economically viable strategy for future renewable-dominated power systems, ensuring stable operation even under high converter penetration and deep series compensation.

Acknowledgement

First and foremost, I express my heartfelt gratitude to the **Almighty God** for His infinite blessings, grace, wisdom, strength, and guidance throughout my doctoral journey. His divine presence has given me the courage and perseverance to overcome every challenge and successfully complete this research work.

I express my sincere gratitude to **Dr. Prateek Sharma**, Hon'ble Vice Chancellor, **Delhi Technological University**, for providing an excellent academic environment and the necessary facilities to pursue and complete my doctoral research. I am grateful to **Prof. Narendra Kumar-II**, Head, Department of Electrical Engineering, Delhi Technological University, for his encouragement, support, and for providing a conducive environment for research.

I express my sincere gratitude to my respected supervisor, **Prof. Narendra Kumar-I**, for his valuable guidance, constructive suggestions, encouragement, and continuous support throughout the course of this research.

I would also like to express my sincere thanks to the faculty and staff of the **Junior Machine Laboratory**. I am especially grateful to **Prof. J. N. Rai**, **Dr. Ajendra Singh**, and **Ms. Shalini Gupta** for their support, encouragement, and assistance during my research work.

I would like to extend my heartfelt thanks to my senior and mentor, **Dr. Rajeev Kumar**, for his constant motivation, valuable guidance, and encouragement throughout my Ph.D. journey. I also sincerely thank **Dr. Saket Gupta** and **Dr. Geeta** for their valuable suggestions, support, and encouragement. I am equally thankful to my colleagues and juniors, **Dr. Brijendra Sangar** and **Dr. Monika Sharma**, for their cooperation, encouragement, and support.

A very special note of gratitude goes to my beloved husband, **Shivendra Kumar**, for his unconditional love, patience, understanding, and unwavering support throughout

this journey. His constant encouragement, belief in me, and strength have been a source of confidence and motivation during every phase of my doctoral research.

I owe my heartfelt gratitude to my beloved father, **Shri Mast Ram Verma**, whose unconditional love, sacrifices, and constant encouragement have been the foundation of my achievements. I am equally grateful to my loving mother, **Smt. Vindoo Devi**, for her endless love, prayers, blessings, and unwavering support.

I extend my special thanks to my elder brother, **Sandeep Verma**, who has always been like a brother and a father figure to me, for his constant encouragement, guidance, and unwavering support throughout my academic journey. His belief in me and his reassuring presence during challenging times have been a source of strength and confidence. I am equally grateful to my sister-in-law, **Shreya Verma**, for her care, encouragement, and continuous support, which have always motivated me. I also thank my brother **Anoop Verma** and **Pooja Verma** for their love and encouragement. My heartfelt thanks also go to my loving nephews, **Sriyan** and **Shivansh**, and my little niece, **Siya**, whose innocent smiles have always filled my life with happiness and positivity.

I would also like to express my sincere gratitude to my parents-in-law and all my family members for their love, blessings, encouragement, and continuous support throughout this journey. Finally, I wish to express my love to the precious little life growing within me. Your presence has been a source of hope and happiness, and I look forward to welcoming you into our lives.

Last but not least, I extend my sincere thanks to everyone who has directly or indirectly contributed to the successful completion of this research work. Their support, encouragement, and goodwill are deeply appreciated and will always remain cherished.

Thank you all.

Neevatika Verma

Table of Content

Title **Page No.**

Candidate's Declaration ..... **iii**

Certificate by the Supervisor ..... **iv**

Abstract ..... **vi**

Acknowledgement ..... **ix**

Table of Content ..... **xi**

List of Tables ..... **xvi**

List of Figures ..... **xvii**

List of Abbreviations and Nomenclature ..... **xx**

CHAPTER 1 INTRODUCTION **1**

1.1 Overview 1

1.2 Background 2

1.3 Subsynchronous Interaction (SSI) 3

1.3.1 Key Characteristics of SSI 3

1.3.2 Dominant Trigger Mechanisms of SSI 4

1.3.3 Consequences of Unmitigated SSI 5

1.4 Motivation 6

1.5 Research Gap 6

1.6 Objectives 8

1.7 Scope of Thesis 9

1.8 Chapter Organization 9

CHAPTER 2 REVIEW OF SSI: CLASSIFICATION, CHALLENGES, AND MITIGATION **12**

2.1 Introduction 12

2.2 IEEE standard terms for SSI and its classification 12
2.2.1 History of IEEE standards terminology 12
2.2.2 IEEE's Classifications 14
2.2.3 Other Emerging Terminologies 17
2.3 Proposed Classification of SSI 17
2.3.1 Sub-Synchronous Resonance (SSR) 18
2.3.2 Sub-Synchronous Converter Control Interaction 19
2.3.3 Sub-Synchronous Torsional Control Interaction 22
2.4 SSI Analysis techniques 25
2.4.1 Frequency scanning technique 25
2.4.2 Complex torque coefficients 25
2.4.3 Eigenvalue analysis 25
2.4.4 Impedance-based model analysis 26
2.4.5 Transient simulation analysis 26
2.5 Mitigation techniques and their challenges 28
2.5.1 Reduce the degree of series compensation 28
2.5.2 Improve grid strength 28
2.5.3 Bypassing series capacitor 28
2.5.4 Damping control by FACTS devices 28
2.5.5 Shunt-VSC 29
2.5.6 PV Solar based damping 29
2.5.7 Damping controls via HVDC 29
2.5.8 Industrial Sub-harmonic Relay 30
2.5.9 Regulating control parameters of WTC 30
2.5.10 Installing heterogeneous wind power plant 31
2.5.11 (on/off) switching of WPP 31

2.5.12 Virtual synchronous generator control 31
2.5.13 SDC with GSC 31
2.5.14 SDC with RSC 34
2.5.15 SDC at both RSC and GSC 37
2.5.16 Battery energy storage system based damping controller 37
2.6 Future trends, Challenges and Recommendations 42
2.7 Conclusion 42
CHAPTER 3 SUBSYNCHRONOUS INTERACTION IN WIND POWER SYSTEMS: MODELING AND ANALYSIS 44
3.1 Introduction 44
3.2 System modeling 44
3.2.1 Modeling of wind turbine 45
3.2.2 Modeling of Shaft System 47
3.2.3 Modeling of DFIG 48
3.2.4 Modeling of DC link 49
3.2.5 Series Compensated Transmission line modeling 49
3.2.6 Modeling of DFIG converter 50
3.2.7 Integrated system modeling 51
3.3 Small Signal Stability Analysis 52
3.3.1 Eigen value analysis 52
3.3.2 Different compensation level 53
3.3.3 Different wind speed 55
3.4 Model Validation 56
3.4.1 Time-domain analysis 56
3.5 Conclusion 58

CHAPTER 4 MITIGATION OF SSR IN DFIG-BASED WPPs USING BESS DAMPING CONTROLLERS 60

4.1 Introduction 60

4.2 Study system 61

4.3 Design of Battery Energy Storage System Damping Controller 61

4.3.1 Modeling of Battery 62

4.3.2 Control System of BESDC 65

4.3.3 Design of the Supplementary Damping Signal 66

4.3.4 Input control signal 68

4.4 Result and discussion 69

4.4.1 Eigenvalue analysis without damping controller 69

4.4.2 Small-signal model validation 71

4.4.3 Eigenvalue analysis with BESDC 73

4.4.4 Time-domain Analysis for BESDC 74

4.5 Conclusion 80

CHAPTER 5 INTELLIGENT BESS DAMPING CONTROLLER BASED ON UPSO 82

5.1 Introduction 82

5.2 Modelling of BESDC 82

5.3 Optimized BESDC design 85

5.4 Upgraded Particle Swarm Optimization Algorithm 87

5.4.1 Optimization Problem Formulation 88

5.5 Result and Discussion 89

5.5.1 Empirical Case Studies and Simulation-Based Validation 92

5.6 Comparison with PSO and UPSO 96

5.7 Conclusion 98

CHAPTER 6 STUDY OF TRANSFORMER SATURATION UNDER SSI..... 100

6.1 Introduction 100

6.2 Study System..... 101

6.3 Mathematical Modeling 101

6.3.1 Transformer flux dynamics and saturation condition..... 101

6.4 Demodulation due to transformer saturation..... 103

6.5 Simulation results and case studies 105

6.5.1 Frequency response analysis of the system model..... 105

6.5.2 Time-domain simulations..... 106

6.6 Conclusion 112

CHAPTER 7 CONCLUSION, FUTURE SCOPE AND SOCIAL IMPACT.... 114

7.1 Conclusion 114

7.2 Future Scope 117

7.3 Social Impact..... 118

REFERENCES..... 119

APPENDIX..... 11433

PLAGIARISM PROOF..... 11435

LIST OF PUBLICATION 136

PROOF OF PUBLICATION..... 145

CURRICULUM VITAE 114

List of Tables

Table 2.1 Comparison analysis of proposed classifications and historical events due to SSI 24
Table 2.2 Comparison of SSI Analysis methods 27
Table 2.3 Summarization of Solutions Techniques and challenges for SSI Mitigation 38
Table 3.1 Mechanical Power, Torque, Rotor Speed (Pu), and Wind Speed 47
Table 3.2 Eigen Value Analysis of the complete system Model With 50% Compensation and a Wind Speed of 7 M/S 53
Table 3.3 Eigen value analysis of mode 3($\lambda_{5,6}$) at varying series compensation 54
Table 3.4 Eigen value analysis of the complete system model with 30% compensation and a wind speed of 7 m/s 55
Table 3.5 Eigen value analysis of mode 3($\lambda_{5,6}$) at varying wind speed and % of series compensation 56
Table 4.1 parameters for the supplementary damping signal 67
Table 4.2 Eigenvalues of the study system model with 50% FSC level, at 7 m/s wind speed 69
Table 4.3 Mode-3 eigenvalue at varying % of series compensation and wind speed70
Table 4.4 Eigenvalues of the study system model with BESDC at 50% FSCTL and 7m/s wind speed 73
Table 4.5 Mode-3 eigenvalue at varying % of series compensation and wind speed with BESDC 74
Table 5.1 Eigenvalues of SSR modes under varying wind speed with and without BESDC, BESDC with PSO and BESDC with UPSO 91
Table 5.2 Quantitative Performance Comparison of PSO vs. UPSO for BESDC Tuning 97

List of Figures

Fig 2.1 Summary of evolution for traditional SSO terminology 13
Fig 2.2 Classification of SSO by IEEE 14
Fig 2.3 Proposed classification of SSI 18
Fig 2.4 Timeline of reported SSCCI events due to involvement of WPP and series compensated transmission line/weak grids 20
Fig 2.5 DFIG based WTC control structure 30
Fig 2.6 With an auxiliary SSR damping at q-axis loop 32
Fig 2.7 GSC SDC with multichannel gain and phase shifters 32
Fig 2.8 PSO optimized with lead-lag networks(b) fuzzy controller 33
Fig 2.9 State-feedback controller, LQR as state observer 33
Fig 2.10 PFL based current controller 34
Fig 2.11 The supplementary SSI damping Observer-based state-feedback controller 35
Fig 2.12 2DOF added current control loop of RSC 36
Fig 2.13 Feedback filtering (LLC and BPF) 36
Fig 2.14 Feedforward filtering (BSF) 37
Fig 3.1 IEEE first benchmark model of DFIG-based WPP 45
Fig 3.2 Relationship between wind power wind speed and rotor speed 46
Fig 3.3 (a) RSC, (b) GSC control loop of DFIG 51
Fig 3.4 Electrical power dynamics response at (a) 30%, (b) 40%, (c) 50% and (d) 60% compensation at fixed wind speed 7m/s 57
Fig 3.5 Electrical power dynamics response at (a) 30% (b) 40%, (c) 50% and (d) 60% compensation at fixed wind speed 9m/s 58
Fig 4.1 Proposed system model under study for the mitigation of SSR 62
Fig 4.2 Electrical battery model [166] 62
Fig 4.3 Traditional control strategy of BESS 64
Fig 4.4 BESDC controller for the SSR mitigation 66
Fig 4.5 Supplementary damping signal 68

Fig 4.6 Dynamic behavior of the active power (pe), reactive power (Qe), and dc-link voltage (Vdc) of DFIG at a fixed series compensation of 50% 71
Fig 4.7 Dynamic behavior of the electromagnetic torque (Te) of 40 %, 50%, and 60% compensation level at 9m/s wind speed (a) FFT analysis for 40% series compensation (b) 50% series compensation (c) 60% series compensation 72
Fig 4.8 Dynamic behavior of the electromagnetic torque (Te) of 7m/s, 9m/s and 11m/s wind speed at 50% series compensation (a) FFT analysis for 7m/s wind speed (b) 9m/s wind speed (c)11m/s wind speed 72
Fig 4.9 Time responses of the system comprising DFIG (a)output active power, (b)reactive power, (c)electromagnetic torque (d)dc-link voltage with and without the proposed Battery energy storage system damping controller 75
Fig 4.10 The output active power of DFIG with and without BESDC at (a)50% series compensation and 9m/s wind speed (b) 60% series compensation at 9m/s wind speed 76
Fig 4.11 DC-link voltage with and without BESDC at (a) 50% series compensation and 9m/s wind speed (b) 60% series compensation at 9m/s wind speed 77
Fig 4.12 The output active power of DFIG with and without BESDC at (a) 7m/s wind speed (b) 11m/s wind speed at 50% series compensation..... 77
Fig 4.13 DC-link voltage with and without BESDC at (a) 7m/s wind speed (b) 9m/s wind speed,50% series compensation 78
Fig 4.14 The output active power without and with BESDC under three-phase fault condition..... 78
Fig 4.15 The phase output voltage of DFIG at Bus1 79
Fig 4.16 DC-link voltage without and with BESDC under three-phase fault condition 80
Fig 5.1 Model of the proposed system developed for SSR mitigation 83
Fig 5.2 BESDC controller for SSR mitigation..... 84
Fig 5.3 Block diagram of supplementary damping signal 85
Fig 5.4 Flowchart of Enhanced BESDC layout 86
Fig 5.5 Objective function convergence comparison between conventional PSO and upgraded PSO algorithms 90

Fig 5.63D surface plot of damping ratio variation with wind speed and series compensation for four control strategies 91
Fig 5.7 Output response of DFIG at 50% SCTL and 9 m/s wind speed for with, without BESDC and Enhanced BESDC (a) Active power output (b) Electromagnetic torque, (c) DC-link voltage of DFIG 93
Fig 5.8 The output response of with, without and enhanced BESDC at 40% series compensation of (a) Electromagnetic torque(pu) (b) DC link voltage of DFIG 94
Fig 5.9 The output response of with, without and enhanced BESDC at 60% series compensation of (a) Electromagnetic torque(pu) (b) DC link voltage of DFIG 94
Fig 5.10 The output response of with, without and enhanced BESDC at 7m/s wind speed and 50% SCTL (a) Electromagnetic torque(pu) (b) DC link voltage of DFIG 95
Fig 5.11 The output response of with, without and enhanced BESDC at 11m/s wind speed and 50% SCTL (a) Electromagnetic torque(pu) (b) DC link voltage of DFIG 96
Fig 5.12 Simulation result of PSO and UPSO at 50% SCTL, 9m/s wind speed of (a) Active output power (b) DC-link voltage 97
Fig 6.1 Single line diagram of considering power system 101
Fig 6.2 Workflow for transformer saturation and stability assessment during faults 103
Fig 6.3 Positive sequence impedance versus frequency characteristics of a series compensated power system at 30% of series compensation 105
Fig 6.4 (a)Three-phase line to ground fault current at line 2. (b) Bus voltage at B2. (c) Frequency spectrum of bus voltage of phase A. 108
Fig 6.5 Impact of transformer saturation at a subsynchronous frequency:(a) Transformer core flux (b) Transformer magnetizing current 109
Fig 6.6 Impact of transformer saturation at a subsynchronous frequency (a)Frequency spectrum of magnetizing current with series compensated (b)Without series compensation..... 109
Fig 6.7 Magnetizing current spectrum of the transformer during fault clearing, with and without series compensation(SSR at f1) 110
Fig 6.8 SSR frequencies vs. compensation showing dangerous 20 Hz/10 Hz resonances at 30% compensation (torsional zone: gray). 111

Fig 6.9 Stability thresholds vs. compensation. 30% case (marked) in marginal zone with flux gain >1.25 and damping ratio near instability limit 112

List of Abbreviations

HVDC	High-Voltage Direct Current
FACTS	Flexible AC Transmission Systems
SSI	Subsynchronous Interaction
WECS	Wind Energy Conversion System
SSO	Subsynchronous Oscillations
WPPs	Wind Power Plants
SSR	Sub-Synchronous Resonance
RSC	Rotor-Side Converter
GSC	Grid-Side Converter
BESS	Battery Energy Storage System
BESDC	BESS-based Damping Controllers
UPSO	Upgraded Particle Swarm Optimization
IGE	Induction Generator Effect
TI	Torsional Interaction
TA	Torque Amplification
SSTI	Sub-Synchronous torsional interactions
DDSSO	Device-Dependent Sub-Synchronous Oscillations
SCTL	Series Compensated Transmission Lines
SSTCI	Sub-Synchronous Torsional Control Interaction
SSCCI	Sub-Synchronous Converter Control Interaction
LCC	Line commutated converter
MMC	multi-level converter
PSS	Power System Stabilizer
PLL	Phase-locked loop
LLC	Lead-Lag Compensator
ICS	Input Control Signal
WAMS	Wide Area Measurement Systems
FBM	First Benchmark Model
SDS	Supplementary Damping Signal

PMU	phasor measuring units
VSI	Voltage Source Inverter
PWM	Pulse width modulation
FFT	Fast Fourier transform
PSO	Particle Swarm Optimization
UPSO	Upgraded Particle Swarm Optimization

Nomenclature

ρ	Air density(kgm^{-3}),
V_{wi}	wind speed(m/s)
R	Rotor radius(m) of wind turbine
A	Blade sweep area(m^2)
C_f	Design constant of wind turbine blade
λ	Tip speed ratio
Ω_m	Mechanical angular velocity
ω_t	Shaft speed of Wind turbine
ω_r	Shaft speed of DFIG
T_g	Internal torque of the system
T_m	Electromagnetic torque of the Generator
D_t	Damping coefficient of Wind turbine
H_t	Inertia constant of Wind turbine
H_g	Inertia constant of Wind generator
D_{tg}	Damping coefficient of Wind generator
K_{tg}	Shaft stiffness of the coupling between two masses
ω_e	Synchronous Reference Speed
ψ_{qm}, ψ_{dm}	Quadrature and direct axes air gap flux linkage
i_{qr}, i_{dr}	Quadrature and direct axes DFIG rotor current component

i_{qs}, i_{ds}	Quadrature and direct axes DFIG stator current component
X_M	Magnetizing Reactance
i_{0s}, i_{0r}	Stator and Rotor zero sequence current components
v_{qs}, v_{ds}	Quadrature and direct axes components of the terminal bus voltage
v_{qr}, v_{dr}	Quadrature and direct axes components of the DFIG rotor voltage
v_{0s}, v_{0r}	Stator and Rotor zero sequence voltage components
X_r, X_s	Rotor Reactance and Stator Reactance
ω_b	Base Speed(2.pi.60rad/s)
R_r	Rotor Resistance
X_{ls}, X_{lr}	Stator and rotor leakage reactance
P_R	RSC power
P_G	GSC power
v_{qg}, v_{dg}	Quadrature and direct axes components of the grid side voltage
i_{qg}, i_{dg}	Quadrature and direct axes components of the grid side current
ω_s	Angular synchronous frequency
V_{dc}	Voltage of DC link
C_{dc}	Capacitor of DC link
R_l	Resistance of transmission line
i_l	Transmission line current
v_c	Capacitor voltage
v_s	Generator bus voltage
V_B	Infinite bus voltage
X_c	Series Capacitor Reactance
V_{Bq}, V_{Bd}	Quadrature and direct axes of the infinite bus voltage
X_l	Total reactance of transmission line
i_{dl}, i_{ql}	Components of transmission line current in direct and quadrature axes
X_{tg}	Reactance at gride side converter

R_{RSC}, L_{RSC}	Resistance and inductance at RSC
R_{GSC}, L_{GSC}	Resistance and inductance at GSC
Q_s	Delivering reactive power through a DFIG stator

CHAPTER 1

INTRODUCTION

1.1 Overview

The global power system is undergoing a profound transformation driven by the pursuit of decarbonization and sustainability. This transition is marked by the large-scale integration of renewable energy sources, particularly wind and solar, supported by advanced transmission technologies such as High-Voltage Direct Current (HVDC) links and Flexible AC Transmission Systems (FACTS). While these developments strengthen clean energy deployment, they also fundamentally alter system dynamics. Unlike traditional synchronous machine-based grids, modern power-electronics-dominated networks exhibit complex interactions and reduced inherent inertia, making them more vulnerable to new forms of instability[1], [2].

Among these challenges, Subsynchronous Interaction (SSI) has emerged as a critical concern. SSI represents a class of oscillatory phenomena that occur at frequencies below the nominal grid frequency (50/60 Hz). These interactions may arise between electrical networks, mechanical shaft systems, and converter controls, potentially leading to equipment stress, power quality deterioration, and even large-scale instability[3]. The risks associated with SSI have been highlighted by real-world incidents across the globe, underscoring the urgent need for accurate modeling and effective mitigation strategies.

This thesis positions itself within this context, focusing on the analysis, classification, and mitigation of SSI in modern power systems, with special emphasis on DFIG-based wind farms integrated through series-compensated transmission networks. It not only addresses the electromechanical aspects of SSI but also extends to the impact of SSI on transformer saturation—a relatively underexplored domain with significant implications for grid reliability. By combining theoretical frameworks, nonlinear modeling, and simulation-based investigations, this work aims to provide a

comprehensive understanding of SSI and propose practical control strategies to enhance overall grid performance.

1.2 Background

The rapid growth in global electricity demand has accelerated the adoption of renewable energy sources, with wind power emerging as a cornerstone of the clean energy transition. Wind energy is abundant, cost-effective, and environmentally friendly, making it one of the most promising alternatives to conventional fossil-based generation. Studies suggest that utilizing only a small portion of global landmass for wind turbine installations could meet a substantial share of global energy needs[4],[5].

Among various wind turbine technologies, the Type-3 wind power system, also known as the DFIG-based Wind Energy Conversion System (WECS), has gained dominant importance in large-scale wind farms. This configuration is widely preferred due to its variable-speed operation, ability to function in both sub- and super-synchronous modes, reduced converter rating, and overall cost-effectiveness[6]. The power generated from Type-3 wind farms can be efficiently integrated into existing transmission networks either by reinforcing infrastructure or by incorporating advanced technologies such as series compensation, HVDC links, and FACTS devices to enhance power transfer capability[7]–[11].

Despite these advantages, the same technologies introduce new challenges in system stability. In particular, series-compensated transmission lines and fast-switching power-electronic converters can give rise to Subsynchronous Oscillations (SSO)[12]. The destabilizing form of these oscillations, known as SSI, occurs when mechanical shaft modes or converter control modes interact with the network at subsynchronous frequencies. Historical events—including shaft damage in conventional generators and large-scale disconnections in wind farms—demonstrate the severity of SSI and its consequences for both operational security and equipment health[13]–[16].

1.3 Subsynchronous Interaction (SSI)

SSI represents a broad class of destabilizing dynamic phenomena that arise when the electrical network exchanges energy with mechanical components, such as turbine-generator shafts, or with power electronic converters at frequencies below the fundamental system frequency (typically 50/60 Hz)[17]. These interactions can lead to sustained oscillations, excessive mechanical stress, and severe system instability, posing significant challenges to the secure operation of modern power systems integrating renewable and power-electronic interfaced generation sources[3].

1.3.1 Key Characteristics of SSI

SSI encompasses multiple subtypes of oscillatory interactions—each characterized by specific coupling pathways and excitation mechanisms. The fundamental distinction lies in the frequency domain and the source of electromechanical coupling involved in the instability.

(i) Frequency Range

The subsynchronous frequency components occur below the system fundamental frequency, typically in the range of 5–55 Hz for 60 Hz systems (and proportionally for 50 Hz systems). Mathematically, the subsynchronous frequency component can be represented as[18]:

$$f_{sub} = f_0 - f_n \tag{1.1}$$

Where, f_0= Fundamental system frequency (50/60 Hz)

f_n = Natural torsional/converter mode

In practical systems, Subsynchronous (f_{sub}) and Supersynchronous ($f_{sub} + f_n$) frequency components coexist. However, it is primarily the subsynchronous component that contributes to negative damping and destabilization, leading to torsional or converter-induced oscillations[19].

(ii) Fundamental Mechanism

The core mechanism of SSI lies in bidirectional electromechanical coupling, which can occur via two principal pathways[20]:

- **Electrical ↔ Mechanical coupling:**

Subsynchronous electrical currents induce oscillatory electromagnetic torques on the turbine-generator shaft system, exciting torsional modes. This coupling can amplify shaft vibrations if the electrical network provides negative damping at the modal frequency[21].

- **Electrical ↔ Control System coupling**

Power electronic converters with fast dynamic controllers (e.g., in DFIGs, HVDC, or STATCOMs) can interact with the grid impedance, creating resonant conditions that amplify subsynchronous oscillations. These control-induced oscillations are prevalent in weak-grid environments and wind farms employing high converter penetration[1], [2], [20]. In both mechanisms, the negative damping effect results from a net energy transfer from the electrical system into the oscillatory mode, leading to instability if not properly mitigated.

1.3.2 Dominant Trigger Mechanisms of SSI

Modern power systems, particularly those with high levels of renewable and converter-based integration, exhibit SSI through three principal mechanisms:

(i) Series Compensation Induced SSR: The use of fixed or variable series capacitors for transmission line compensation reduces effective line reactance but introduces an LC resonance with the line inductance. This resonance may interact with turbine-generator torsional modes, leading to classical Sub-Synchronous Resonance (SSR)[22]. Historical incidents, such as the Navajo Project (1970s), demonstrated severe turbine shaft failures due to this phenomenon[23], [24].

(ii) Converter-Induced Subsynchronous Interactions: In wind and HVDC systems, converter control loops (current or voltage regulators) can couple dynamically with the network impedance, producing Sub-Synchronous

Control Interactions. A notable example occurred in Texas (2009), where a large-scale wind farm experienced amplified 35 Hz oscillations due to controller-grid interaction, eventually leading to converter damage and wind turbine trips[25]–[29].

(iii) Weak-Grid and Low-Inertia Conditions: Offshore or remote-area grids, characterized by low short-circuit capacity and reduced inertia, exhibit poor damping of subsynchronous modes. Long HVDC links and extensive cabling further aggravate the resonance, allowing minor perturbations to evolve into destructive oscillations, particularly in large wind installations[1][16].

1.3.3 Consequences of Unmitigated SSI

If suitable preventive actions are not quickly implemented, the SSI could result in at least one or more subsequent consequences[30], [31]:

(i) **Equipment damage:** The voltage overshoots in SSI in such a way that in milliseconds, the voltage tends to reach the overvoltage pick-up value of a relay. For such quick overshoots, the protective relay will not isolate the feeder instantaneously. The overvoltage generated in quick time may damage the equipment[26], [32].

(ii) **Power generation loss:** Due to unstable oscillating overshoots of voltage at the point of common coupling, wind turbine generators (WTGs), wind farms, and conventional generating power stations may trip, and the total power generated will thus be reduced [20]. This can lead to financial as well as asset loss for the organization [21, 22]. From a historical event, it is evident that in Guyana (in China), the power was reduced from 219 to 75 MW due to a typical SSI event. Similar events occurred in the Hami wind power system, where a 600 MW steam turbine was tripped by torsional relays due to SSI. Since SSI introduces harmonics in the system, it degrades the power profile of a system. The oscillating voltage can also lead to various equipment damage installed in wind energy systems[33], [34].

(iii) **Power quality:** Another observable effect is that SSI brings subharmonic and inter-harmonic components, therefore degrading the power quality and

imperilling the performance of installed equipment. For example, the inter-harmonic currents develop a loud noise and derate the efficiency of transformers[35], [36].

1.4 Motivation

The large-scale integration of Type-3 (DFIG-based) wind farms into series-compensated transmission networks has introduced SSI as a major stability concern in modern renewable-rich power systems. Real-world events across the U.S., China, and Europe have shown that SSI can lead to rapid oscillation growth, turbine–generator shaft failures, wind farm tripping, equipment damage, and severe power quality deterioration—often beyond the capability of conventional protection and stabilizing schemes. At the same time, the shift from synchronous to power-electronic-dominated grids has created new forms of SSI that traditional IEEE classifications and simplified analytical models cannot adequately represent. Existing studies frequently overlook detailed converter dynamics, grid-strength variations, and transformer behavior under subsynchronous excitation, leaving critical gaps in understanding system vulnerability.

Furthermore, while damping techniques such as FACTS controllers have been explored, they are often ineffective or uneconomical for converter-rich wind farms. Battery Energy Storage Systems (BESS) offer fast and flexible control suitable for damping subsynchronous oscillations, yet their application for SSI—especially optimized, robust damping controller design—remains insufficiently studied.

These gaps motivate the need for accurate modeling, comprehensive SSI analysis, investigation of transformer saturation effects, and development of advanced, optimization-based BESS damping controllers to ensure the stable and reliable operation of future renewable-integrated power systems.

1.5 Research Gap

Although extensive research has been carried out on SSI in conventional synchronous generator-based systems, the advent of converter-interfaced renewable generation has

introduced new and more complex forms of SSI that are not yet fully understood. The review of existing literature reveals several notable gaps that justify the present research:

1. The traditional IEEE classification of SSO is unable to categorize the complex SSI introduced by converter-based resources like DFIGs. Particularly, unable to distinguish between converter-grid and converter-generator interactions.
2. Many previous studies have oversimplified DFIG models, neglecting the detailed analysis of dynamics of the Rotor-Side Converter (RSC) and Grid-Side Converter (GSC), by modelling them as constant voltage sources. This leads to an inaccurate assessment of system stability.
3. Many analytical studies have been limited to frequency-domain impedance analysis without correlating results through time-domain simulations or benchmark model validation (e.g., IEEE FBM). This limits their applicability for practical system design. There is a clear need for simulation-based verification of SSI phenomena under varying grid strengths, compensation levels, and wind speeds.
4. Conventional SSR damping methods, such as FACTS or PSS-based damping, are not directly applicable to converter-dominated systems. Modern research lacks effective control-oriented solutions, such as Battery Energy Storage System (BESS)-based damping controllers, specifically designed to mitigate SSI specially SSR mode while maintaining grid support functions. Current literature does not sufficiently address how the inclusion of BESS might impact the stability margins, resonance modes, or damping ratios of such systems.
5. Few studies have explored metaheuristic optimization of damping controller parameters to achieve robust SSI suppression under varying operating conditions. The absence of such adaptive and intelligent control frameworks limits the practical deployment of mitigation strategies in dynamic renewable environments.
6. While the impacts of SSI on turbine-generator shafts and converter stability are well documented, the transformer's response to subsynchronous excitation—

particularly core saturation, flux excursions, and harmonic distortion—has received minimal attention.

Despite the significant advancements in understanding SSI within power systems, several critical research gaps persist—particularly in the context of Type-3 wind power systems (DFIG-based) connected via series-compensated transmission networks. The integration of BESS as a means of damping SSI remains an underexplored area in current literature.

1.6 Objectives

To address these identified research gaps, the present work is guided by the following primary and secondary objectives:

Primary Objective: To develop a comprehensive framework for the analysis and mitigation of SSI in DFIG-based wind power systems connected to series-compensated transmission lines, with the aim of enhancing overall system stability and protecting critical assets from adverse dynamic interactions.

Secondary Objectives:

1. To reclassify SSI phenomena, review analysis and mitigation techniques, and propose effective damping control strategies ensuring stable operation of wind-integrated power systems.
2. To develop a detailed DFIG-based WPPs model, including RSC–GSC dynamics, and to analyse small-signal stability in order to identify the critical SSR mode.
3. To design a BESS-based Damping Controller (BESDC) for SSR mitigation in DFIG-based WPPs.
4. To design an optimized BESDC that enhances SSR damping and system stability across varying wind speeds and compensation levels.
5. To evaluate the impact of SSI on transformer saturation of the series-compensated line.

1.7 Scope of Thesis

The scope of this thesis is carefully defined to provide a focused yet comprehensive investigation of SSI in Type-3 wind power systems. The key boundaries of the research are:

- **System Under Study**: The thesis primarily investigates Type-3 (DFIG-based) wind farms connected to series-compensated transmission lines, modelled using the IEEE benchmark system.

- **Phenomena Considered**: The study focuses on SSI, including its electromechanical aspects, converter-control-induced interactions, and its impact on transformer flux dynamics and saturation. Other forms of instability, such as transient voltage collapse or frequency stability, are beyond the current scope.
- **Analysis Techniques**: Both frequency-domain impedance analysis and time-domain nonlinear simulations are employed to examine SSI. Eigenvalue analysis is used to assess small-signal stability, while nonlinear flux modeling is used to evaluate transformer behaviour.
- **Mitigation Strategies**: The thesis evaluates control-based damping methods, including supplementary damping controllers and energy-storage-assisted solutions, to enhance system stability. Hardware prototyping and field testing are excluded from this work.
- **Broader Relevance**: While the analysis is conducted on Type-3 wind systems, the insights and mitigation strategies developed are extendable to renewable-integrated, power-electronic-dominated grids with similar dynamic challenges.

1.8 Chapter Organization

This thesis is organized into seven chapters, each addressing a specific stage of the investigation into SSI in Type-3 wind power systems and the development of advanced damping strategies. The chapters are structured as follows:

Chapter 1 – Introduction: Establishes the context of renewable energy integration, highlighting the role of Type-3 wind farms in modern grids. It introduces the problem of SSI, presents the motivation and objectives, specifies the scope of the work.

Chapter 2 – Review of SSI: Classification, Challenges, and Mitigation: This chapter provides the foundational basis for the thesis through a critical review and reclassification of SSI phenomenon. It highlighted the shortcomings of the IEEE classification, particularly its inadequacy in representing interactions in renewable-rich grids. This new framework provides an enhance and comprehensive taxonomy for understanding oscillation events in modern power systems and its mitigating techniques, by connecting it to historical events like the Navajo project (SSR) and the Texas wind farm event to describe different SSI interactions.

Chapter 3– Sub-Synchronous Interaction in Wind Power Systems: Modeling and Analysis: Develops a detailed model of a Type-3 wind power system connected through a series-compensated transmission line. Using the IEEE First Benchmark Model, eigenvalue analysis, frequency-domain impedance studies, and nonlinear time-domain simulations are conducted to assess the onset, severity, and modes of SSI under different operating conditions.

Chapter 4 – Mitigation of SSR in DFIG-based WPPs using BESS-based Damping Controllers: Introduces BESS-based Damping Controllers for SSR mitigation in Type-3 wind farms. Different configurations are modelled and evaluated using eigenvalue analysis and time-domain studies, demonstrating their ability to improve damping, reduce oscillations, and enhance system stability.

Chapter 5 – Intelligent BESS damping controller based on UPSO: Focuses on optimizing the design of the BESDC using Upgraded Particle Swarm Optimization (UPSO). The chapter presents the controller structure, tuning methodology, and simulation studies, showing how UPSO significantly improves damping ratios, stabilizes critical modes, and ensures robustness across wind speeds and compensation levels.

Chapter 6 – Study of transformer saturation under SSI: Investigates the nonlinear behaviour of transformers under subsynchronous excitation. A flux–voltage integral model is applied to study core saturation, flux excursions, and harmonic distortion caused by SSI. The analysis demonstrates the vulnerability of transformers to SSR-driven phenomena, emphasizing their importance in stability studies.

Chapter 7 – Conclusion, Future Scope, and Social Impact: Summarizes the key findings and contributions of the thesis, emphasizing the novel insights into SSI and transformer saturation in Type-3 wind farms, as well as the effectiveness of optimized damping controllers. It outlines limitations of the current work, suggests directions for future research, and highlights the broader societal and industrial impacts of secure renewable integration.

CHAPTER 2

REVIEW OF SSI: CLASSIFICATION, CHALLENGES, AND MITIGATION

2.1 Introduction

This chapter provided an in-depth review of SSI phenomena in wind-integrated power systems, particularly focusing on DFIG-based WPPs interfaced through series-compensated transmission lines. The growing integration of power electronics and renewable generation has given rise to new challenges in system stability, with SSI emerging as one of the most critical concerns. The traditional classification of SSI was examined along with the IEEE's original definitions and the evolving terminology. It was noted that recent system disturbances and events cannot be fully explained by existing standards, leading to the need for updated classification schemes. Numerous real-world incidents from the U.S., China, and Europe were analysed to illustrate the diversity of SSI mechanisms. The review also explored key mitigation strategies, including damping controllers, parameter tuning, FACTS devices and HVDC systems, and BESS etc; while highlighting the limitations and challenges associated with each.

2.2 IEEE standard terms for SSI and its classification

2.2.1 History of IEEE standards terminology

Earlier in the 1930s, synchronous machines were found to act as an induction machine due to a series capacitor's participation that generates a sub-synchronous current[40]. Later this occurrence is referred to as the induction generator effect (IGE), and an incident occurred at the Mohave power station in Southern Nevada in 1970[41] due to the interaction of the electromechanical devices and the involvement of the series capacitor during which the generator shaft was seriously damaged. Later, the name was referred to as torsional interaction (TI), while another incident occurred in 1971 at the same generator power station [42]. Following the two consecutive incidents, this topic gained serious attentions on terms such as IGE, TI, torque amplification (TA),

and SSR, which were debated in 1973[43]. Besides, some researchers concluded that the above phenomenon occurred due to the Series Compensated Transmission Lines (SCTLs) and minimizing damping torsional vibrations, which resulted in SSR participation[44]. Later, an IEEE committee was created, and a report on SSR studies was published in 1976[45]. A square Butte HVDC test was conducted in USA in 1977, and the results revealed that HVDC converters could also introduce adverse subsynchronous frequency interactions with turbine generators, which is now known as sub-synchronous torsional interactions (SSTI) [46]. Following these incidents, researchers have been focusing their efforts on reducing SSR and SSTI due to SCTLs and the involvement of power converters[47], [48]. In its first bibliographic appendix published in 1979, an IEEE working committee summarized the SSR literature and categorized SSR into IGE and torsional oscillations[49]. To unify academia and industry on the SSR issue, standard IEEE terminologies and SSR definitions were proposed in 1980. It further categorized SSR into IGE, TI, and TA, and provided a standard definition of each terminology.

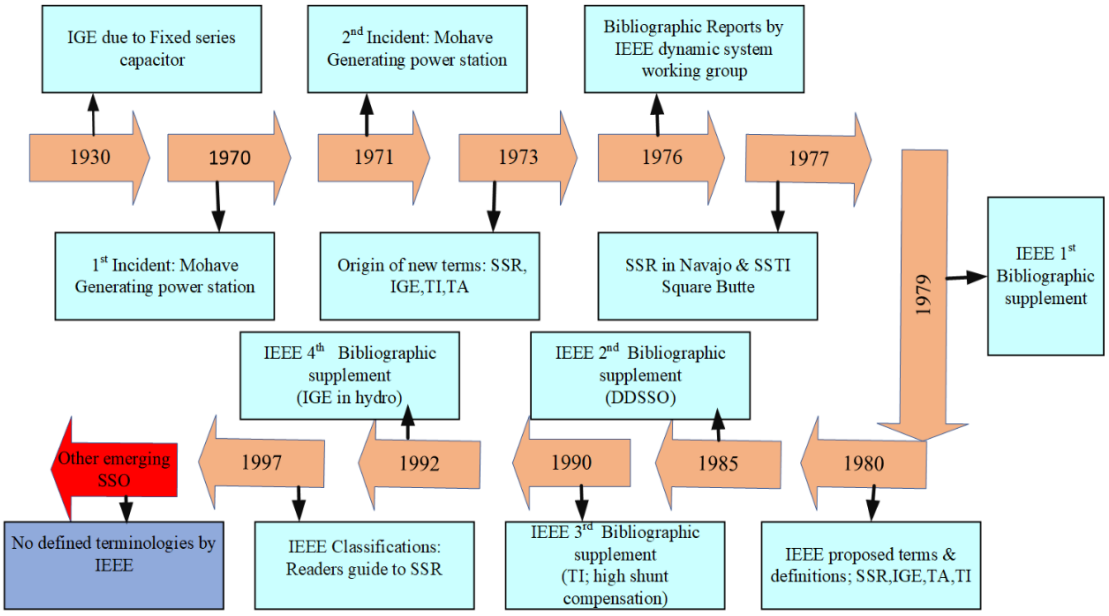

Fig 2.1 Summary of evolution for traditional SSO terminology

In 1985, the second bibliographic supplement introduced device-dependent sub-synchronous oscillations (DDSSO), a concept that covered a wide variety of control devices[50], [51]. This effect was found during the commissioning stage of Ontranio hydro units in 1985 [56]. The third bibliographic supplement published in 1990,

claimed that SSR events could occur due to a transmission line with high shunt compensation[45]. An IEEE committee gave a standard classification and definition for SSR and countermeasure techniques in 1992[52]. SSI between hydro turbines and series compensated transmission lines was started in the fourth bibliographic supplement published in 1997[53]. The timeline in Fig.2.1 summarizes a brief overview of the evolution of SSO terminologies.

2.2.2 IEEE's Classifications

"Sub-Synchronous Resonance Working Group of the System Dynamic Performance Subcommittee" presented standard terminologies, definitions, and classifications after many attempts[54]. SSR and DDSSO come into the SSO phenomenon, as shown in Fig. 2.2 During the SSR phenomenon, there must be involvement of SCTLs, whereas in DDSSO, there are participation of fast control devices, i.e., HVDC, SVCs, PSSs, governor control, and variable speed drives[44]. Thus, SSO is classified into SSR and DDSSO as fallows.

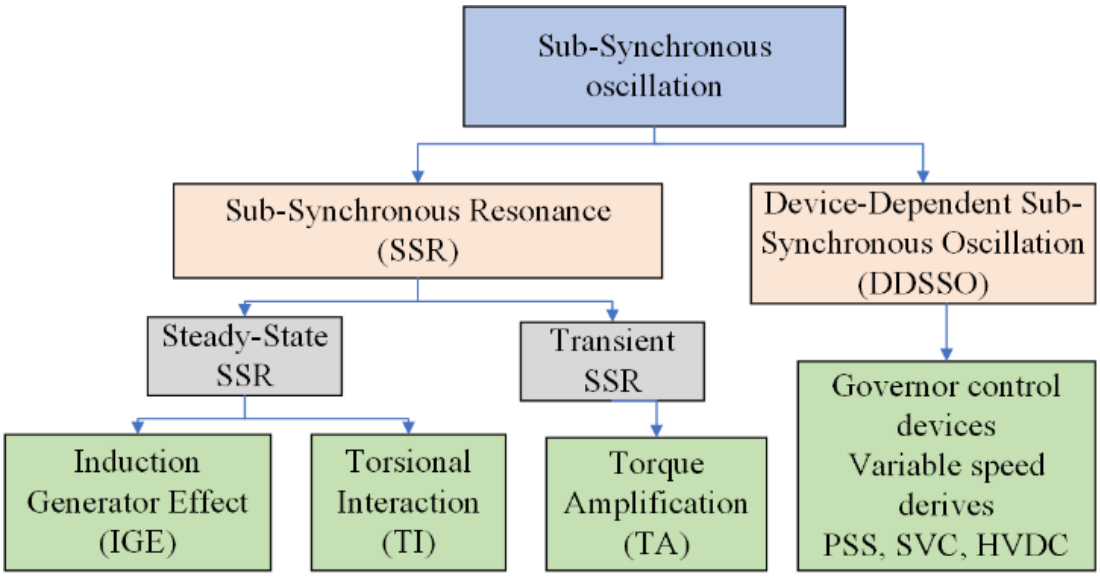

Fig 2.2 Classification of SSO by IEEE

(a) Sub-Synchronous Resonance (SSR)

SSR is prompted by SCTLs connected through a turbine-generator mechanism and exchanges energy at a frequency below the fundamental frequency[55]. Due to the series capacitor, a resonance condition appears in a system as an L-C circuit[56], and the resonance frequency can be calculated as:

$$f_{er} = f_s\sqrt{\frac{Xc}{Xl}} \tag{2.1}$$

where f_s is the synchronous frequency, Xc is the reactance of the series-connected capacitor, and Xl is the total reactance available in the system, including the generator, transmission line, and transformer of the system. The positive sequence current of the armature current at resonant frequency f_{er} produces a stator flux, and the rotor winding induces voltage, resulting in a current at a frequency of $f_r = f_0 - f_{er}$, where f_0 is the rotor frequency generated due to its rotation. These currents, which may maintain subsynchronous armature currents, are generated in the rotor as a result of sub-synchronous stator voltage at subsynchronous frequency [62]. The sub-synchronous frequency current, however, results in a torque that dampens negatively. Subsynchronous currents' negative dampening impact can eventually cause the generator shaft to fail.

The IEEE categorizes SSRs into two categories at the outset: (a) Steady state; and (b) Transient state, also known as torque amplification.

(b) Steady state: Steady state comprises Torsional Interactions and Induction Generator Effect.

Induction Generator Effect: IGE is only caused due to available electrical machines in the network, while it does not involve a generator-turbine mechanism. The series capacitor compensated system is excited due to the IGE. The rigid rotor is responsible for the IGE caused in the system, and the synchronous generator acts as an induction machine for a sub synchronously rotating stator flux due to resonance in the circuit. The slip at a subsynchronous frequency can be defined as [54], [57]

$$S_{SSR} = \left(f_{er} - \frac{f_0}{f_{er}}\right) \tag{2.2}$$

The equivalent rotor resistance at a subsynchronous frequency is

$$R_{eq=}\frac{R}{S_{SSR}} \tag{2.3}$$

If $f_{er} < f_0$, the resistance becomes negative, reflecting that the damping is negative, and an overdamped oscillation of voltage and current would be observed[59].

Torsional Interactions: Synchronous generator rotor produces oscillation frequency f_{en} due to torsional frequency f_n, which is responsible for generating armature voltage at subsynchronous frequency range. The oscillating frequency is $f_{en} = f_0 - f_n$. If this voltage component frequency (f_{en}) matches the system's electrical resonating frequency, the electromagnetic torque produced will enhance the torsional oscillation, which reflects in the mechanical system [58]. Generally, the torsional oscillation is close to the electrical resonant frequency.

As same as IGE, TI also guides the self-excitation of the generator at sub-synchronous frequencies. Torsional oscillation is developed because of electrical and mechanical systems' interaction at a specific frequency, whereas IGE is a purely electrical phenomenon and doesn't depend on mechanical systems.

(c) Torque Amplification

The transient electric torque is developed on the generator rotor due to a significant disturbance in the network [65]. These transient electrical torques oscillate, and some components include sub-synchronous torques. The sub-synchronous torque oscillates when the frequency is close to the mechanical system's torsional frequency. This has be referred to as torque amplification[58].

(d) Device-Dependent Sub-Synchronous Oscillations

SSO in turbine generators are caused by interactions with other parts of the power system in addition to interactions between turbo-generator set and series capacitor compensated networks. PSSs, HVDC converter controls, SVC, controls for high-speed governors and converters for variable speed drives, are further potential sources. Possible sources for the excitation of SSO can be any devices that regulate/reacts quickly to power/speed fluctuations in the sub-synchronous frequency range[52]. For instance, PSS dampens oscillations in the power system at low frequencies. The parameters of PSS and feedback signals, which have one or more oscillatory signals corresponding to the natural torsional modes of the shaft system, may be injected into the generator field windings. As a result, the torsional modes may be excited into SSO. Similarly, the HVDC converter and a governor control action can also excite SSO[3].

2.2.3 Other Emerging Terminologies

With the growing penetration of renewable energy and advancements in power electronic devices, system efficiency has improved, but complexity has also increased[59]. Since the IEEE's 1992 classification, there has been little update to reflect recent developments.

Power electronic converters, due to their fast control actions, can induce SSO[30]. A notable incident occurred in 2009 within ERCOT, termed Sub-Synchronous Control Interaction (SSCI), involving interaction between a wind turbine and a SC transmission line[60]. SSCI primarily addresses issues between SC lines and wind turbines[61]. However, IEEE's classifications lack clarity on the dominant source of such oscillations.

To address this, Shair et al. proposed a broader classification of SSO into three types: (i) inductor-capacitor (L-C), (ii) torsional oscillations, and (iii) converter-grid interactions[20]. However, this model remains complex and does not clearly identify dominant causes or future interaction scenarios. Another classification by the author in[62] focuses on SSR in conventional generators and wind power systems. Additionally, some studies[55] use the term SSI instead of SSO, but no consistent standard classification or terminology exists to guide future research in this field.

2.3 Proposed Classification of SSI

This section proposes a new classification along with previous IEEE standards [52]. Extending classification to get more defined knowledge of the emerging SSO phenomenon and covering all types of interactions in the conventional and renewable power system have been done precisely and efficiently. In the proposed classification, DDSSO is classified into sub-synchronous torsional control interactions (SSTCI) and sub-synchronous converter control interactions (SSCCI). As DDSSO individually cannot define the dominant source of interaction, while as the name suggests, SSTCI shows the interaction between turbo-generator and control devices or any FACTS devices. In contrast, the name SSCCI suggests that interaction is between converter control and series compensated line/FACTS control devices. The detailed

classification of an entire sub-synchronous phenomenon is shown in Fig.2.3 and discussed in detail.

Generally, SSI refers to energy exchange between two systems at natural frequencies below the fundamental frequency. In an electrical system, many elements are involved, such as generator's mechanical shaft, capacitor, reactor for reactive power compensation, and various control equipment used to optimize the power utilization. Based on these elements, SSI can be further classified into SSR, SSCCI, and SSTCI.

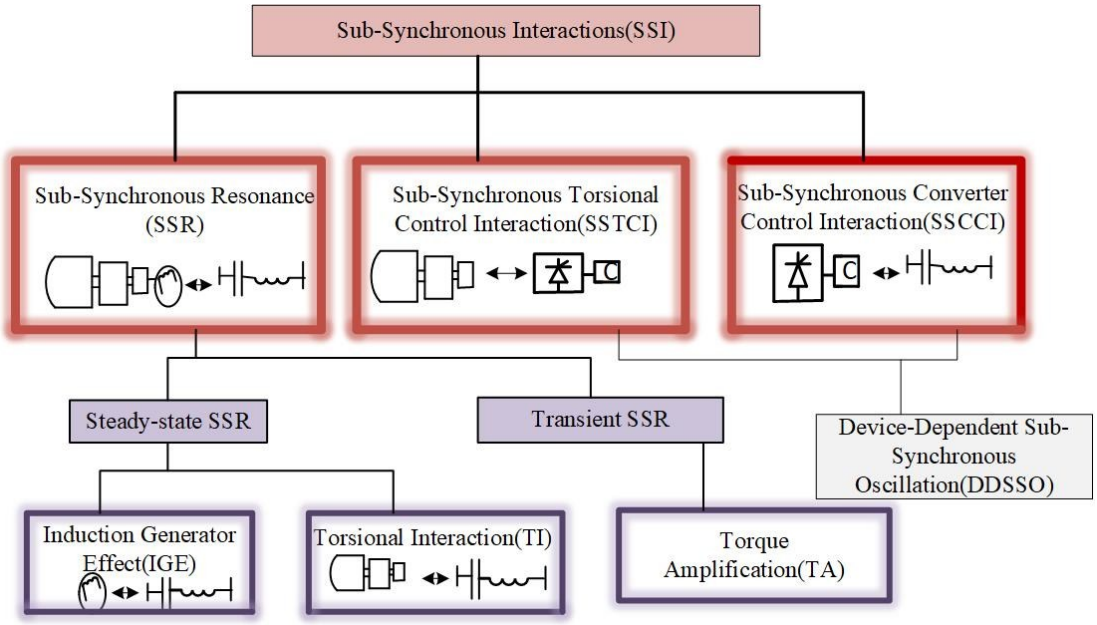

Fig 2.3 Proposed classification of SSI

2.3.1 Sub-Synchronous Resonance (SSR)

As described in Section 2.2.2, SSR exchanges energy at a frequency lower than the fundamental frequency and is triggered by SCTLs connected via a turbine-generator mechanism[55]. Due to the series capacitor, a resonance condition appears in a system[56]. As mentioned earlier, an SSR is produced due to the interaction of stator flux with rotor flux at a frequency f_0, and the torque is developed at the frequency of $f_r = f_0 - f_{er}$. If the developed torque frequency f_r matches the natural frequency of the mechanical generator-shaft combination, torsional stress is developed in the shaft,

and an undamped oscillation will be produced, leading to the failure of the mechanical systems[63], [64].

The conventional SSR occurs in a synchronous machine of thermal power plant, transmission line associated with series capacitance, wind energy system under certain circumstances. SSR may further be divided as due to Induction Generator Effect and Torsional Interaction [52]. The further classification of SSR is the same as the classification proposed by the IEEE, which has already been discuss in Sect. 2.2.2. The current research status of SSR is focusing on SSR analysis techniques and mitigation techniques, which will be discussed in upcoming chapters.

2.3.2 Sub-Synchronous Converter Control Interaction

SSCCI refers to interaction between the power electronics converter control circuits and SCTL. The resonance frequency is not fixed in SSCCI, which depends upon a particular situation of the converter control algorithm[14]. It is of utmost necessity to control these oscillations, which can build up drastically because of converter control and a pure electrical network. The control system associated with the wind turbines' converter generates a negative resistance under SSR[47]. A power electronic circuit produces multiple slip frequencies caused by switching of rotor current, and a negative resistance is generated, which is responsible for the undamped oscillation produced in the network[65]. However, SSCCI is a multi-variable dependent phenomenon, making it challenging to forecast any relationship.

There have been many incidents occurred due to the involvement of wind turbine converter control and series compensated transmission line/weak grid. The timeline of the practical events is shown in Fig.2.4 due to SSCCI phenomenon. A 100 MW DFIG-based WPP that was accidentally left radially linked to a 345 kV SCTL in south central Minnesota in 2007, was the first SSCCI event resulting in SSO around 9–13 Hz[60], [66]. In 2009, a similar incident took place in Texas, which harmed the series capacitor and crowbar circuits. A DFIG-based WPP was connected with a 50–70% fixed SC transmission line, and SSCCI was triggered at 22 Hz causing the current and voltage to increase very quickly up to 300% in 0.4 s, resulted in the damage of the series capacitor in 0.2 s[67]. Oscillations around 4 Hz were observed at

a PMSG based WPP in Texas (2011) region after a transmission line was tripped[25]–[29]. Between 2012 and 2016, the Guyuan wind power system experienced several SSCCI occurrences. More than 58 oscillation incidents with oscillation frequencies between 6–9 Hz were observed in 2012 in Guyuan grids, where DFIG-based WPP having double circuits of SCTLs connected to Guyuan station with Inner Mongolia and North China grids[39], [68].

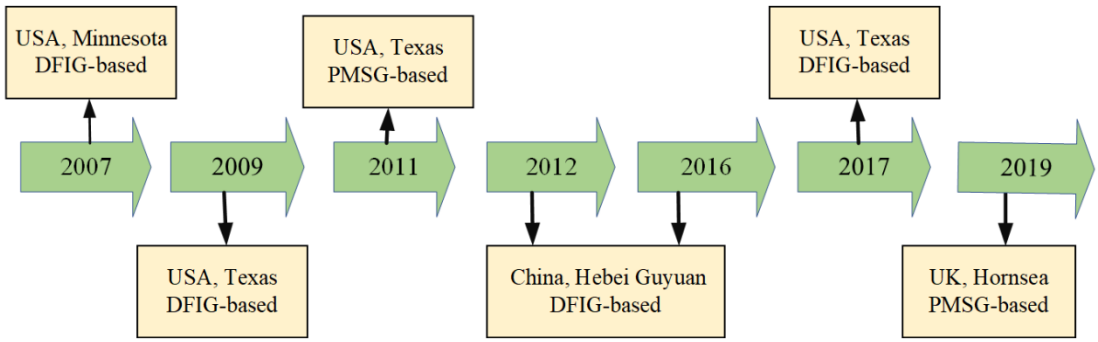

Fig 2.4 Timeline of reported SSCCI events due to involvement of WPP and series compensated transmission line/weak grids

In 2016, in a 600 MW DFIG-based WPP in Northwest China (300 turbines of 2 MW), instantaneous voltages and currents were found to oscillate at frequencies of 37 Hz and 63 Hz[68] [41], [73]. The oscillations were eliminated by strengthening the grid (a second 500 kV line was built and placed into service) and updating the WPP converter control. For the Texas ERCOT wind farm in 2017, SSCCI occurrences were documented. The instantaneous current frequency range is 22–26 Hz, and by updating the WPP converter control software, WPP vendors resolved the problem[69]. The interaction of the DFIG control system and a SCTL was the cause of all the aforementioned events. The majority of incidents were caused by a transmission line failure, which left the wind farm radially connected to a SCTL. Ten minutes prior to the interruption of the Great Britain power grid (Hornsea) in August 2019, oscillations with a frequency of 9 Hz were seen. It was later discovered that weak grid oscillations were also accountable for the 800 MW offshore WPP reaching the de-loading stage[70]. After that, the control software was upgraded by the WPP vendor. On August 24th, 2021, oscillations of 8 Hz in RMS voltage were noted in Scotland. The disturbances occurred twice, each lasting 20–25 s, with around 30 min apart. After re-

introducing a few traditional plants to the system, the oscillations were reduced. The oscillation's underlying cause is currently being investigated[41]. It has been observed that SSCCI is an entirely electrical phenomenon and that a large amount of energy is transferred between the converters of WPP and the series compensated network [6].

In addition, a majority of studies have proven that wind farms using DFIGs are susceptible to SSCCI[71][72][73]. As a consequence, research community pays significant attention to SSCCI and the accompanying countermeasures. The root cause of SSCCI accidents is the subject of much investigation, and it has been observed in [9] that SSCCI is intimately related to the proportional integral (PI) controller of the current loop of the RSC. The magnitude and frequency range in which the DFIG shows negative resistance are both influenced by the bandwidth of the current controller loop. Resonant current in the stator of the DFIG produces a similar sub-synchronous current in the rotor when a disturbance occurs. When the sub-synchronous current is detected, the PI controller of the RSC's current loop then modifies the output voltage, which can boost the disturbance and sub-synchronous current, leading to SSCCI. Therefore, by adjusting the PI parameters of the DFIG converter controller, several mitigating techniques have been proposed[74]–[76]. The proportional gain of the RSC current loop is reduced in [88], which is a damping approach to lessen SSCCI. Although it has limited capability, changing the control parameters may degrade the original control performance.

To overcome these challenges, supplementary wide-band damping control strategy for MMC-STATCOM has been proposed to mitigate SSCCI. This method adopts a notch filter to filter only synchronous frequency components to produce the damping control signal, and obtains the corresponding sub-synchronous component to makes MMC-STATCOM exhibit positive resistance even at varying sub-synchronous frequency range[77]. A supplementary damping controller can be applied to a multi-Terminal DC system and wind turbine converter to effectively secure the integration of WPP and series compensated transmission line[78].

2.3.3 Sub-Synchronous Torsional Control Interaction

SSTCI refers to a problem when a turbo-generator set is connected to power electronic controller, and the mechanical system generates undamped torsional oscillations at sub-synchronous frequencies. The control devices in FACTS and HVDC converter circuits, rapidly change parameters according to the system's power variation in sub-synchronous frequencies[74], [79]. This may cause negative damping, and similar to TI, an undamped oscillation may be produced, which can damage the shaft of a mechanical system. Due to SSTCI, the first accidents happened in 1980 at the Square Butte HVDC and nearby Milton Young turbine plant, while similar events occurred in Ontario and Chester, USA in 1983 and 1987 respectively[51], [75], [80]–[82]. The latest incident occurred in Hami Wind power system China in 2015, which has a 3000 MW type-4 PMSG based WPP, and power is transmitted through both AC and HVDC transmission lines[83]. Many SSO events were found in 2014, but a severe one was detected on 1 July 2015, in which the torsional oscillation occurred in a conventional turbine generator which is 300 km away from the wind farm. The torsional protective device tripped 3 units of the traditional turbo-generator, resulting in the loss of 1250 MW power generation. The fundamental reason behind the incident was the interaction between the HVDC line and traditional turbo-generator [96].

As per the proposed classification in[20], this incident comes under grid-converter oscillations. However, the oscillations propagated into the transmission line and matched the turbine generator's torsional frequency. Subsequently, the three units were tripped due to the protection scheme, and varying resonance frequencies were detected between 27 and 33 Hz for 3 h and 20 min since the interactions occurred between converter and turbo-generator. Hence, it comes into the SSTCI phenomenon. Usually, the rectifier sides of HVDC converter control are responsible for the negative damping. The degree of sub-synchronous interaction is influenced by a number of variables, but the management strategy utilized by HVDC to keep power transmitted around a single constant amount is the key reason for the reduced sub-synchronous damping. Constant current or constant power control is a common HVDC rectifier control method for achieving constant power characteristics. Equidistant firing control, which controls the timing of valve firing, is another built-in feature of contemporary

HVDC systems that results in reduced sub-synchronous damping. The original HVDC systems' equiangle firing control was intended to be replaced[84], as the equidistant firing control increased the side effect of HVDC on subsynchronous damping since it essentially eliminated the harmonic generation issue brought on by the previous equiangle firing control [38, 100], though other controllers may also have an effect on it[84].

In particular, the parameters and structure of the rectifier current controller are crucial in determining the level of interaction. A supplementary control circuit may have an impact on the behavior of the control system on the crucial torsional frequencies of a particular unit since the control system, or more specifically, the HVDC control principle, is what causes the interaction[84]. The transfer function of rectifier control is impacted by this supplementary control, also known as sub-synchronous damping control. As a result, the control system related phase shift that causes increasing sub-synchronous oscillation at a certain natural frequency is eliminated. The current research is on Line commutated converter (LCC)-HVDC systems, as LCC-HVDC has rapidly grown in China[85], [86]. An analysis of SSTCI was done for LCC-HVDC and modular multi-level converter (MMC)-HVDC in a power system. It produces higher risk of SSTCI as compared to HVDC systems only[87]. Introducing MMC-STATCOM can reduce the negative damping of existing LCC-HVDC system, while the risk of SSTCI may be further reduced by increasing the PLL gain on the rectifier sides of HVDC[88]. The proposed classification and the historical events are summarized in Table 2.1

Table 2.1 Comparison analysis of proposed classifications and historical events due to SSI

Type of proposed SSI phenomenon	**Triggering Factor**	**Characteristics**	**Practical Incidents**		
			Location	Year	Severity
SSR	Realistic level of series compensation in a transmission line.	Weak damping caused by negative rotor apparent resistance. Interaction between shaft system and series capacitor. 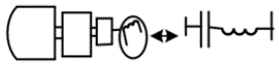	Mohave, California, USA [16], [56]	1970	Failure
			Navajo, USA [23]	1976	Test
			Cholla, USA [24]	1978	Test
			Shangdu, China [89]–[91]	2011	Test
SSTCI	Rectifier side of the HVDC system. Inappropriate parameter tuning of Power conveters.	Fast control action of devices causes variable torsional frequency. Interaction between shaft system and power converters/fast control devices. 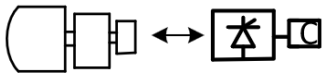	Square Butte, USA [80], [81]	1980	Test
			Ontario, USA [51]	1983	Test
			Chester, USA [75], [82]	1987	Test
			Hami, Xingjiang, China [34], [76], [92]	2015	Failure
SSCCI	Level of series compensation. Weak AC system without involving of series compensation. Power electronics devices with inappropriate parameter tuning.	Wide-ranging transformation between a system with several sources and multiple terminals. Variable resonance frequency. Adverse impacts on the other existing stable modes in the system. Interaction between power converters/fast control devices and a series compensated line. 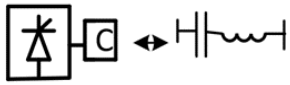	Minnesota, US [60], [66]	2007	Failure
			ERCOT, Texas, USA [25]–[29]	2009	Failure
			Guyuan, Hebei, China [39], [93]	2012	Failure
			ERCOT, Texas, USA [69]	2017	Test
			Hornsea U.K [70]	2019	Failure
			Scottish wind farm [41]	2021	Test

2.4 SSI Analysis techniques

Various methods are used to analyse SSI, including frequency scanning, complex torque coefficient analysis, eigenvalue analysis, impedance-based modeling, and transient simulation. This section reviews these commonly used approaches. Table 2.2 summarizes their applications, features, and limitations, as reported in existing literature.

2.4.1 Frequency scanning technique

Linear analysis in frequency scanning uses a positive sequence network and equivalent circuit modeling. It determines the system's transient impedance Z(s) as a frequency function from a single point. Stability is assessed by identifying sub-synchronous frequencies where reactance is zero and resistance is negative. Tools like PSCAD/EMTDC/MATLAB support implementation[94]. While simple and effective for preliminary SSI risk screening, this method is limited for systems with multiple power electronic devices and does not capture dynamic wind turbine behaviour during faults[95].

2.4.2 Complex torque coefficients

I.M. Canay[96] proposed the complex torque coefficients method to assess sub-synchronous oscillation by calculating the mechanical damping D_M and electrical damping D_E. A periodic disturbance is applied to the generator rotor, and the torque increment ratio is expressed as:

$$\frac{\Delta T_E}{\Delta \delta} = K(\mathcal{F}) + j\mathcal{F}D(\mathcal{F}) \tag{2.4}$$

System stability at a given frequency is analysed by comparing $K(\mathcal{F})$and $D(\mathcal{F})$. Although it may not fully predict system behavior across all frequencies, the method effectively visualizes damping using time-domain simulations or linear models[97] [99]. It remains a conventional tool for SSO analysis[98].

2.4.3 Eigenvalue analysis

Eigenvalue analysis is widely used for small-signal stability studies. It begins by modeling system components with state and algebraic equations, then linearizing to form the state-space matrix [64]

$$\Delta\dot{X}=A\Delta X \tag{2.5}$$

Eigenvalues of matrix A represent oscillation modes real parts indicate damping and imaginary parts denote oscillation frequency. Due to its accuracy, eigenvalue analysis helps assess the impact of wind speed, operating conditions, compensation level, and controller settings on SSI modes[99], and supports mitigation strategies[85]–[88]. However, it becomes complex in high-order systems ("dimension disaster") and only provides damping at specific frequency points, limiting its effectiveness in general frequency domain analysis[100].

2.4.4 Impedance-based model analysis

Impedance-based analysis in the frequency domain is categorized into stationary frame (phase domain) and synchronous frame (d-q domain) models[101]. The system is typically divided into source (e.g., converters, wind farms, generators) and load (e.g., transmission lines). System stability is assessed using the source-load impedance ratio with the generalized Nyquist criterion (GNC) [71]. Widely applied in studying SSI in wind farms, this method accommodates both power electronic converters and conventional generators. With growing use of power electronics, impedance-based analysis holds strong potential, though improved modeling techniques are still needed[102].

2.4.5 Transient simulation analysis

Transient simulation analysis displays time-domain variable trends and includes electromagnetic, electromechanical, and dynamic mechanical simulations. Electromagnetic transient simulation effectively validates SSI models and complements methods like frequency scanning and eigenvalue analysis[101]. It is particularly suited for analysing SSI in wind farms[103]. However, increasing use of converter controls challenges simulator accuracy and speed[71]. While time-domain simulations show variable trends, they do not reveal deeper system variable relationships crucial for understanding oscillation mechanisms and suppression strategies.

Table 2.2 Comparison of SSI Analysis methods

Analysis Techniques	**Advantage**	**Limitations**	**Applications**
Frequency scanning techniques	• Simple and easy to implement by utilizing equivalent circuits or simulation tools. • Computational attractive • Cost-effective	• Approximate method • For accuracy, the results must be verified using time domain simulation. • It is not possible to consider the dynamic properties of systems during faults.	• To identify steady-state SSR ,SSTCI and SSCCI • To determine the system operating circumstances that influence SSI.
Eigenvalue analysis	• Accurate analysis and provides a clear insight into Subsynchronous interactions • Reveals details about the damping and frequency of every system mode. • Finding the involvement of state variables and component sensitivity is simple.	• Restricted to very large systems • Nonlinearities cannot be included • Device switching characteristics are ignored • Expensive method • Require detailed system representation • Fails to identify transient SSR	• Helpful for creating SSI countermeasure controllers • To determine the system's operational circumstances that affect SSI
Complex torque coefficients	• Displaying the mechanical and electrical damping coefficient trends over a wide range of frequencies	• Mostly applied to the mechanical oscillation	• To identify SSTCI and torsional interaction of SSR
Impedance-based model analysis	• Finding the oscillation path and component sensitivity is possible due to the impedance-network model, which preserves the network topology.	• Improved modeling methods and suitable stability criteria are required. • Challenging frequency domain modeling techniques	• Used for SSCCI analysis
Transient simulation analysis techniques	• Allows for precise SSI investigations under varied disturbances	• For self-excitation study, not recommended • Needs a thorough system representation • Not helpful for determining the internal relationships among different variables	• Verify the outcomes of the eigenvalue and frequency scanning techniques

2.5 Mitigation techniques and their challenges

Several techniques exist to mitigate SSI. This section reviews mitigation methods and their challenges based on literature addressing the classified emerging SSI phenomenon. Table 2.3 summarizes their features, limitations, and applicability to both network and generation sides.

2.5.1 Reduce the degree of series compensation

Higher compensation level causes higher risk of SSR, and thus it requires to reduce the series compensation at the planning stage. However, an incident occurred in Guyan, China, due to SSCCI with the compensated line approx. 6.67% [60], [104].

2.5.2 Improve grid strength

Generally, power plants are located far away from the grid or local load. The required long transmission lines increase the net reactance thus, reduce the short circuit ratio, resulting in weaker grid. As a result, the steady state based SSR phenomenon can arise. This can be mitigated by improving the AC system strength by introducing, e.g., a voltage source converter, HVDC line etc., though it may cause risk of SSCCI[105], [106]. This is revealed when an SSCCI incident occurred in Hami PMSG based WPP connected with a weak AC grid system[99].

2.5.3 Bypassing series capacitor

This technique is inexpensive and feasible for practical systems by developing an intuitive oscillation sensing algorithm. If the calculated magnitude of synchronous current exceeds a specific set value. In that case, the algorithm provides command and bypasses the series capacitors at particular instant. In contrast, a reinsertion algorithm is applied to reinsert the series capacitors when the voltage level is under the threshold value[107]. However, SSI can happen in a system without series compensation as stated hereinbefore.

2.5.4 Damping control by FACTS devices

FACTS devices effectively mitigate SSI while fulfilling their primary functions—voltage and power flow control, reactive compensation, stability, and power quality[108][109]. By adjusting internal controls, they damp SSR by reshaping

network impedance without disrupting core operations. Devices like SVC, STATCOM, TCSC, GCSC, UPFC, and SSSC have proven effective[110]–[112]. However, high cost is a major drawback, especially for new installations. VSC-based FACTS may also risk triggering SSCCI[74], [79].

2.5.5 Shunt-VSC

Due to the fundamental operating frequency, cost, rating, and equipment size increase, using FACTS devices to mitigate SSI may not be economically feasible. However, the cost of FACTS devices could be reduced by designing a special-purpose shunt-VSC to generate a compensated signal at the extracted sub-synchronous frequency instead of the fundamental frequency. The sub-synchronous component is extracted by a notch filter and a bandpass filter[113], [114]. The challenge in this technique is the accurate extraction of the sub-synchronous frequency because of varying sub-synchronous and fundamental frequencies with time during SSI events. Thus, it is challenging to track the exact frequency while it's devoted only to SSI damping without performing other tasks[115].

2.5.6 PV Solar based damping

Although FACTS devices can alleviate the SSR issue proficiently, they can't exchange active power with the network and are also costly. Reference[116] utilized a PV solar farm as STATCOM, namely PV-STATCOM, to mitigate SSR in a steam turbine-driven system with SC transmission lines. The PV solar farm can work as a STATCOM with its whole inverter limit for SSR alleviation from evening to nighttime. If a system deficiency/ fault triggers SSR during the daytime. In that case, the PV solar stops its normal active power generation and its whole inverter ability works as PV-STATCOM for SSR counteraction. When the SSR is damped, the PV solar farm returns back to its ordinary real power generation. However, VSC-based PV-STATCOM raises the risk of SSCCI[117], [118].

2.5.7 Damping controls via HVDC

Bulk power can be transferred using an HVDC transmission system from a remote location to grid utility efficiently and effectively. A converter controller is used at sending end and receiving end[119]. A proportional resonate controller is applied at

sending end of modular multi-level converter HVDC link to suppress SSTCI[120], and some further supplementary damping controllers can be used to existing HVDC converters. However, a VSC-based HVDC converter may destabilase other stable mode of the existing system.

2.5.8 Industrial Sub-harmonic Relay

Industrial sub-harmonic relays and active damping controllers are used to detect and damp SSTCI. Microprocessor-based sub-harmonic protection estimates SSTI but is prone to errors, requiring analog sensors for correction. Overall, these mitigation techniques are costly[121]. According to the authors, limited literature exists on SSTCI mitigation, with current research focusing mainly on SSTCI analysis[86], [122], [123].

2.5.9 Regulating control parameters of WTC

The DFIG-based wind turbine control (WTC) structure is shown in Fig. 2.5. Controller parameters, especially PI controller gains in the RSC and GSC, significantly affect SSCCI damping.

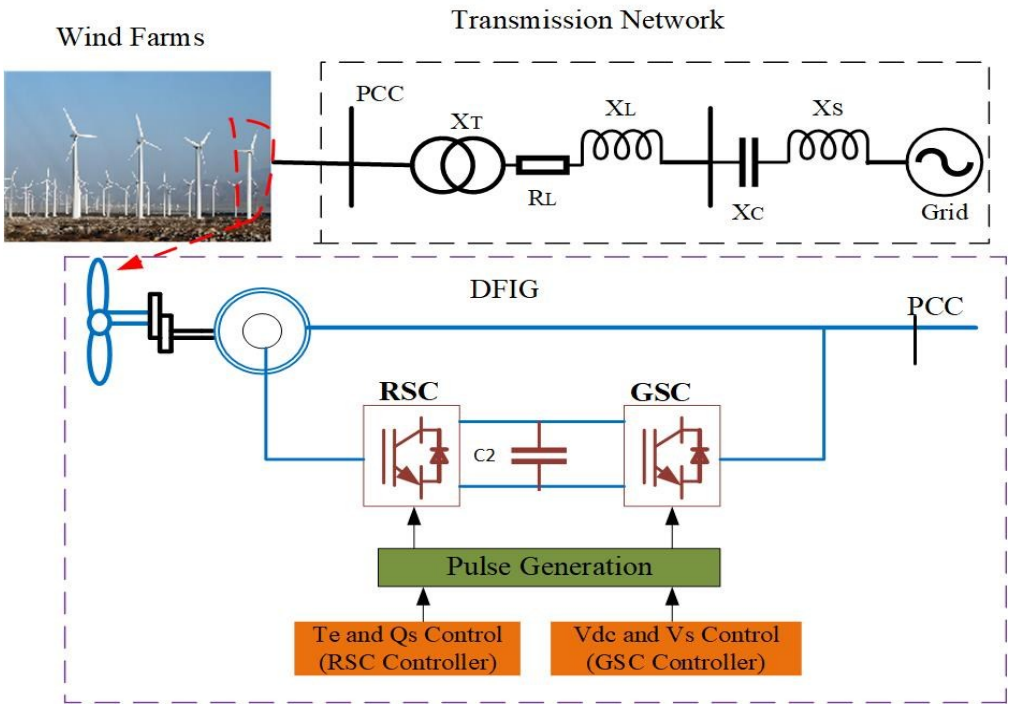

Fig 2.5 DFIG based WTC control structure

Higher current controller gain reduces the damping ratio, as confirmed by eigenvalue analysis[79,83,94]. Torque loop gain and reactive power control also lower

SSCCI damping. A mitigation approach involves real-time detection of sub-synchronous components to reduce RSC gain. Enhancing RSC rise time and optimizing PI parameters can improve damping, but exceeding limits may impair DFIG fault sensing[95].

2.5.10 Installing heterogeneous wind power plant

Deploying a different type of wind farm instead of the same type of wind farm is less prone to SSCCI[37], for example, adding Type-4 (PMSG with full scale converter) wind turbines, which are able to provide positive damping to Type-3 (DFIG with partial scale converter) wind turbines[124], [125]. This can be adopted to mitigate the effect of SSCCI in the WPP. However, it is difficult to model and study the wind farm as it cannot be accumulated to signify the entire wind farm.

2.5.11 (on/off) switching of WPP

In this strategy, selecting a suitable number of WPP and turning off the entire WPP by providing a tripping signal helps stabilize the unstable mode of SSCCI [22]. This is accomplished by determining the equivalent impedance[34],[39]. This arrangement is suitable for the global protection of power systems from SSCCI. However, separate communication is required for the command and coordination unit, and the major drawback is the cost of power loss.

2.5.12 Virtual synchronous generator control

This technique recently has been developed to mitigate SSCCI by providing virtual inertia. It can simulate the dynamic stability characteristics of a wind farm by providing virtual inertia via controlling the back-to-back converter of the wind turbines[126], [127]. Most of the current research is on the design of an SDC to reshape the system's overall impedances. There is not much literature on virtual synchronous generator control found on the impact of SSO caused by SSCCI, while this technology is not mature and is an expensive solution.

2.5.13 SDC with GSC

The GSC control loop enables integration of a damping controller, offering damping capabilities similar to STATCOM but at reduced cost[128], [129]. Supplementary

damping can be added in the q-axis of the stator voltage control loop, as shown in Fig.2.6, to mitigate SSCCI by modulating the reference signal. This concept has been explored in multiple studies[23], [130], [131].

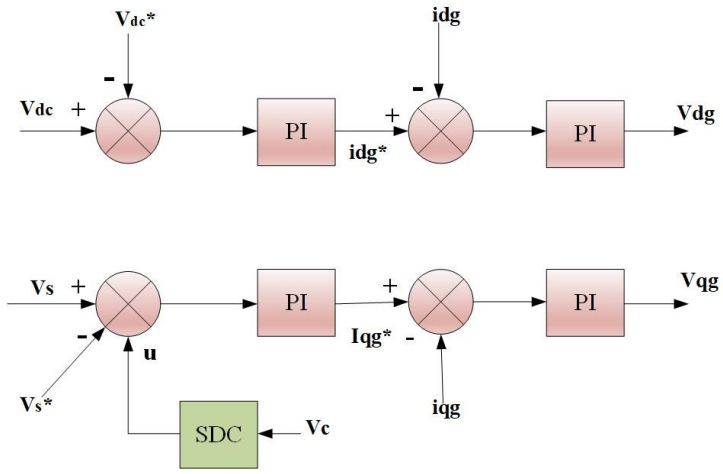

Fig 2.6 With an auxiliary SSR damping at q-axis loop

A multichannel damping controller is proposed, where each channel uses modal speed as input and applies phase and gain compensators to damp oscillations, as illustrated in Fig.2.7 [132]. A PSO-based technique was later applied to optimize the Lead-Lag Compensator (LLC), but its applicability is limited to specific operating points. Given the nonlinearity and wide operational range of WPPs, an adaptive fuzzy logic-based damping controller was introduced, showing better performance in comparison studies with PSO-based controllers, as shown in Fig.2.8[23].

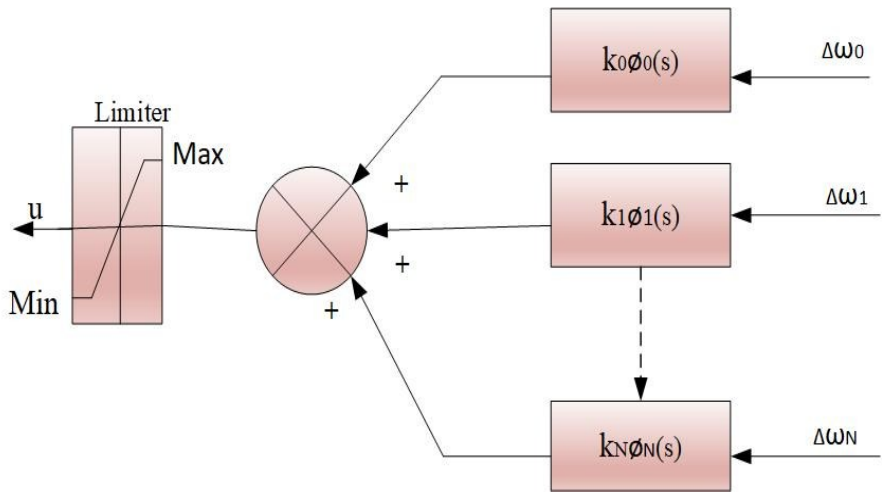

Fig 2.7 GSC SDC with multichannel gain and phase shifters

However, most techniques used speed deviation as the Input Control Signal (ICS), which is suboptimal. A more effective ICS is the voltage across the series capacitor[32], though it must be transmitted via a separate communication link, possibly causing delays.

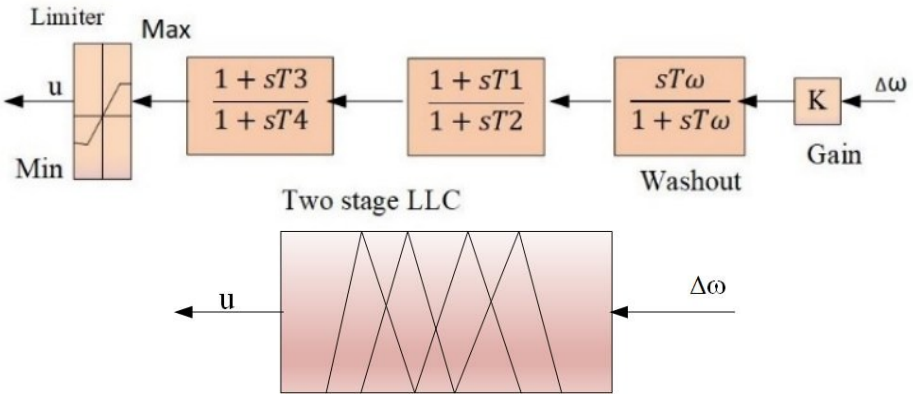

Fig 2.8 PSO optimized with lead-lag networks(b) fuzzy controller

To address this, a state feedback controller using an optimal quadratic method was developed to regulate the GSC terminal voltage[133]. It uses stator current (d-q components) as input and includes a high-pass filter for noise blocking. The controller output is applied to the stator-voltage control loop of the GSC, as shown in Fig.2.9**.** Despite satisfactory performance, its complexity—due to model order reduction and state estimation—limits practical application in large wind farms.

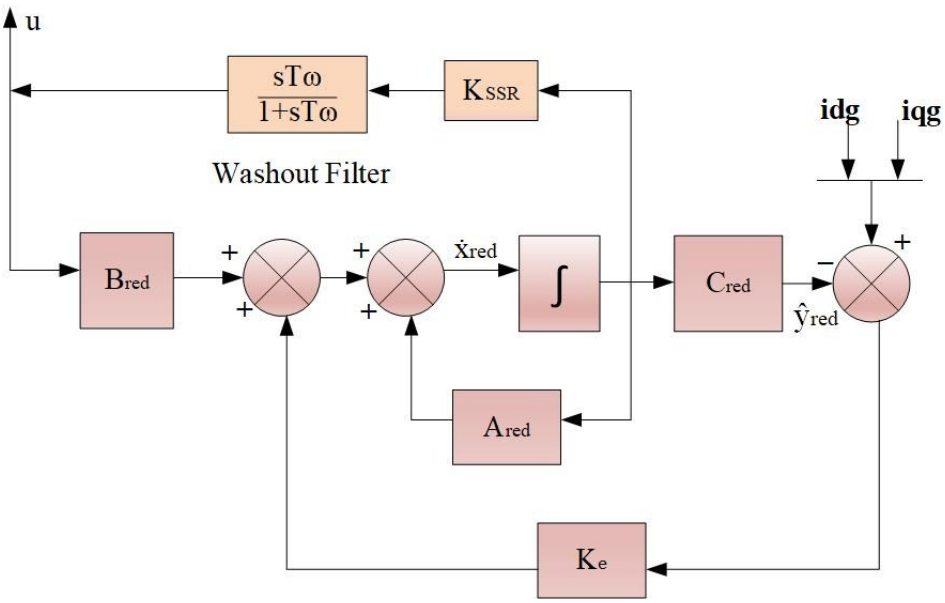

Fig 2.9 State-feedback controller, LQR as state observer

To overcome this, a feedback linearized sliding mode controller was designed for robust control across a wide range, with output applied to the stator control loop of the GSC[134]. A probabilistic DFIG-based PSS using LLC and capacitor voltage as ICS was also introduced[124].

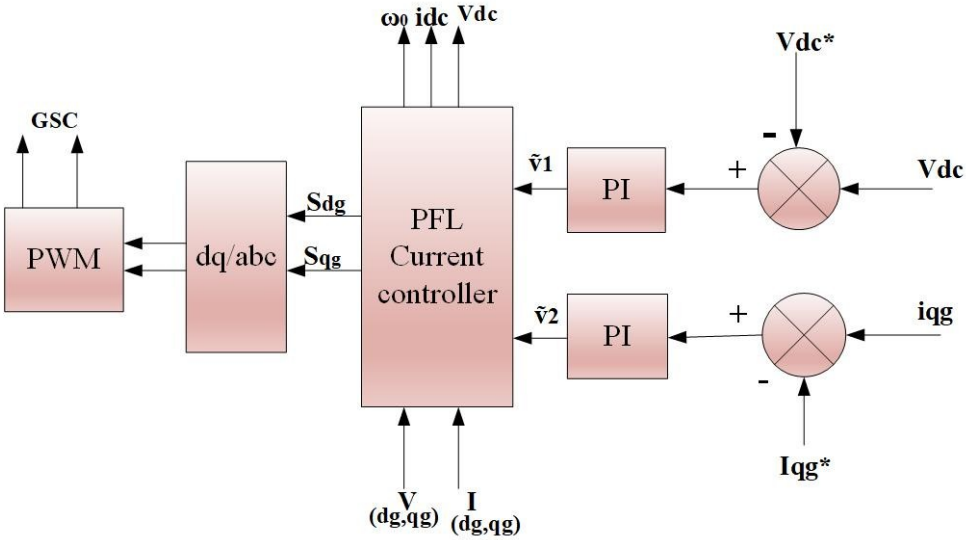

Fig 2.10 PFL based current controller

In a more recent study[135], the traditional PI-based current controller was replaced with partial feedback linearization, which transforms the nonlinear model into a low-order, partially linearized model to enable wide-range SSI mitigation with reduced mathematical complexity, as shown in Fig.2.10[103].

2.5.14 SDC with RSC

RSC offers superior damping performance over GSC when equipped with an auxiliary damping controller, especially under high series compensation, due to its high controllability and direct influence on rotor resistance[136]. A supplementary damping controller is implemented in the RSC's inner control loop using a multi-input multi-output state-space approach with rotor and stator currents as input signals[17], [137], as shown in Fig.2.11. However, its performance can degrade during DFIG transients. To address this, a linear matrix inequality (LMI)-based method and a two-degree-of-freedom (2DOF) derivative control strategy were proposed, applied to the d-q axis of RSC's inner voltage loop, enhancing SSCCI damping and fault ride-through (FRT)

capability, as shown in Fig. 2.12[138]. Further improvements involve integrating LLC and a low-pass filter (LPF) to suppress high-frequency noise[139].

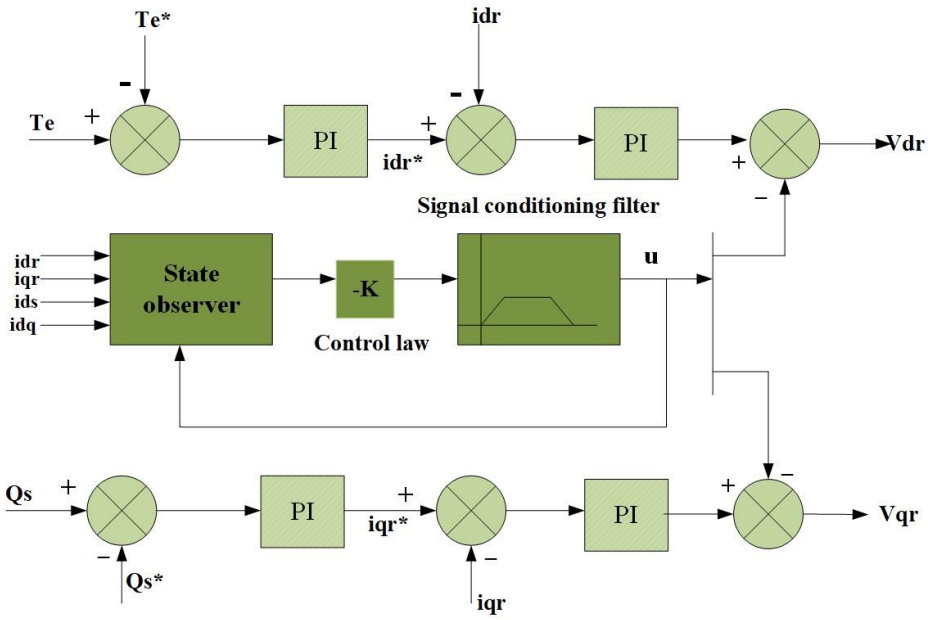

Fig 2.11 The supplementary SSI damping Observer-based state-feedback controller

PFL-based nonlinear feedback controllers have been developed to replace the RSC current controller[103], [135]. An H-infinity-based robust nonlinear current controller was also proposed, outperforming traditional PI controllers across various compensation levels and wind speeds [140]. Another approach integrates filters into the RSC control loop to mitigate SSCCI[141]. Two filtering methods exist: (i) Bandpass filtering of the input control signal (ICS) to isolate sub-synchronous components. A combination of LLC and bandpass filter (BPF) with PSO-optimized gain ratio is applied, using speed deviation as ICS, with output fed to both d-q axes of the RSC, as shown in Fig. 2.13[142]. This method, however, struggles in time-varying systems. (ii) Notch filtering adds a band-stop filter at the RSC's d-q axis control loop using a feedforward approach to block sub-synchronous frequencies. Placement and design are detailed in Fig. 2.14[143]. While simple and cost-effective, tuning is needed for specific frequencies.

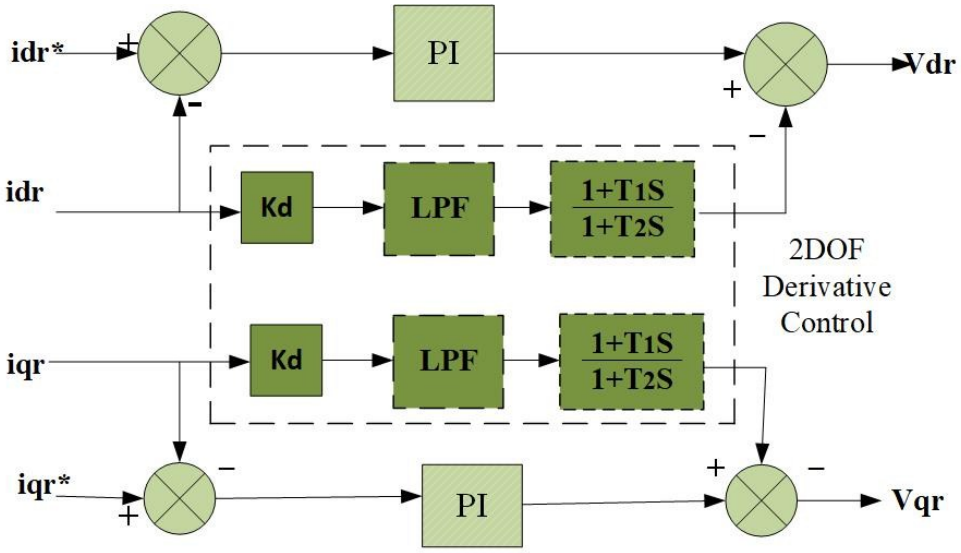

Fig 2.12 2DOF added current control loop of RSC

An SDC is also implemented on the RSC-side active power control loop, using turbine-generator speed as ICS. In a real-world Argentinian power system with series-compensated transmission lines, SDC was added at the d-axis rotor voltage loop, using the wind farm's active power as feedback to suppress SSCCI[144].

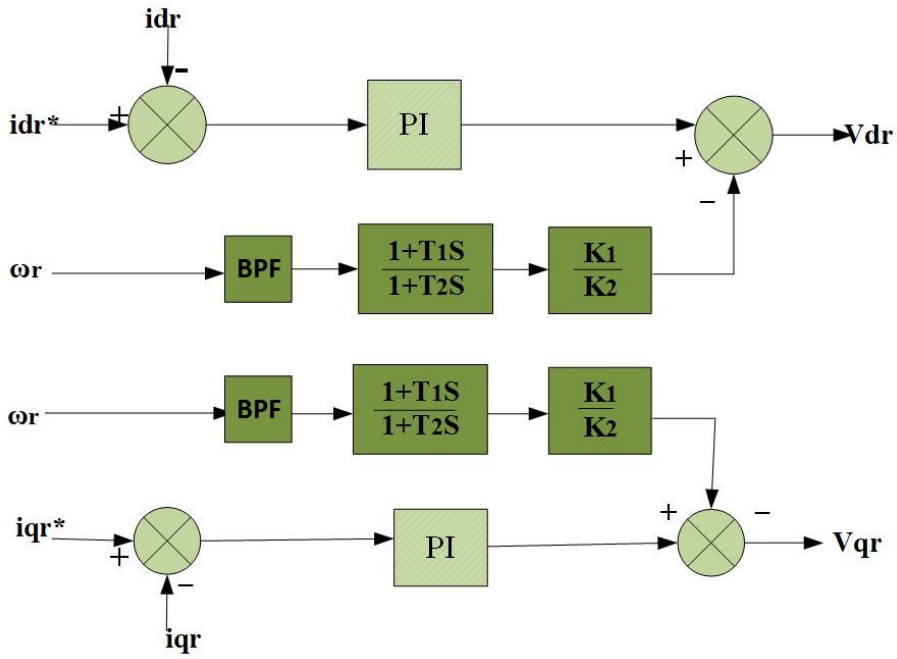

Fig 2.13 Feedback filtering (LLC and BPF)

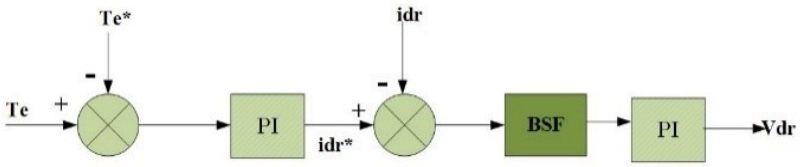

Fig 2.14 Feedforward filtering (BSF)

2.5.15 SDC at both RSC and GSC

Implementing supplementary damping controllers in both RSC and GSC enhances control capability and system stability. In [145], the conventional PI controllers were replaced with exact feedback linearization controllers, which transform the nonlinear system into a linear one, ensuring stability across a wide range of sub-synchronous frequencies—unlike PI controllers, which lack guaranteed stability. Later, a state-feedback linearization controller was proposed to replace PI controllers in both RSC and GSC[135]. However, these methods face challenges such as complex implementation and potential converter saturation issues.

2.5.16 Battery energy storage system based damping controller

BESS not only enables optimal renewable energy storage but also ensures smooth PV output, load shedding, and power balancing[146]. A typical BESS includes a step-up transformer, passive filter, DC/AC converter, and battery bank. Due to its low cost and flexible installation, BESS is gaining popularity. However, research on BESS-based controllers for SSR damping remains limited. Tsang et al. proposed BESS solutions for inter-area oscillation attenuation[147], while Y. Zhu et al. optimized BESS placement for damping purposes[148]. J. Khazaei et al. showed BESS effectiveness in mitigating SSR during heavy load variations[149]. A study by[150] used STATCOM with BESS to enhance grid stiffness in weak wind farm connections. M. F. Ahmed et al. proposed a fuzzy-based BESS to reduce torsional oscillations in steam turbine shafts[151]. In wind power plants, M. Beza et al. developed an adaptive damping controller using a BESS-coupled bidirectional converter to regulate active/reactive power via the GSC[152]. However, this method is flexible for integration into existing systems, with low maintenance costs and additional active and reactive power support.

Table 2.3 Summarization of Solutions Techniques and challenges for SSI Mitigation

Proposed classification	Mitigation Techniques	Advantages	Challenges	Applicable for	
				Generation side	Network side
SSR	Reduce the degree of series compensation [22],[79]	• Not required any expensive damping methods	• Only appropriate for the designing stage. • The risk of SSCCI maybe rise.		✓
SSR	Improve grid strength [80],[89],[99]	• Not required expensive damping methods	• Only appropriate for the designing stage. • The risk of SSCCI may be a rise.		✓
SSCCI	Installing heterogeneous wind power plant[16],[81],[82]	• Wind plant more stable Invulnerable to SSCCI	• Complications in modeling and studies cannot be accumulated to signify the entire wind farm. • Risk of SSCCI.	✓	
SSR	Bypassing series capacitor[30]	• Inexpensive efficiently executed to practical system	• It can itself cause the Sub-synchronous phenomenon • Loss of power		✓
SSCCI	(on/off) switching of WPP[18],[74]	• Total protection	• Require advance equipment for detection. • Loss of power	✓	
SSR	Damping control by FACTS devices[55],[56][84-86]	• Flexible and robust for a wide range of operation • Effectively mitigate SSI	• Expensive • VSC based FACTS devices can also trigger SSCCI event		✓

Proposed classification	Mitigation Techniques	Advantages	Challenges	Applicable for	
				Generation side	Network side
SSTCI	Damping controls via HVDC[89-91]	• Easily added SSDC to HVDC	• VSC based HVDC can trigger SSCCI event		✓
SSTCI	Industrial Sub-harmonic Relay	• Detect the time varying oscillations	• Source of Error • Expensive		✓
SSR	Shunt-VSC[92][98]	• Inexpensive efficiently executed to practical system	• Only devoted for SSI damping, not perform other tasks		✓
SSCCI	Regulating control parameters of WTC[79][83][94], [95]	• Not required any expensive equipment	• The control parameters of the WTC are not easily accessible. • Various manufacturers may have different WTC controls. • Individually adjusting each WG of a wind farm is impractical and uneconomical.		✓
SSCCI	Virtual synchronous generator control[94],[95]	• Stabilize Sub-synchronous oscillation along with providing inertia	• Expensive • Technology is not mature	✓	
SSR	PV Solar based damping[96-98]	• Controllability of both active and reactive power	• Expensive • An SSCI event can be participated by VSC-based converters.		✓

Proposed classification	Mitigation Techniques	Advantages	Challenges	Applicable for	
				Generation side	Network side
SSCCI	SDC with GSC[20][82][99-107]	• Assemble in converter controller. • Inexpensive solution • Reactive power control capability can be utilized for damping. • Effective SSI mitigation	• Low rated • Control capability is less for damping SSI. • It required greater damping control. • At low wind speed and a high degree of compensation, • voltage control capability would be restricted • Require cautious tuning parameter	✓	
SSCCI	SDC with RSC[106-117]	• Assemble in converter controller. • High rating as compared to GSC controller; Control capability is more than the GSC. • Active and reactive power are directly control. • Effective mitigation at high compensation • It required lesser effort for damping control.	• It might be destabilized in another mode. • Require extra work and care for tuning. • It can destabilize the Sub-synchronous mode due to the high gain of the RSC controller. • Due to increased current control, gain reduces aggregate equivalent resistance. • It deteriorates the control bandwidth of DFIG and does not meet the FRT requirement.	✓	

Proposed classification	Mitigation Techniques	Advantages	Challenges	Applicable for	
				Generation side	Network side
		• The controllability index is high for rotor voltage control during SSI. • RSC controller directly affects the rotor resistances.			
SSCCI	SDC at both RSC and GSC[106][118]	• Improve FRT capability along with other parameters. • Increases control capability	• Complex approaches • Saturation of converter	✓	
	BESS damping controller	• Provides both active and reactive power support for damping SSI. • Fast dynamic response enhances transient stability and inertia support. • Modular, flexible, and easily integrated into existing converter control schemes. • Effective under varying wind speeds and compensation levels. • Low maintenance and supports grid recovery during faults.	• Requires optimal sizing and placement for effective damping. • Cost of large-scale battery systems remains high. • Controller coordination with DFIG and grid converters is complex. • Aging and state-of-charge (SOC) management affect performance.	✓	✓

2.6 Future trends, Challenges and Recommendations

With the increasing shift toward renewable energy, power electronic devices are now integral to power generation and utilization. However, several recent power failures in the U.S. and China have been linked to SSI in renewable power systems, drawing significant attention from researchers. This review highlights various SSI phenomena and mitigation strategies, though practical implementation still faces challenges:

1. **Limited model access**: Due to commercial privacy and lack of standardization, turbo-generator models are often inaccessible or unvalidated, hindering early SSI analysis in system planning.
2. **Oversimplified models**: Aggregated models typically assume identical turbines connected to a single bus, whereas real-world systems involve diverse wind farms with different generators and controllers—affecting the accuracy of mitigation strategies.
3. **Lack of practical solutions**: Many proposed SSI damping methods are theoretical, with limited focus on real-world deployment. A fast and easily implementable control strategy is urgently needed.
4. **Time-varying frequencies**: SSI frequencies change over time, making real-time tracking of sub-, super-, and synchronous components complex, yet essential for effective mitigation.

In this regard as per the authors' best knowledge, a few publications on battery energy storage system have been published. BESS have shown promise for SSI damping due to their fast response, scalability, and ability to provide active/reactive power support. Additional advantages include modularity, low maintenance, ease of integration, grid support during faults, and enhancement of system inertia making BESS a robust and flexible tool for mitigating SSI in modern power systems.

2.7 Conclusion

This chapter has presented a detailed classification of SSI and reviewed a broad range of mitigation strategies implemented in wind power systems. A new categorization

based on the dominant source of oscillation—Torsional Interaction, SSR, SSCCI, and SSTCI—has been proposed to enhance the understanding of evolving SSI phenomena in modern grids with high renewable penetration.

Various control approaches, including active damping methods, parameter tuning techniques, and converter-based solutions, have been analysed with their respective benefits and implementation challenges. Given the growing complexity and scale of wind power integration, the requirement for robust, economical, and scalable damping systems is evident. Among the explored methods, BESS have emerged as a highly promising solution for mitigating SSI due to their fast dynamic response, bidirectional power control, and capability to support both active and reactive power. Furthermore, BESS offers modularity, ease of integration into existing systems, low maintenance costs, and enhanced grid support during disturbances, making it a strategic component in future SSI damping solutions.

CHAPTER 3

SUB-SYNCHRONOUS INTERACTION IN WIND POWER SYSTEMS: MODELING AND ANALYSIS

3.1 Introduction

The integration of large-scale wind power into modern power systems introduces new dynamic challenges, particularly related to sub-synchronous interaction. SSI refers to the adverse interaction between the electrical network and mechanical components of generation systems at frequencies below the system's fundamental frequency. In wind power systems, especially in DFIGs interconnected SCTLs, this phenomenon can lead to SSR, potentially compromising system stability. As wind penetration increases globally, understanding and mitigating SSI is essential to ensure reliable and secure grid operation. This chapter focuses on the modeling and analysis of SSI in DFIG-based WPP. It develops a simplified dynamic model to study the interaction mechanisms, identifies key influencing factors, and provides insight into system behaviour under various fixed series compensation and operating conditions.

Several previous research works discuss detailed mathematical modeling of a DFIG-based WPS[126], [153]–[157] However, the RSC, GSC dynamics have not been considered for the modeling and system analysis. The RSC and GSC have been considered to be a constant voltage source model[100], [154], [158] and a constant DC connection voltage amongst the RSC and the GSC. The RSC, as well as GSC must be simulated and included in the system modelling for internal dynamic analysis as they can introduce significant impact in the overall system dynamics. The dynamics of DFIG, RSC and GSC can be included in the stability analysis to improve its accuracy.

3.2 System modeling

Instead of a synchronous generator combined with a series compensated transmission lines, the IEEE first benchmark model has been updated to investigate the SSI phenomena in DFIG based wind energy conversion systems, as illustrated in

Fig.3.1[154], [159]. A 161kV SCLT connects an infinite bus to a 100MW DFIG based WPP in this study. The DFIG has a 575 V rated voltage and a 60 Hz frequency. The 67 wind turbines that make up the 100-megawatt wind farm each having a 1.5MW capacity. In the Appendix, parameters for both the aggregated model and the single model are given. The examined system depicted in Fig.3.1 must be constructed using state-space equations, as will be discussed below, in order to investigate the effect of the SSI phenomenon on system stability.

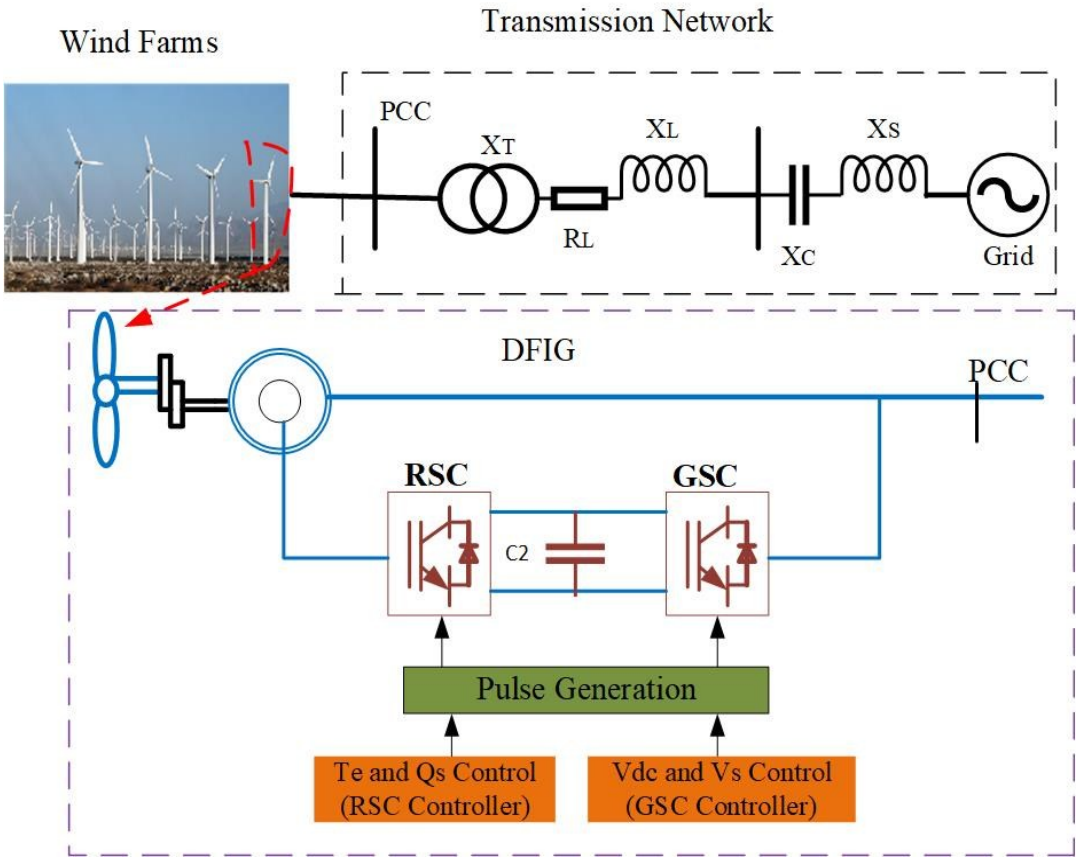

Fig 3.1 IEEE first benchmark model of DFIG-based WPP

3.2.1 Modeling of wind turbine

A wind turbine's mechanical output torque is proportional to the wind speed and can be expressed as[160]:

$$T_m = \frac{\rho R A C_p V_{wi}^2}{2\lambda} \tag{3.1}$$

C_p denotes the blade power coefficients, which is determined by the blade pitch angle 'θ' and tip speed ratio as fallow:

$$C_p = 0.5\left(\frac{RC_f}{\lambda} - 0.022 * \theta - 2.0\right)e^{-0.255\left(\frac{RC_f}{\lambda}\right)} \tag{3.2}$$

The tip speed ratio is expressed as:

$$\lambda = \frac{\Omega_m R}{V_{wi}} \tag{3.3}$$

Fig.3.2 depicts the link between wind speed, mechanical power and rotor speed, all these values in per unit system, for a 1.5MW wind turbine when the pitch angle 'θ' is zero with 200ft rotor radius is assumed.

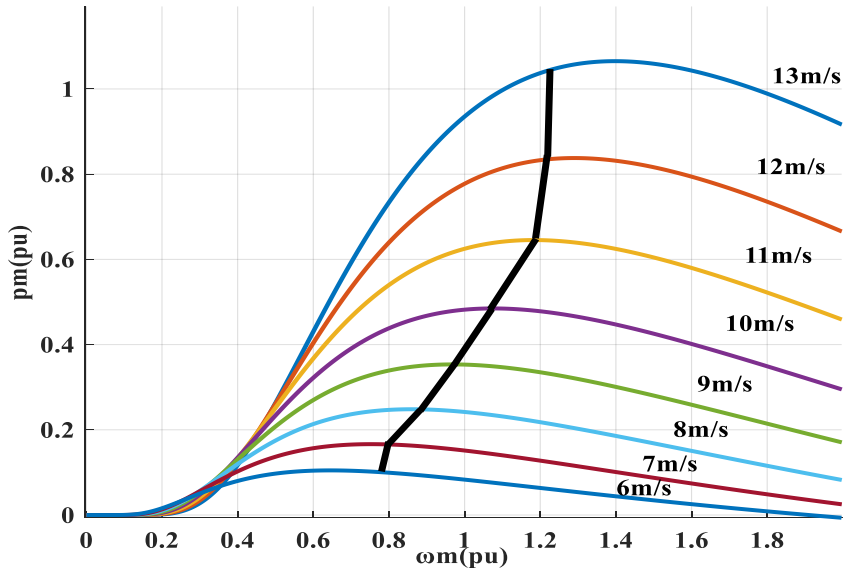

Fig 3.2 Relationship between wind power wind speed and rotor speed

We can develop a lookup table as shown in Table 3.1 that lists the various wind speeds and the rotor speed, maximum mechanical power, and shaft torque. It should be emphasized that in the small-signal analysis technique, Table 3.1 depicts the wind turbine model. This Table, by means of including a torque control loop, can obtain the desired optimum rotor speed.

Table 3.1 Mechanical Power, Torque, Rotor Speed (Pu), and Wind Speed

Wind speed (V_{wi})	**7m/s**	**8m/s**	**9m/s**	**10m/s**	**11m/s**	**12m/s**
ω_m	0.8	0.88	0.97	1.06	1.18	1.2
P_m	0.18	0.28	0.39	0.47	0.64	0.84
T_m	0.22	0.32	0.4	0.46	0.54	0.7

3.2.2 Modeling of Shaft System

In power system analysis, the two-mass system frequently represents torsional dynamics. The first mass is represented by wind turbine shaft, which has a low speed, and a DFIG high-speed shaft system represents the second mass system; and a state-space representation of a two-mass system is as follows[160], [161]:

$$\frac{d}{dt}\begin{pmatrix}\omega_t\\ \omega_r\\ T_g\end{pmatrix}=\begin{pmatrix}\frac{-D_t-D_{tg}}{2H_t} & \frac{D_{tg}}{2H_t} & \frac{-1}{2H_t}\\ \frac{D_{tg}}{2H_g} & \frac{-D_g-D_{tg}}{2H_g} & \frac{-1}{2H_g}\\ K_{tg}\omega_g & -K_{tg}\omega_e & 0\end{pmatrix}\begin{pmatrix}\omega_t\\ \omega_r\\ T_g\end{pmatrix}+\begin{pmatrix}\frac{T_m}{2H_t}\\ \frac{-T_e}{2H_t}\\ 0\end{pmatrix} \tag{3.4}$$

ω_t, ω_r and T_g are the state variables. T_m and T_e are the input side of the shaft system model. The constant of a two-mass model system is D_t, H_t, H_g, D_{tg} and K_{tg}. The optimal wind turbine torque T_m is obtained from Table 3.1 at any required wind speed, whereas T_e it could be written as air gap flux leakage and currents of the DFIG is express:

$$T_e = \psi_{qM} i_{dr} - \psi_{dM} i_{qr} \tag{3.5}$$

The air gap flux linkage is obtained as follows:

$$\psi_{qM} = X_M \left(i_{qs} + i_{qr}\right) \tag{3.6}$$

$$\psi_{dM} = X_M \left(i_{ds} + i_{dr}\right) \tag{3.7}$$

3.2.3 Modeling of DFIG

The modeling of DFIG with RSC, a dynamic model of the sixth order is used. The model is characterized as[21]**:**

$$\dot{X} = A_D X_D + B_D U_D \tag{3.8}$$

where the state variables are denoted by X_D , and U_D denotes the inputs of DFIG, B_D denotes the constants of electrical parameter, and A_D Represents the constants of state variables.

$$X_D = \left[i_{qs}; i_{ds}; i_{0s}; i_{qr}; i_{dr}; i_{or} \right] \tag{3.9}$$

$$U_D = \left[v_{qs}; v_{ds}; v_{0s}; v_{qr}; v_{dr}; v_{or} \right] \tag{3.10}$$

The parameters i_{0s}, i_{0r}, v_{0s} and v_{0r} are equal to zero because the system is balanced.

A_D and B_D is expressed as:

$$A_D = -B_D \begin{pmatrix} R_S & \frac{\omega_S}{\omega_b} X_S & 0 & 0 & \frac{\omega_S}{\omega_b} X_M & 0 \\ -\frac{\omega_S}{\omega_b} X_S & R_S & 0 & -\frac{\omega_S}{\omega_b} X_M & 0 & 0 \\ 0 & 0 & R_S & 0 & 0 & 0 \\ 0 & \frac{\omega_S - \omega_r}{\omega_b} X_M & 0 & R_r & \frac{\omega_S - \omega_r}{\omega_b} X_r & 0 \\ -\frac{\omega_S - \omega_r}{\omega_b} X_M & 0 & 0 & -\frac{\omega_S - \omega_r}{\omega_b} X_r & R_r & 0 \\ 0 & 0 & 0 & 0 & 0 & R_r \end{pmatrix}$$

$$B_D = -\omega_b \begin{pmatrix} X_S & 0 & 0 & X_M & 0 & 0 \\ 0 & X_S & 0 & 0 & X_M & 0 \\ 0 & 0 & X_{lS} & 0 & 0 & 0 \\ X_M & 0 & 0 & X_r & 0 & 0 \\ 0 & X_M & 0 & 0 & X_r & 0 \\ 0 & 0 & 0 & 0 & 0 & X_{lr} \end{pmatrix}^{-1} \tag{3.11}$$

Except for ω_b, ω_r and ω_s, which are in rad/sec, all parameters and variables are in per-unit.

3.2.4 Modeling of DC link

A first-order model describes the dynamics of the capacitor in the DC link between the GSC and the RSC[21].

$$C_{dc}V_{dc}\frac{dV_{dc}}{dt} = P_R - P_G \tag{3.12}$$

$$\mathrm{P}_R = \frac{1}{2}\left(v_{qr}i_{qr} + v_{dr}i_{dr}\right) \tag{3.13}$$

$$\mathrm{P}_G = \frac{1}{2}\left(v_{qg}i_{qg} + v_{dg}i_{dg}\right) \tag{3.14}$$

V_{dc} is the actual value whereas, $v_{qr}, i_{qr}, v_{dr}, i_{dr}, v_{qg}, i_{qg}, v_{dg}, i_{dg}$ are in per-unit system.

3.2.5 Series Compensated Transmission line modeling

Generally, the dynamics of the series compensated model are ignored, but for the SSR analysis it is essential. The transmission line can be electrically depicted as lumped series RLC circuit and adopts the synchronous reference frame to modeling the series compensated transmission line. Per phase dynamics equations is expressed as[63]:

$$R_l.i_l + L\frac{di_l}{dt} + v_c = v_s - V_B \tag{3.15}$$

$$C\frac{dv_c}{dt} = i_l \tag{3.16}$$

The series compensated transmission's line state-space representation is expressed as:

$$\frac{d}{dt}\begin{pmatrix} i_{ql} \\ i_{dl} \\ v_{cq} \\ v_{cd} \end{pmatrix} = \begin{pmatrix} -\frac{R_l}{X_l} & -\omega_e & -\frac{1}{X_l} & 0 \\ -\omega_e & -\frac{R_l}{X_l} & 0 & -\frac{1}{X_l} \\ X_c & 0 & 0 & -\omega_e \\ 0 & X_c & \omega_e & 0 \end{pmatrix}\begin{pmatrix} i_{ql} \\ i_{dl} \\ v_{cq} \\ v_{cd} \end{pmatrix} + \omega_b \begin{pmatrix} \frac{v_{qs} - V_{Bq}}{X_l} \\ \frac{v_{ds} - V_{Bd}}{X_l} \\ 0 \\ 0 \end{pmatrix} \tag{3.17}$$

The synchronous reference speed and the base speed both are1pu or 377rad/s.

3.2.6 Modeling of DFIG converter

This study aims to look at both RSC and GSC converter controllers. In previous research, RSC and GSC converter controllers are considered constant voltage sources[21], [63], [100], while the dynamics of RSC and GSC may cause an enormous variation in a system model. The system model cannot be used to analyse the internal dynamics of the system if RSC and GSC are not taken into account. The following state space equations governing the dynamics of the RSC-GSC converter.

$$\frac{d}{dt}\begin{pmatrix} i_{dr} \\ i_{qr} \\ i_{dg} \\ i_{qg} \end{pmatrix} = \begin{pmatrix} -\frac{R_{RSC}}{L_{RSC}} & \omega_s & 0 & 0 \\ -\omega_s & -\frac{R_{RSC}}{L_{RSC}} & 0 & 0 \\ 0 & 0 & \frac{R_{RSC}}{L_{GSC}} & -\left(\omega_s - X_{tg}\right) \\ 0 & 0 & -\left(\omega_s + X_{tg}\right) & \frac{R_{GSC}}{L_{GSC}} \end{pmatrix} \begin{pmatrix} i_{dr} \\ i_{qr} \\ i_{dg} \\ i_{qg} \end{pmatrix}$$

$$+ \begin{pmatrix} \frac{1}{L_{RSC}} & 0 & 0 & 0 \\ 0 & \frac{1}{L_{RSC}} & 0 & 0 \\ 0 & 0 & \frac{1}{L_{GSC}} & 0 \\ 0 & 0 & 0 & \frac{1}{L_{GSC}} \end{pmatrix} \begin{pmatrix} v_{dr} \\ v_{qr} \\ v_{dg} \\ v_{qg} \end{pmatrix} \tag{3.18}$$

Vector-controlled techniques is adopted in this study[161]. The control loop is shown in Fig.3.3. For the RSC controller, Table 3.1 is used for the obtain the optimal reference torque. The value remains constant when the wind speed surpasses the rated speed. The reference torque is the torque that delivers the maximum rotational speed at the measured rotational speed when the wind speed is less than the rated speed. Using this lookup table, the wind turbine can extract the maximum amount of wind energy feasible.

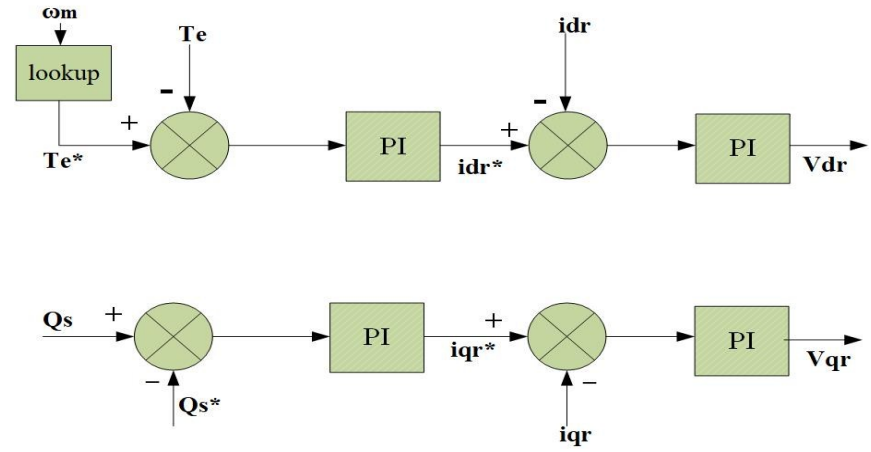

(a)

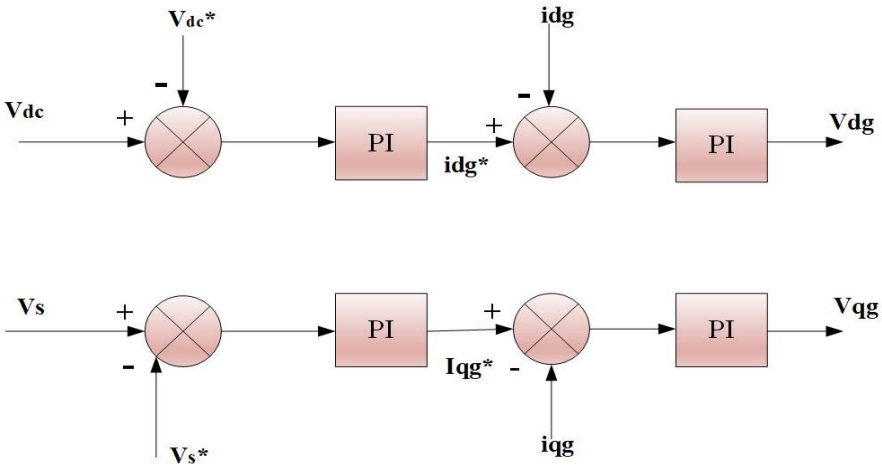

(b)

Fig 3.3 (a) RSC, (b) GSC control loop of DFIG

3.2.7 Integrated system modeling

To understand the complete system, it is useful to think of it as an integration of the various subsystems. Equation expresses the entire system model[63].

$$\left(\dot{X}\right)=\left(A_{sys}\right)\left(X_{sys}\right)+\left(B_{sys}\right)\left(U_{sys}\right) \tag{3.19}$$

Where $\left(X_{sys}\right)=\left(X_{shaft} \quad X_{DFIG} \quad X_{tl} \quad X_{dc}\right)$ (3.20)

The system matrix of the entire system is given by

$$\left(A_{sys}\right)=\begin{pmatrix} A_{shaft} & 0 & 0 & 0 \\ 0 & A_{DFIG} & 0 & 0 \\ 0 & 0 & X_{tl} & 0 \\ 0 & 0 & 0 & A_{dc} \end{pmatrix} \tag{3.21}$$

These interconnected subsystems are able to communicate with each other via state and control variables in the individual subsystems. Algebraic Equations of v_{ds}, v_{qs}, i_{ds} and i_{qs} are used to link the controllers. Now v_{ds}, v_{qs}, i_{ds} and i_{qs} expressed as:

$$v_{ds} = v_{dg} + X_{tg} i_{qg} \tag{3.22}$$

$$v_{qs} = v_{qg} + X_{tg} i_{dg} \tag{3.23}$$

$$i_{ds} = i_{dg} - i_{dl} \tag{3.24}$$

$$i_{qs} = i_{qg} - i_{ql} \tag{3.25}$$

Developed torque and stator reactive power is given by:

$$T_g = X_m \left(i_{dr} i_{qs} - i_{ds} i_{qr}\right) \tag{3.26}$$

$$Q_s = \frac{1}{2}\left(v_{qs} i_{ds} - v_{ds} i_{qs}\right) \tag{3.27}$$

A state-space model is used to investigate the system's small signal stability, which leads to time-domain simulation analysis and eigenvalue computation.

3.3 Small Signal Stability Analysis

To analysis the effect of the SSI on system stability eigen value analysis has been done. A simulation-based time domain analysis has also been done to validate the findings of the eigen value analysis.

3.3.1 Eigen value analysis

The eigen value approach is one of the most critical approaches for studying a dynamic system's small-signal stability. Based on the order of the system matrix, this analysis generates a collection of eigen values. The eigen values can be used to determine a

system's stability; if the real component of an eigen value is positive, the system is unstable; if the real part is negative, the system is stable. The frequency of oscillations is represented by the imaginary portion. The size of the system matrix (A_{sys}) is determined in Section 3.2, which is the 22x22 size of the matrix, resulting in 22 eigen values. In eigen value analysis, chosen two case to investigate (i) Different compensation level of a transmission line and (ii) Different wind speed.

3.3.2 Different compensation level

In order to identify the effect of different compensation level to the sub-synchronous frequency at which system is to be unstable. Table 3.2 displays the set of eigen values from (λ_1-λ_{22}) for fixed wind speeds at 7m/s and at a constant capacitive compensation level of 50%.

Table 3.2 Eigen Value Analysis of the complete system Model With 50% Compensation and a Wind Speed of 7 M/S

Mode	Eigenvalue	Frequency (Hz)	Description
$\lambda_{1,2}$	-1790±j889	141	Very high freq.
$\lambda_{3,4}$	-19.2±j568.2	90.4	Sup-sync
$\lambda_{5,6}$	**1.6±j187.8**	**29.9**	**SSR**
$\lambda_{7,8}$	-52.4±j7.9	1.25	Electromechanical
$\lambda_{9,10}$	-0.63±j18.8	2.86	Electromechanical
$\lambda_{11,12}$	-6.41±j8.6	1.36	Electromechanical
$\lambda_{20,21}$	-0.0±j0.0	0	PI Controller
λ_{13}	-5.9	0	No oscillatory
λ_{14}	-7.4	0	No oscillatory
λ_{15}	-5.8	0	No oscillatory
λ_{16}	-5.6	0	No oscillatory
λ_{17}	-1.9	0	No oscillatory
λ_{18}	-48.2	0	No oscillatory
λ_{19}	-37.7	0	No oscillatory
λ_{22}	-0.0	0	No oscillatory

At resultant the eigen values (λ_5) and (λ_6) has found unstable at these operating circumstances, and at this condition the system becomes increasingly unstable. The oscillating frequency at which the system is unstable at the sub-synchronous frequency which is responsible for the SSR. The remaining computed eigen values operate in a variety of ways. Electromechanical modes with eigen values of (λ_7 -λ_{12}) are reported to be responsible for electromechanical system dynamics. (λ_1, λ_2) and (λ_3, λ_4) belongs to the extremely high frequency and super synchronous modes, respectively, because the frequency of these dynamics is higher than the system's, they are always stable. The (λ_{13}-λ_{22}) do not have any frequency terms and are classified as oscillatory as positive modes or non-oscillatory as a negative mode, with amplitudes which are variable as a function of compensation levels as well as wind speeds.

Table 3.3 Eigen value analysis of mode 3($\lambda_{5,6}$) at varying series compensation

%Compensation	**Mode3 ($\lambda_{5,6}$)**		**Remarks**
	Eigen value	**Frequency (Hz)**	
10	-4.7±j291.2	46.36	Stable
20	−3.02±j256	40.76	Stable
30	-1.5±j229	36.46	Stable
40	**0.01±j207**	32.96	Unstable
50	**1.6±j187.8**	29.90	Unstable
60	**3.16±j170**	27.07	Unstable
70	**4.8±j155.8**	24.80	Unstable
80	**6.4±j142.3**	22.65	Unstable

From above result we observed that mode (λ_5, λ_6) is only unstable. Therefore, it is necessitating to check this mode at different level of series compensation and to observe the pattern. From Table 3.3 observed that at 30% of series compensation and below to 30% of series compensation the system becomes stable and the real part of eigen value of (λ_5, λ_6) decreases as compensation decreases and amplitude of oscillating frequency increases accordingly. Above 30% of series compensation the system becomes tends to unstable mode due to decrement of positive damping coefficient. It is verified from eigen value analysis is that the 30% of series compensation would be the safe value of compensation for which the stability of the

system can be ensured without compromising its performance. A detailed eigen value analysis of the complete system model with 30% series compensation at a 7m/s wind speed is shown in Table 3.4 and observed that all the system modes are in stable condition.

Table 3.4 Eigen value analysis of the complete system model with 30% compensation and a wind speed of 7 m/s

Mode	Eigenvalue	Frequency (Hz)	Remark
$\lambda_{1,2}$	-1794±j887.5	141.3	Stable
$\lambda_{3,4}$	-16.1±j524.8	83.6	Stable
$\lambda_{5,6}$	-1.5±j229.2	36.5	Stable
$\lambda_{7,8}$	-49.1±j10.9	1.73	Stable
$\lambda_{9,10}$	-0.63±j18.8	2.99	Stable
$\lambda_{11,12}$	-4.56±j10.2	1.62	Stable
λ_{13}	-7.51	0	Stable
λ_{14}	-5.9	0	Stable
λ_{15}	-5.7	0	Stable
$\lambda_{16,17}$	-2.2±j0.4	0.06	Stable
$\lambda_{18,19}$	-0.01±j0.07	0.01	Stable
λ_{20}	-0.00	0	Stable
λ_{21}	-48.2	0	Stable
λ_{22}	-37.7	0	Stable

3.3.3 Different wind speed

In order to identify the effect of different wind speed to the sub-synchronous frequency at which system is to be unstable. Considering the typical wind speed of 7m/s, 9m/s and 11m/s and the fixed series compensation level of 30%, 40%, 50% and 60% as an example, as compensation increases, the real part of eigen value (λ_5, λ_6) grows in size, and the system becomes increasingly unstable, as seen in Table 3.5. However, as the wind speed increases the real part of mode (λ_5, λ_6) very slightly decreases. With this result, we can conclude that the wind speed has an insignificant impact on the SSI. The

system stability is observed too dependent on the percentage of compensation offered to the transmission line while fairly insensitive to change in wind speed.

Table 3.5 Eigen value analysis of mode 3($\lambda_{5,6}$) at varying wind speed and % of series compensation

Compensation (%)	**Wind Speed**	**Mode3 ($\lambda_{5,6}$)**		**Remark**
		Eigen value	**Frequency (Hz)**	
30	7m/s	-1.5±j229.23	36.50	Stable
	9m/s	-1.54±j229.20	36.49	Stable
	11m/s	-1.6±j229.11	36.48	Stable
40	7m/s	**0.01±j207**	32.96	Unstable
	9m/s	-0.04±j206.9	32.94	Marginally Stable
	11m/s	-0.12±j 206.8	32.92	Stable
50	7m/s	**1.6±j187.8**	29.90	Unstable
	9m/s	**1.5±j187.7**	29.88	Unstable
	11m/s	**1.4±j187.5**	29.85	Unstable
60	7m/s	**3.2±j170.9**	27.21	Unstable
	9m/s	**3.1±j170.73**	27.18	Unstable
	11m/s	**2.9±j170.4**	27.13	Unstable

3.4 Model Validation

3.4.1 Time-domain analysis

To verify the eigen value analysis results, MATLAB/Simulink has been employed for time-domain analysis. Based on the time- domain result depicted in Fig.3.4 and Fig.3.5 on increasing the series compensation level, the system loses its stability. At a constant wind speed of 7m/s, Fig.3.4 displays the electrical power (Pe) dynamic response at 30%, 40%, 50%, and 60% of series compensation values. It has been noticed that above 30% of series compensation, the dynamic response of the active power of the system becomes unstable. At 30% of series compensation, the response tends to stabilize. The second case shown in Fig.3.5 considers a specific wind speed at 9 m/s with the same various compensation values and obtained the result that after varying

the wind speed, there is a slight improvement in their damping. The positive damping decreases as the compensating level rises.

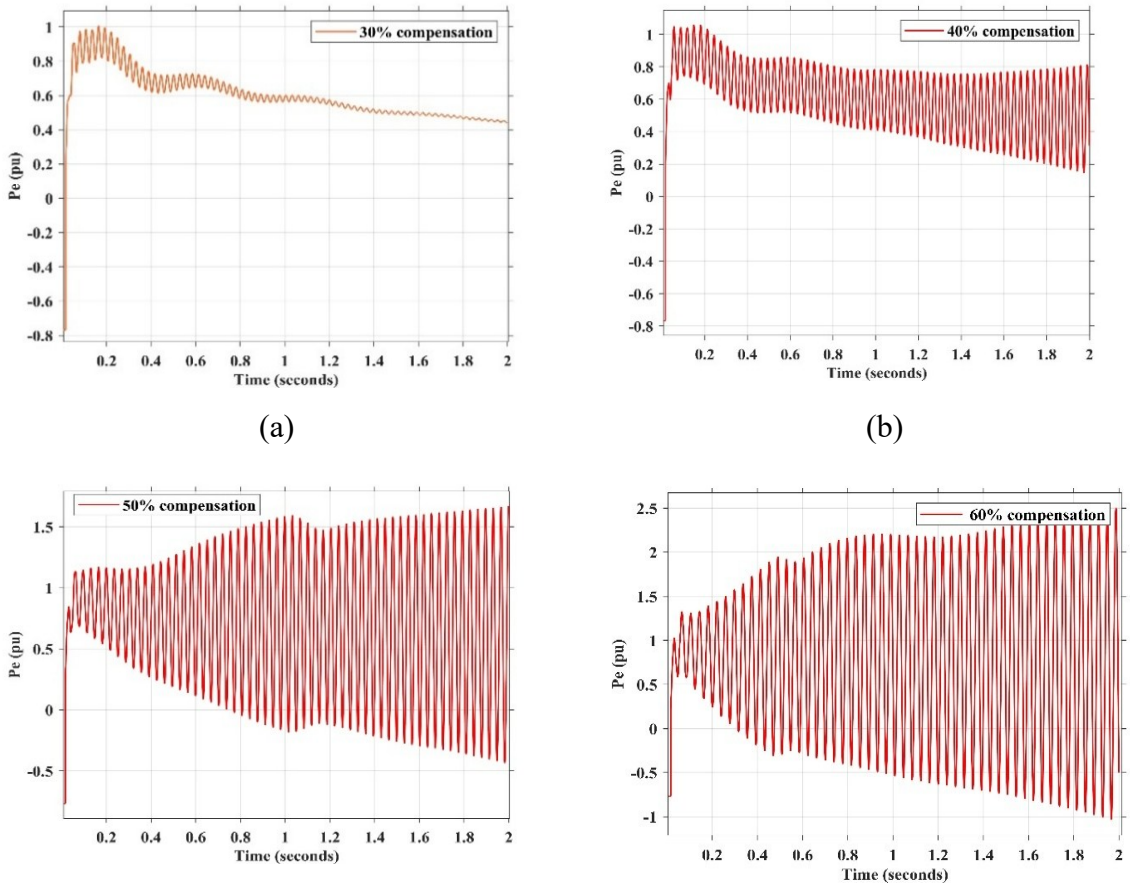

Fig 3.4 Electrical power dynamics response at (a) 30%, (b) 40%, (c) 50% and (d) 60% compensation at fixed wind speed 7m/s

The above result reveals that as the compensation level is raised, the SSR frequency rises while the damping decreases at resultant increased amplitude of oscillation. While on increasing wind speeds the sub-synchronous frequency and amplitude of oscillation decreases in to some extent manner. These data support the theory that the dominant mode becomes slightly unstable when wind speed decreases.

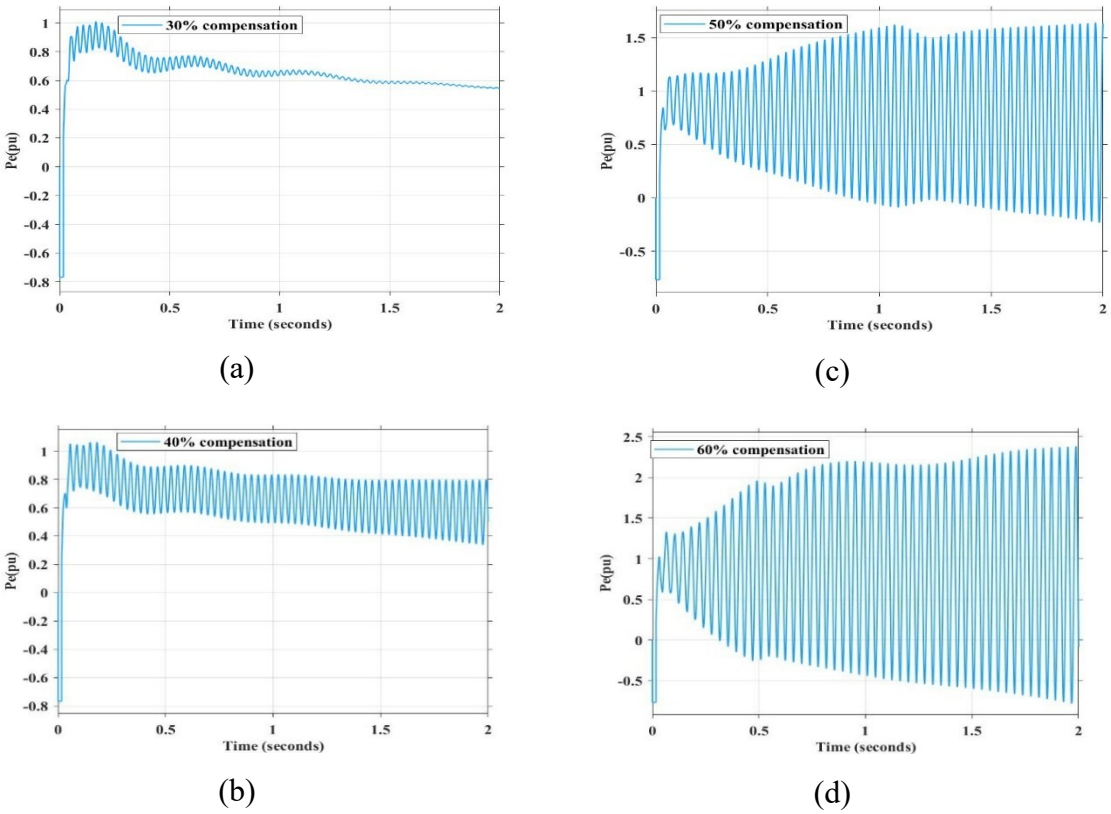

Fig 3.5 Electrical power dynamics response at (a) 30% (b) 40%, (c) 50% and (d) 60% compensation at fixed wind speed 9m/s

3.5 Conclusion

In this chapter, the phenomenon of SSI in WPS particularly DFIG-based WPS interconnected SCTL has been systematically analysed. A comprehensive dynamic state-space model was developed to represent the key components of the system, including the wind turbine, DFIG, converter control loops, and the series-compensated network. A detailed mathematical model of the 100MW grid-connected DFIG-based WPS based on the IEEE first benchmark model, as well as a dynamic model of the RSC and GSC converters, has been done. The numerous modes of oscillations present in the integrated system can be easily discovered using eigen value analysis. The stability of the various oscillating modes can be identified by analyzing the nature of eigen values. Accordingly, in this chapter, SSI analysis has been carried out using an eigen value technique for various wind speeds and series capacitance compensation levels and got different oscillation modes, i.e., SSR mode, Super-synchronous mode, electromechanical mode, and some non-dominant modes have been explored. The time

domain analysis based on the nonlinear simulation has been employed to validate the eigen value outcome. The following conclusion has been obtained:

- The real component magnitude of the eigen value increases as the fraction of series compensation is raised, and the system becomes increasingly unstable.
- The increase in wind speed velocity slightly decreases the amplitude of the real part of eigen value, resulting in a slightly better stable system.

This suggests that the series compensation plays a vital role in the system's stability due to sub-synchronous resonance instead of variation in the wind speed. Nonetheless, the 30% of series compensation could be the safe compensation value for which the system's stability can be ensured without compromising its performance.

CHAPTER 4

MITIGATION OF SSR IN DFIG-BASED WPPs USING BESS DAMPING CONTROLLERS

4.1 Introduction

Nowadays, battery energy storage systems have emerged as a highly promising technology for enhancing power system stability, especially in systems experiencing dynamic disturbances. Their ability to respond rapidly to fluctuations, coupled with their scalability and cost-effectiveness, makes them particularly suitable for damping oscillatory modes such as those caused by SSI. BESS can quickly inject or absorb both active and reactive power through power electronic converters, thereby suppressing oscillations and enhancing overall system performance. Unlike conventional damping methods such as power system stabilizers or FACTS devices, BESS offers operational flexibility and can be deployed more economically, especially in remote or renewable-rich zones. Despite these advantages, existing research falls short in thoroughly exploring the application of BESS-based damping controllers for SSR mitigation in DFIG-based WPSs. In particular, the small-signal stability of BESS-equipped systems under varying wind speeds and transmission line compensation levels remains under-addressed. Moreover, most existing control strategies rely on locally measured feedback signals, which may not adequately capture the global dynamics of a widely distributed power network.

To bridge this research gap, this chapter proposes a novel BESS-based Damping Control (BESDC) loop specifically designed to mitigate SSR in a DFIG-based WPP. A unique aspect of the proposed controller is its use of a supplementary damping signal derived from angular speed deviations measured through Wide Area Measurement Systems (WAMS). This approach provides enhanced observability and better control performance by utilizing real-time system-wide data.

The chapter also presents a comprehensive small-signal stability analysis of a modified IEEE First Benchmark Model (FBM) under various operating scenarios. The effectiveness of the proposed BESDC is validated under different wind speeds and series compensation levels, demonstrating its potential to improve damping of sub-synchronous modes and enhance the operational stability of wind-integrated power systems.

4.2 Study system

A modified IEEE FBM model-based study system has been used to analyze the SSI phenomena which has been discussed in chapter-3 in detailed . A 100-megawatt DFIG-based WPP transmits electrical power to the infinite bus system over a 161 kV fixed series compensated transmission line. The frequency of generated voltage is 60 Hz [25]. The 100-megawatt WPP is composed of 67 wind turbines, each of which has a 1.5-megawatt capacity. An analogous lumped machine represents the aggregate behavior of a set of wind turbines. Several recent studies[162], [163] back up this argument, claiming that wind farm aggregate is a good estimate for investigating system interconnectedness. This method has also been employed in system studies[39], [147], [154], [164], where "simulations of bulk system dynamics using a single machine equivalent are sufficient for most planning investigations". The Appendix contains the parameters for both the single and aggregated models.

4.3 Design of Battery Energy Storage System Damping Controller

A conventional BESS comprises a step-up coupling transformer, a passive inductive filter, DC/AC power converter, and a battery bank [165]. Following this utilizing the DC/AC power converter part of the BESS could alleviate the oscillations due to the SSI phenomenon by using a supplementary damping signal. Therefore, in our proposed system to deal with the SSI phenomenon particularly SSR, a 200kW battery energy storage system has been considered. It’s added to Bus-2 of the 161kV fixed SCTL, which is as directed in Fig.4.1 For designing the BESDC, a Supplementary Damping Signal (SDS) has been added to the active power controller block of the voltage source converter part of the BESS. SDS is triggered during transient conditions to dampen the oscillations. The WAMS and phasor measuring units (PMU) has

utilized in our proposed system to provide real-time information to the supplementary damping signal.

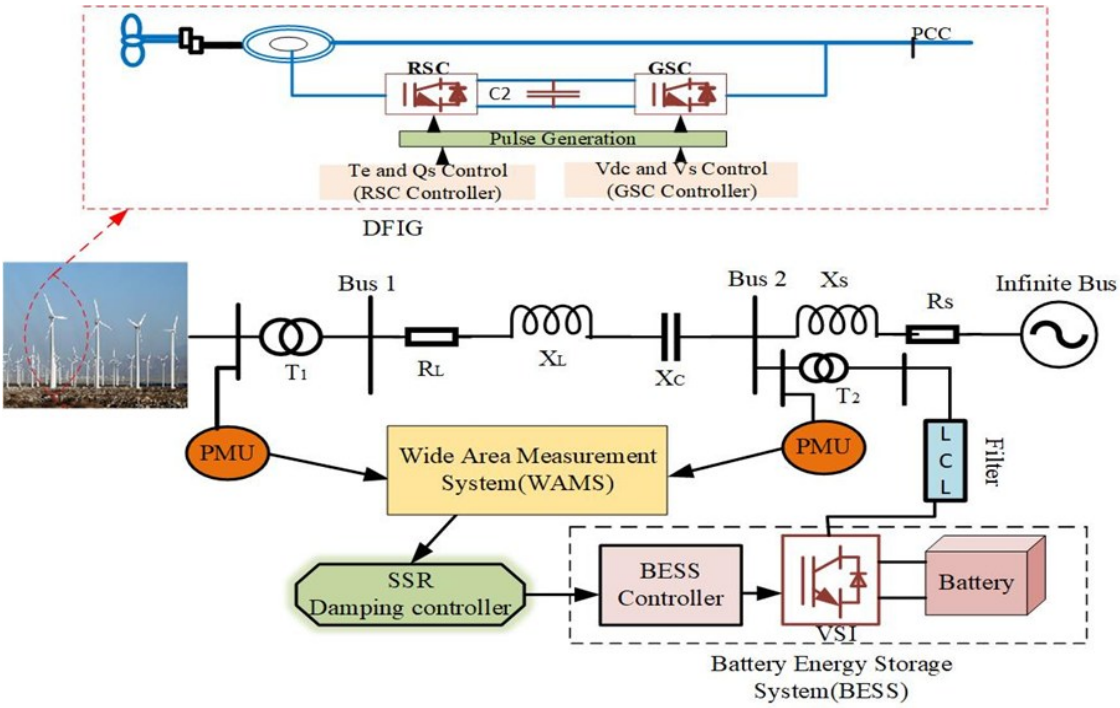

Fig 4.1 Proposed system model under study for the mitigation of SSR

4.3.1 Modeling of Battery

The electrical model parameters are then calculated using[166]. In the first step, a specific capacity for the battery is determined. This diagram depicts the electrical battery in detail, as shown in Fig.4.2 which was modeled in this paper[166].

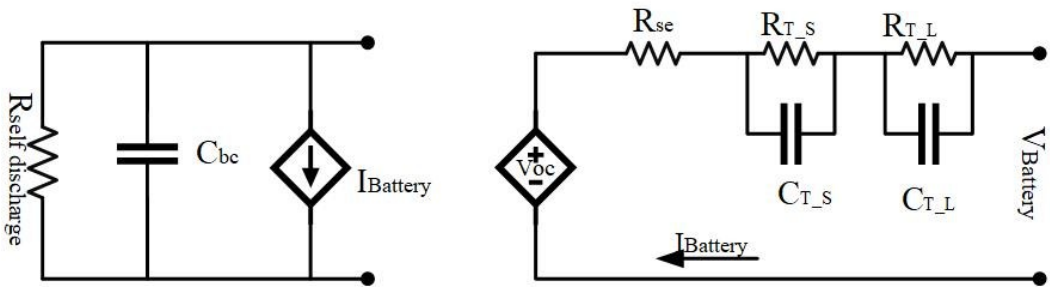

Fig 4.2 Electrical battery model [166]

A Li-ion battery is used as an energy storage system with a capacity of 200 kW has been developed. If each energy storage device's nominal power is 200 kW, the battery capacity can be computed as follows:

$$C_{bc} = Capacity\left(f_{1c}\right)\left(f_{2T}\right)3600 \tag{4.1}$$

Where C_{bc} the capacity of the battery when completely charged is, $Capacity$ is denoted by nominal capacity in Ahr, and the cycle number correction factor is denoted by f_{1c} while the temperature-dependent correction factor is f_{2T} The following parameters have been taken as given in [166]

$$V_{oc} = -1.030e^{-35Sbc} + 3.6 + 0.2Sbc - 0.1S_{bc}^{2} + 0.3S_{bc}^{3} \tag{4.2}$$

$$R_{se} = 0.15620e^{-24.37Sbc} + 0.0744 \tag{4.3}$$

$$R_{T_L} = 6.6030e^{-155.2Sbc} + 0.0498 \tag{4.4}$$

$$C_{T_L} = 6065.0e^{-27.12Sbc} + 4475.0 \tag{4.5}$$

$$R_{T_S} = 0.32080e^{-29.14Sbc} + 0.0466 \tag{4.6}$$

$$C_{T_S} = -752.90e^{-13.51Sbc} + 703.60 \tag{4.7}$$

Where V_{oc} is the battery voltage at open circuit condition, Sbc is the battery cell's state of charge, R_{se} is the resistor in series, and R_{T_S} is the short transient resistors and R_{T_L} is the long transient resistors. Short and long transient capacitors, respectively, are C_{T_S} and C_{T_L}. The generated battery energy is then sent to the grid via a three-phase inverter. As demonstrated in Fig.4.3, BESS employs constant power control and the PQ control technique. The BESS grid voltages are V_{sa}, V_{sb} and V_{sc}, and their dq axis components are V_{sd}, V_{sq}. The BESS controller output voltages are V_{Ba}, V_{Bb} and V_{Bc}, and their dq axis components are V_{Bd}, V_{Bq}. The BESS output currents are i_a, i_b and i_c, and their dq axis components are i_d, i_q. The inductance of the BESS grid line is Ls and ω represents the angular synchronous frequency. DC side capacitors, voltage, and current are referred to as C_{dcB}, V_{dcB} and i_{dcB}. The BESS output currents are i_a, i_b and i_c, and their dq axis components are i_d, i_q. The inductance of the BESS grid line is L_s. DC side capacitors, voltage, and current are referred to as C_{dcB}, V_{dcB} and i_{dcB}.

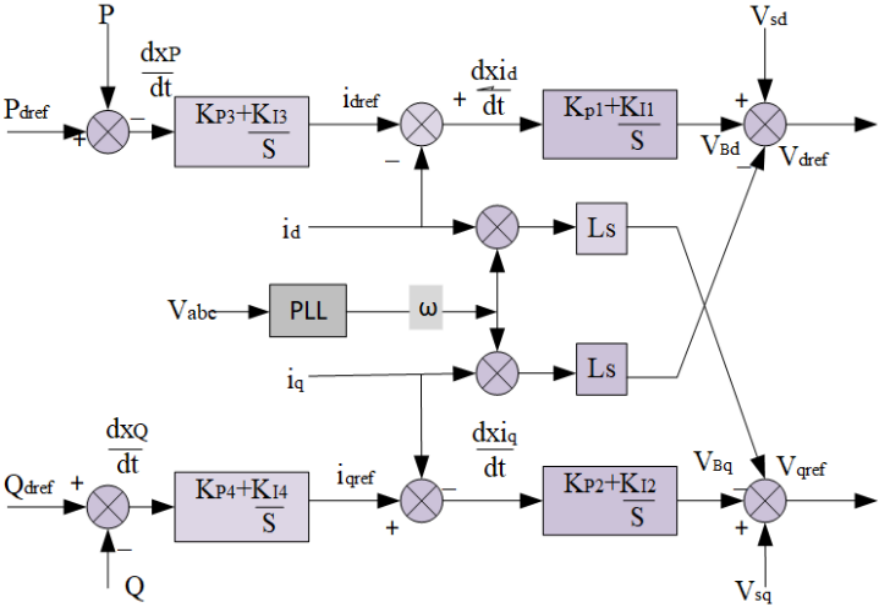

Fig 4.3 Traditional control strategy of BESS

Considering i_d, i_q, x_Q, x_{id}, x_P, x_{iq} and V_{abc} as the state variables, small-signal modes for BESS can be configured as follows [148], [151], [152], [167]:

Transmission lines state equations are:

$$\frac{di_d}{dt} = \frac{\omega}{L_s}\left(V_{dref} + L_s i_q\right) \tag{4.8}$$

$$\frac{di_q}{dt} = \frac{\omega}{L_s}\left(V_{qref} + L_s i_d\right) \tag{4.9}$$

Controller state equation

$$\frac{dx_p}{dt} = P_{dref} - \left(V_{Sq} i_d - V_{Sd} i_q\right) \tag{4.10}$$

$$\frac{dx_{id}}{dt} = K_p\left(P_{dref} - \left(V_{Sq} i_d - V_{Sd} i_q\right) + K_{I1}\left(x_p - i_d\right)\right) \tag{4.11}$$

$$\frac{dx_Q}{dt} = Q_{dref} - \left(V_{Sd} i_d - V_{Sq} i_q\right) \tag{4.12}$$

$$\frac{dx_{iq}}{dt} = K_{p4}\left(Q_{dref} - \left(V_{Sd} i_d - V_{Sq} i_q\right) + K_{I4}\left(x_Q - i_q\right)\right) \tag{4.13}$$

DC capacitor state equation

$$\frac{dV_{dcB}}{dt} = \frac{\omega}{C_{dcB}V_{dcB}}\left(V_{Bd}i_{Bd} + V_{Bq}i_{Bq}\right) \tag{4.14}$$

For the model analysis, the entire system models are represented by:

$$\dot{X} = f\left(X,U\right) \tag{4.15}$$

Whereas, $X = \left(X_{shaft} \quad X_{DFIG} \quad X_{tl} \quad X_{dc} \quad X_{BESS}\right)$ is assembled in MATLAB/Simulink to obtain the eigenvalue analysis.

4.3.2 Control System of BSDC

The configuration of Voltage Source Inverter (VSI)-based BESS is utilized to mitigate the oscillation in WPP due to SSI phenomenon. The major component of the BESS is the inverter controller. Fig.4.4 depicts the schematic diagram of a distinctive grid-connected VSI-based BESS[168]. There are four levels of control involved in the developed controller. Supplementary damping signals, power controller block, inner current controller block, and a Pulse width modulation (PWM) unit. The literature considers WAMS data to obtain the angular speed deviation as an input for the supplementary damping signal. The supplementary damping signal is denoted by U, and this signal is supplemented by the active power of the power controller block as depicted in Fig.4.4, in order to provide damping of the oscillations. The output of the primary power controller block is to provide i_{dref} and i_{qref} reference current to the inner current-controller block. The second control block is the inner current-controller block and this controller block is to regulate the AC side current of the VSI by using a PWM method[116]. Firstly, i_d and i_q are compared to i_{dref} and i_{qref} reference values, respectively, as shown in Fig.4.4 in the current controller block. The decoupling of feed-forward signals is used to improve the outputs of proportional-integral (PI) controllers, which process error signals. For the PI parameter tunning a systematic hit-and-trial approach has been used, to produce the fastest step response, the shortest settling time, and less than 10% overshoot time. The inner controller block provides the dq reference voltage. The dq reference voltages are translated to abc the reference frame and fed into the PWM unit, which generates pulse signal. The LCL

filter is used in the system, which is interconnected through a coupling transformer, to minimize the ripples at the AC side of the VSI so that the systems can deliver low distorted current and voltage at the output[169].

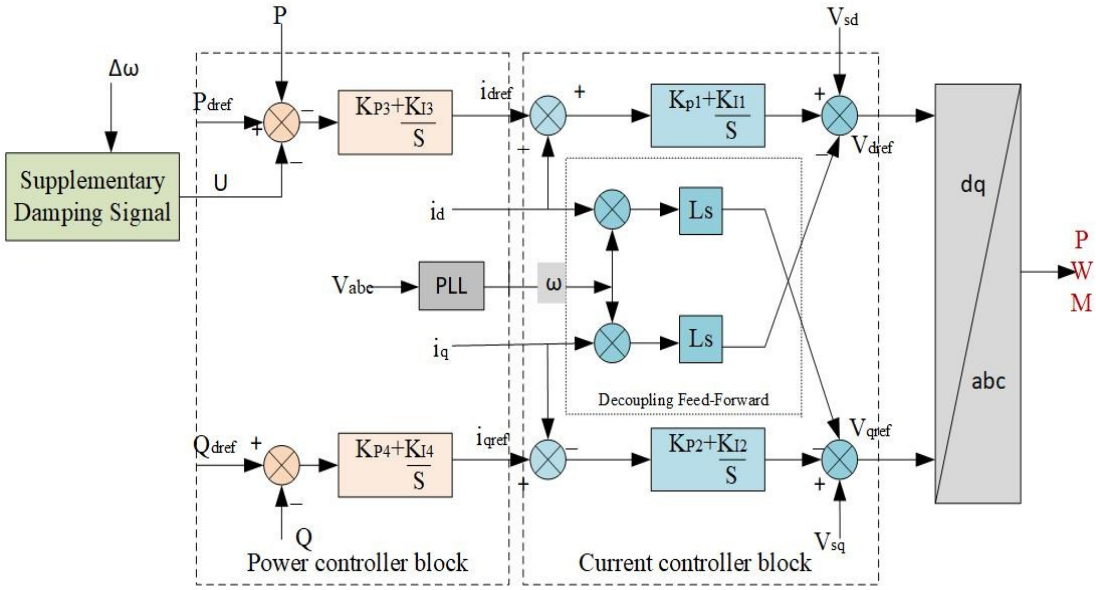

Fig 4.4 BESDC controller for the SSR mitigation

4.3.3 Design of the Supplementary Damping Signal

Fig.4.5 illustrates the configuration of the SDS. The objective of the SDS is to compensate for the negative damping by providing additional damping. This can be achieved without reducing the synchronizing torque. A washout, two lead-lag compensators, gain as well as a limiter block composes the SDS design technique in this study, as illustrated in Fig.4.5 [118], [170]. The design of the SDS transfer function is defined as:

$$SDS(s) = \frac{sT_W}{1+sT_W} T(s) \tag{4.16}$$

were the transfer function of the lead-lag compensator. T(s) is defined as

$$T(s) = \frac{K(1+sT_1)(1+sT_3)}{(1+sT_2)(1+sT_4)} \tag{4.17}$$

Whereas K represents gain of the damping signal. The gain of the controller determines the strength of the damping effect. A higher gain will provide stronger damping, but may also introduce instability. The gain should be carefully tuned to achieve the desired damping effect without introducing instability.

T_W denotes the washout time constant, the objective of the washout block acts as a high pass filter, it prevents from DC component and low-frequency component. T_1, T_3, T_2, and T_4 is the time constants of two stages lead-lag compensator block. The compensator consists of a lead network and a lag network, each of which contributes to the overall phase shift of the system. The phase shift of the lead network should be chosen to align with the frequency of the sub-synchronous oscillation, while the phase shift of the lag network should be chosen to provide additional damping. The gain of the lead-lag compensator should be chosen to achieve the desired level of damping while avoiding instability. The compensator parameters are tuned based on the eigenvalues of the system matrix and analyzing their locations in the complex plane along with systematic hit and trial methods to achieve the desired level of damping.

Since the number of unknown parameters is six which need to determined. The number of algebraic equations must equal the number of the unknown controller parameter according to the model theory. We may quickly and simply obtain the required parameters for the controller by solving the set of linearized algebraic equations (4.15). Therefore, the parameters of the controller are determined by substituting the desired eigenvalues corresponding to Mode 3, Mode 4 and Mode 6 to the closed loop system characteristics equation:

$$|sI - (A + B.SDS(s)C)| = 0 \tag{4.18}$$

Where I is identity matrix of the same dimension as A.

To obtained optimal parameter a systematic hit-and-trial procedure also used to tune the SDS parameters to produce a fast step response, less settling time, and less than 10% overshoot time so that to minimizing the impact on system stability and transient response efficiently. The condition should be fallowed $T_1>T_2$ and $T_3<T_4$. The obtained optimal parameter is shown in Table 4.1

Table 4.1 parameters for the supplementary damping signal

Parameter	K	T_W	T_1	T_2	T_3	T_4	**Min and Max**
Value	1.38	10	0.1	0.01	0.4	2	∓ 0.1

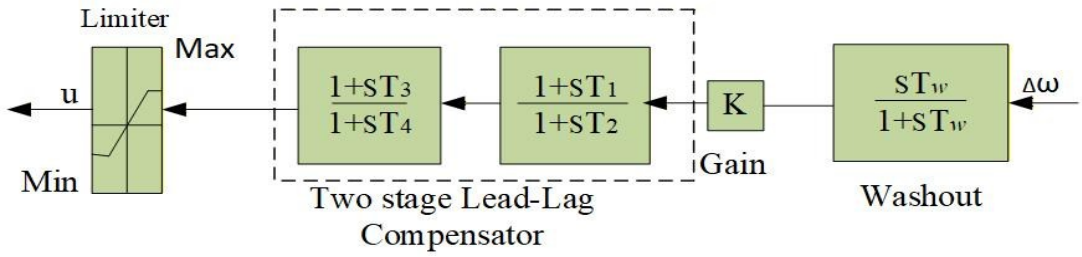

Fig 4.5 Supplementary damping signal

The angular speed deviation signal has been used as the input control signal in this proposed system, and the SDC input is designed to alleviate SSR and measures the frequency deviation of the generator using WAMS. As shown in Fig.4.1, the SDS output is added to the battery controller, which regulates the BESS's reference active power generation.

4.3.4 Input control signal

The major challenge of selecting a speed deviation as an Input Control Signal (ICS) is to capture the angular speed deviations of a generator and transmit them to the other components of the system that is far away from the synchronous generator. Thus, the advancement in the technologies such as WAMS, PMU, and communication networks enable us to get the most accurate and real-time data on the dynamic parameters of a complex power system [171][172]. At the same time, it is essential to have real-time data for the parameter such as frequency, voltage, and current from generating station to the transmission system. However, this study focuses on using speed deviation as an ICS for designing a damping controller to mitigate the SSR. Generally, PMUs are installed to measure the voltage and frequency at a busbar, and that can be transmitted to other substations. The installed PMU captures the data regarding current, voltage, frequency, and other parameters at regular intervals on a sample basis, and this data is stored in data concentrators. Each PMU is generally time synched with the GPS devices, and the data stored in the form of samples are time-stamped which can be used for the analysis of complex power systems. The samples taken from the PMU devices should be in milliseconds so that the exact analysis can be done at the remote end for frequency deviation observed in the synchronous generator[173]. The time-stamped data of analog parameters stored in the data concentrator are transferred to

the remote end with the support of the WAMS network. The role of WAMS is to monitor the data transmission from PMUs to the central controller, ensuring reliable data transfer from several stations to the computation center. This study analyses the BESS technology controller to dampen the SSR oscillation. WAMS serves the purpose of providing real-time data of angular speed deviation at the synchronous generator to the controller input installed in BESS technology at the remote end Bus Bar unit. The details and arguments for employing WAMS to capture rotor speed data have been described in[36] and are not covered in this study.

4.4 Result and discussion

For further analyzing the small signal stability, the eigenvalue method has been used, and, to validate the eigenvalue a time domain analysis also has been done in this section by using MATLAB/Simulink.

4.4.1 Eigenvalue analysis without damping controller

To study the small-signal stability of a dynamic system, the eigenvalue method is one of the fundamental and effective methodologies. In this methodology, the order of the system matrix decided the set of eigenvalues.

Table 4.2 Eigenvalues of the study system model with 50% FSC level, at 7 m/s wind speed

Modes	Eigenvalue	Frequency(Hz)	Description
Mode 1	-1790±j889	141	Very high frequency
Mode 2	-19.2±j568.2	90.4	Super-synchronous
Mode 3	**1.6±j187.8**	**29.9**	SSR
Mode 4	-0.63±j18.8	2.86	Electromechanical
Mode 5	-52.4±j7.9	1.25	Torsional mode
Mode 6	-6.41±j8.6	1.36	Torsional mode

The analysis of eigenvalue decided the stability of the system. The system is unstable if the real component of the eigenvalue is positive, and stable if the real part of the eigenvalue is negative. The oscillating frequency is decided by the imaginary part of the eigenvalue. The eigenvalue analysis exhibits when applied in the above-linearized study system without any damping controller, six unstable modes of oscillatory

behavior. Table 4.2 displays the set of eigenvalues of six modes at a fixed series compensation level of 50% for the 7m/s wind speed. Mode-1 and Mode-2 show the high frequency with a super-synchronous phenomenon, respectively, because they have greater frequencies than the system and are always stable.

Table 4.3 Mode-3 eigenvalue at varying % of series compensation and wind speed

Compensation	**Wind Speed**	**Mode 3**	
		Eigenvalue	**Frequency(Hz)**
40%	7m/s	0.01±j207	32.96
	9m/s	-0.04±j206.9	32.94
	11m/s	-0.12±j206.8	32.92
50%	7m/s	1.66±j187.8	29.90
	9m/s	1.56±j187.7	29.87
	11m/s	1.43±j187.5	29.84
60%	7m/s	3.26±j170.9	27.25
	9m/s	3.15±j170.7	27.14
	11m/s	2.95±j170.4	27.18

Mode-3 is not stable at this operating state, and it belongs to the sub-synchronous frequency range, and the system may become progressively unstable on increasing values of series compensation. Mode 4 is the electromechanical mode that exists due to the dynamics of electromechanical systems, and the remaining two modes, 5 and 6, are the torsional modes. As the series compensation is increased, it can be seen in Table 4.3, that the positive real part of the eigenvalue is increasing which shows the system is tending towards instability. The value of eigenvalue is dependent on the level of series compensation used in high-voltage transmission lines. On the other hand, the real part of the eigenvalue is decreased when the speed of the wind is increased which shows that at a higher speed of the wind, the system becomes more stable. Similarly, as shown in Table 4.3 wind speed rises from 7m/s to 11m/s, and the computed eigenvalue's real part slightly decreased at resultant the overall system at higher wind speed becomes stabilized. The time-domain simulation of the same system is deliberated on in the following subsections.

4.4.2 Small-signal model validation

In order to verify the validity of the small-signal model of the proposed study system, the small-signal model is established in MATLAB.

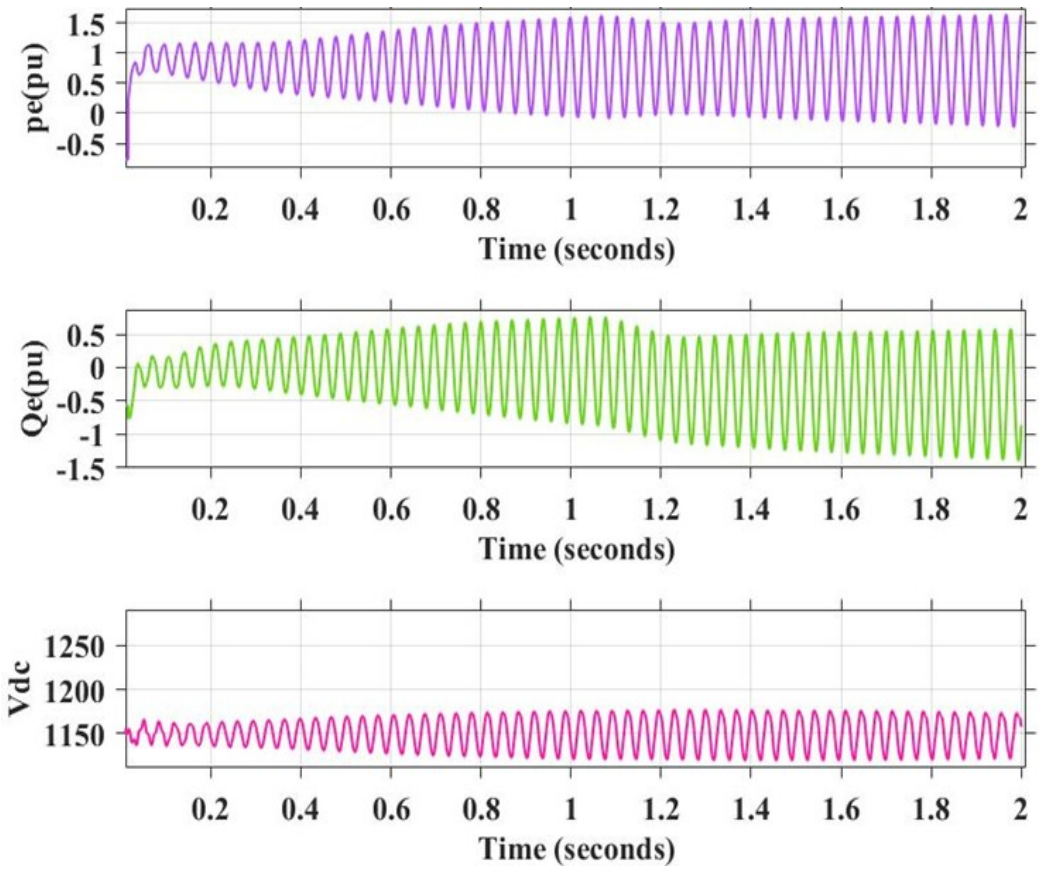

Fig 4.6 Dynamic behavior of the active power (pe), reactive power (Qe), and dc-link voltage (Vdc) of DFIG at a fixed series compensation of 50%

In contrast, the detailed electromagnetic transient model is built in the MATLAB/Simulink simulation platform. Accordingly, IEEE's first benchmark model is simulated at a wind speed of 7 m/s, and 50% of the series compensated transmission line. The output of the dynamic behavior of the active, reactive, and dc-link of DFIG is shown in Fig. 4.7, and the behavior of the waveform shows undamped oscillation. The eigenvalues in Table 4.2 show that Mode-3 is unstable at a wind speed of 7 m/s and 50% of the SCTL. To verify the correctness of the small-signal model to compute the eigenvalue at varying series compensation and wind speed. The obtained eigenvalue of Mode-3 at varying series compensation and wind speed is shown in

Table 4.4. The frequency of Mode-3 is 32.94, 29.87, and 27.14 at series compensation of 40%, 50%, and 60%, respectively. For the validation of the result seen in eigenvalue methods, the time-domain analysis and its Fast Fourier transform (FFT) have been analyzed.

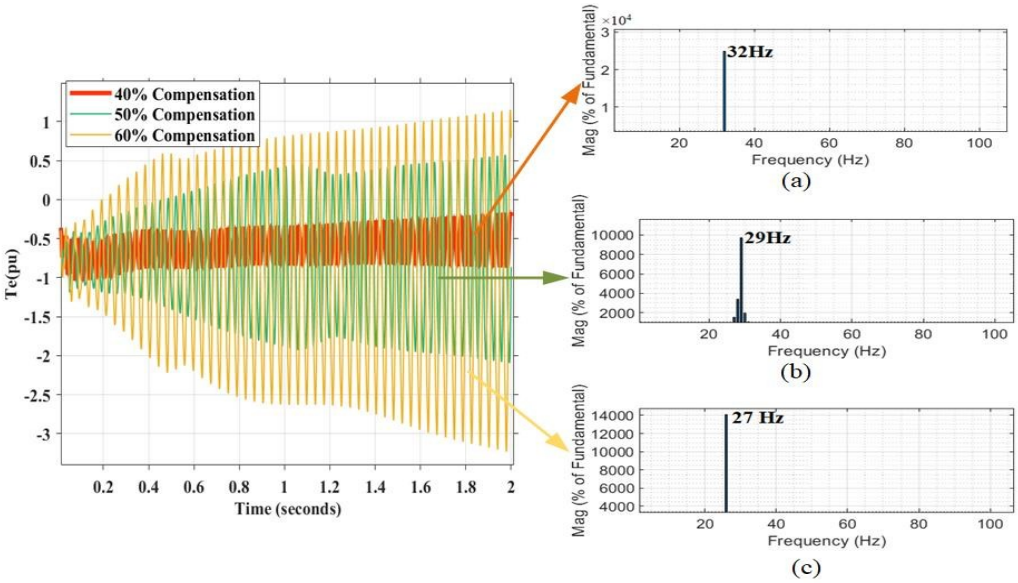

Fig 4.7 Dynamic behavior of the electromagnetic torque (Te) of 40 %, 50%, and 60% compensation level at 9m/s wind speed (a) FFT analysis for 40% series compensation (b) 50% series compensation (c) 60% series compensation

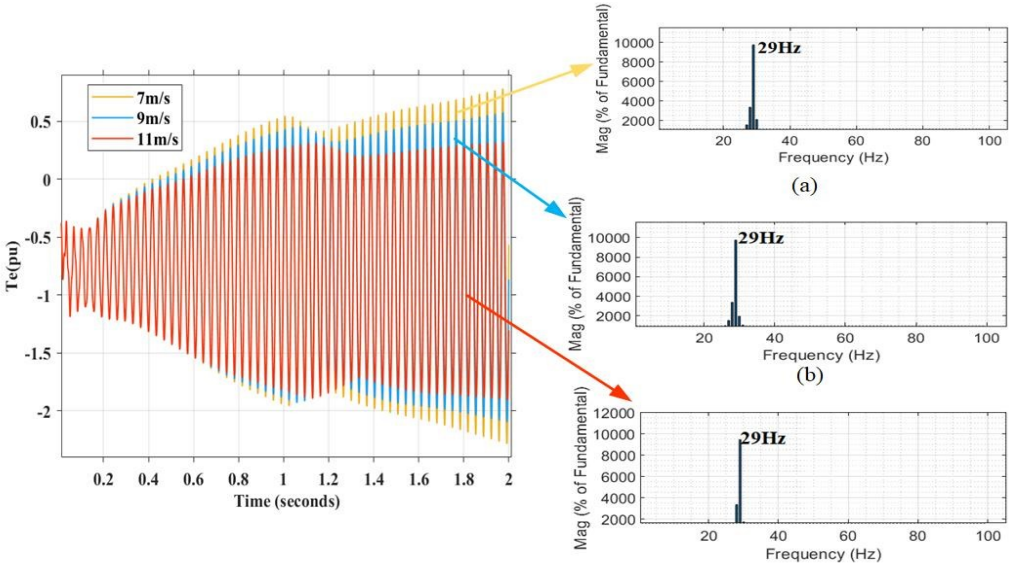

Fig 4.8 Dynamic behavior of the electromagnetic torque (Te) of 7m/s, 9m/s and 11m/s wind speed at 50% series compensation (a) FFT analysis for 7m/s wind speed (b) 9m/s wind speed (c)11m/s wind speed

Fig. 4.7 shows the dynamic behavior of the electromagnetic torque (Te) of 40 %, 50%, and 60% compensation levels at 9m/s wind speed. Fig. 4.8 shows the dynamic behavior of the electromagnetic torque(Te) of 7m/s, 9m/s, and 11m/s wind speed at 50% series compensation. After FFT analysis of the time domain signal, we get the same frequency as get by the eigenvalue analysis shown in Table 4.4. For the validation of the result seen in eigenvalue methods, the time-domain analysis and its FFT have been analyzed.

4.4.3 Eigenvalue analysis with BESDC

The proposed BESDC has been applied in a benchmark model to study the efficacy of a proposed damping controller by eigenvalue analysis. The eigenvalue analysis has been performed without a damping controller in the previous section and obtained six modes of oscillations in which Mode-3 is in unstable mode at sub-synchronous frequency, and this mode becomes undamped. After utilizing the BESDC, it can be concluded that for Mode-3(SSR Mode), the real part of the eigenvalue is more negative hence more stable.

Table 4.4 Eigenvalues of the study system model with BESDC at 50% SCTL and 7m/s wind speed

Modes	Eigenvalue	Frequency(Hz)
Mode 1	-17.93±j887	141.2
Mode 2	-16.2±j524.5	83.51
Mode 3	-1.5±j229.2	36.49
Mode 4	-49.4±j10.9	1.73
Mode 5	-0.63±j18.8	2.99
Mode 6	-4.5±j10.2	1.62

Table 4.5 displays the eigenvalues of the study system with a BESDC, which shows that all modes are stable even when the series compensation is set to 50%. Table 4.6 displays the eigenvalues of the study system with the BESDC at different compensation levels as well as wind speed, and it is found that even after increasing compensation level, the controller is capable of providing positive damping, and at resultant all modes are in stable condition.

Table 4.5 Mode-3 eigenvalue at varying % of series compensation and wind speed with BESDC

Compensation	Wind Speed	Mode 3	
		Eigenvalue	Frequency(Hz)
40%	7m/s	-3.0±j255.9	40.74
	9m/s	-3.04±j255.84	40.74
	11m/s	-3.09±j255.8	40.73
50%	7m/s	-1.5±j229.23	36.50
	9m/s	-1.54±j229.2	36.49
	11m/s	-1.6±j229.1	36.48
60%	7m/s	-1.04±j207	32.96
	9m/s	-1.09±j206.8	32.92
	11m/s	-1.16±j206.82	32.93

4.4.4 Time-domain Analysis for BESDC

The DFIG-based WPP having a series compensated transmission line suffers instability due to SSR and gets increasingly unstable when the compensation level rises. Hence, the BESDC equipped with a SDS composed of the angular speed deviation is used to damp out oscillations due to SSR. To enhance BESDC performance a time-domain simulation has been done in MATLAB/Simulink. The baseline scenario is considered at a wind speed of 9 m/s and 50% FSC and IEEE FBM model is considered to analyse the performances of the proposed damping controller. the equivalent model for the same is shown in Fig.4.1 and the required parameter is illustrated in the appendix.

(i) Damping performance of the BESDC

The simulation has been done for the baseline scenario to verify that the performances of the BESDC can dampen out the undamped oscillation due to SSR. According to simulation results for the baseline scenario, active power of 0.53pu has been achieved with 9m/s wind speed. further power factor is adjusted to 1 at the stator and grid side terminal, ensuring that the expected reactive power for the DFIG for steady-state conditions can be achieved zero. The further point is that the dc-link voltage reference is 1150 V. Fig. 4.9 shows the system's dynamic responses for the DFIG output active

power, reactive output power, electromagnetic torque, and dc-link voltage with and without the application of the proposed BESS damping controller. It shows that the system responses are stable when using the proposed damping strategy based on the BESS. The responses of the following values, Pe is equal to 0.53 pu, Qe is zero, and Vdc is 1150 V of the output active power, reactive power, and dc-link voltage of the DFIG have been achieved at steady state conditions.

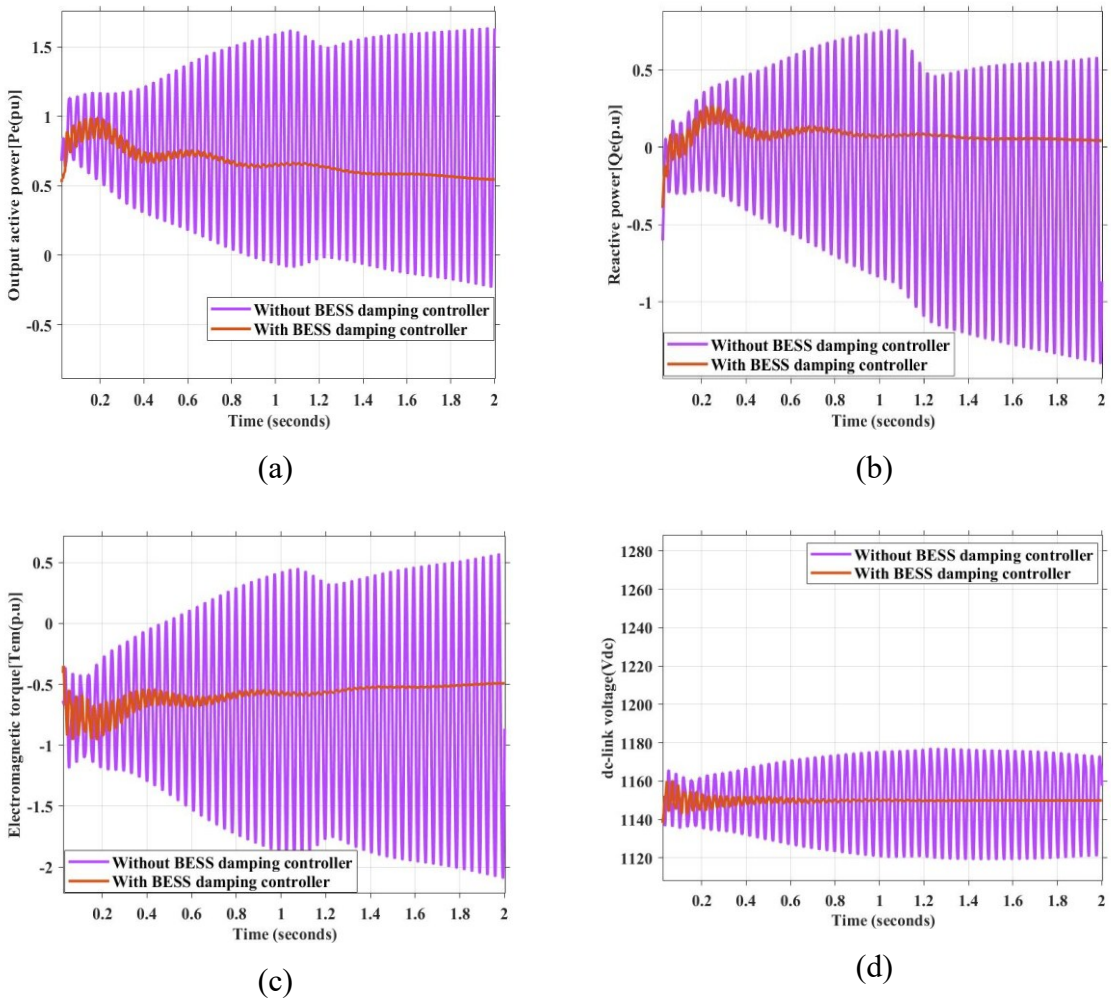

Fig 4.9 Time responses of the system comprising DFIG (a)output active power, (b)reactive power, (c)electromagnetic torque (d)dc-link voltage with and without the proposed Battery energy storage system damping controller

While taking the case without using BESDC, due to SSR, the rotor circuit action on damping SSR is negative. Hence, undamped sub-synchronous oscillations are generated on DFIG responses resulting unstable system. On the other hand, the rotor circuit has a detrimental effect on damping SSR oscillations, resulting in undamped

sub-synchronous oscillation manifest on the DFIG dynamic responses, leading to unstable system behaviour.

(ii) Robustness of the BESDC

The simulation for the baseline scenario is further expanded to validate the robustness of the proposed BESDC to mitigate the sub-synchronous oscillation due to SSR under major three cases as follows: (a) varying fixed series compensation levels (b) varying wind speeds and (c) Three phase fault condition.

(a) Varying fixed series compensation levels:

The baseline scenario is simulated at 50% and then 60% of SCTL while other parameters have been fixed. The system damping is directly related to the fixed series compensation level. We can validate the performance of the proposed BESDC at various series compensation levels, which has equivalent to the performance of BESDC at various damping conditions.

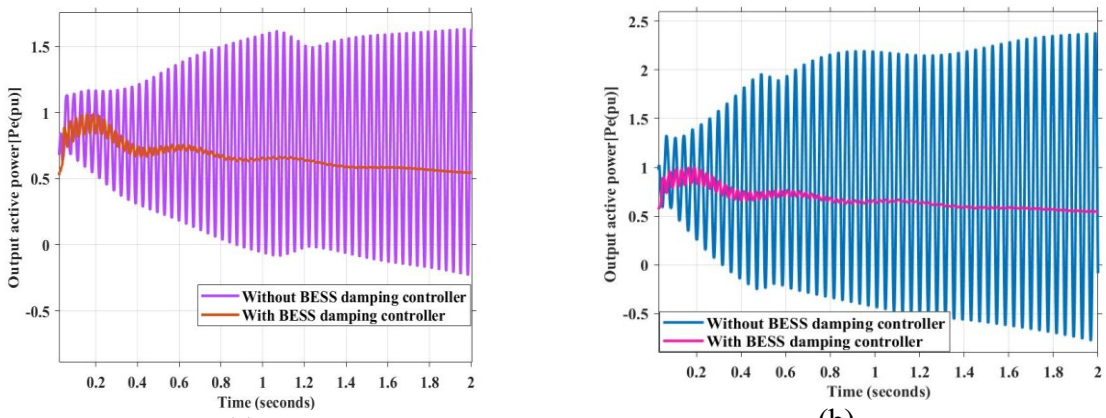

Fig 4.10 The output active power of DFIG with and without BESDC at (a)50% series compensation and 9m/s wind speed (b) 60% series compensation at 9m/s wind speed

As depicted in Fig. 4.8. When the level of series compensation increases, the amplitude of the undamped oscillation increases, and eventually, the system becomes unstable. The amplitude of output power oscillation is reduced when BESDC is added to the system after even though increasing the series compensation level from 50% to 60%. Fig. 4.10 depicts the active power of DFIGs for both with and without BESDC. Fig. 4.11 displays the dc-link voltage of DFIG.

(b) Varying wind speeds:

The baseline scenario is simulated at a wind speed of 11 m/s and 7 m/s rather than 9 m/s, whereas other parameters have been fixed. Fig. 4.12 depicts the active power output of the DFIG with and without BESDC at diverse wind speeds and observed that after using the damping controller the undamped oscillations are damped out. The results validate that the efficacy of the proposed damping controller is proficient in damping out oscillation at different wind speeds. Correspondingly, Fig. 4.13 depicts the dc-link voltage of the DFIGs with and without BESDC

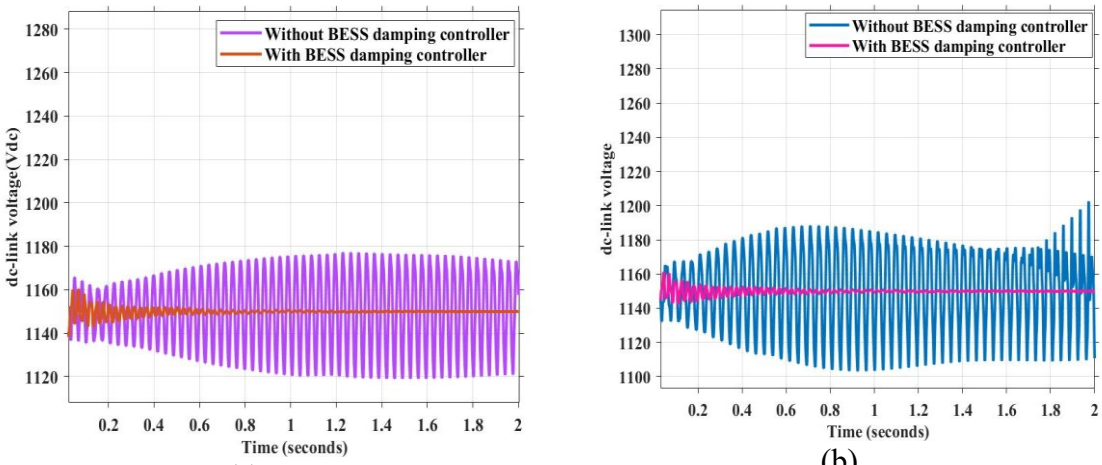

(a) (b)

Fig 4.11 DC-link voltage with and without BESDC at (a) 50% series compensation and 9m/s wind speed (b) 60% series compensation at 9m/s wind speed

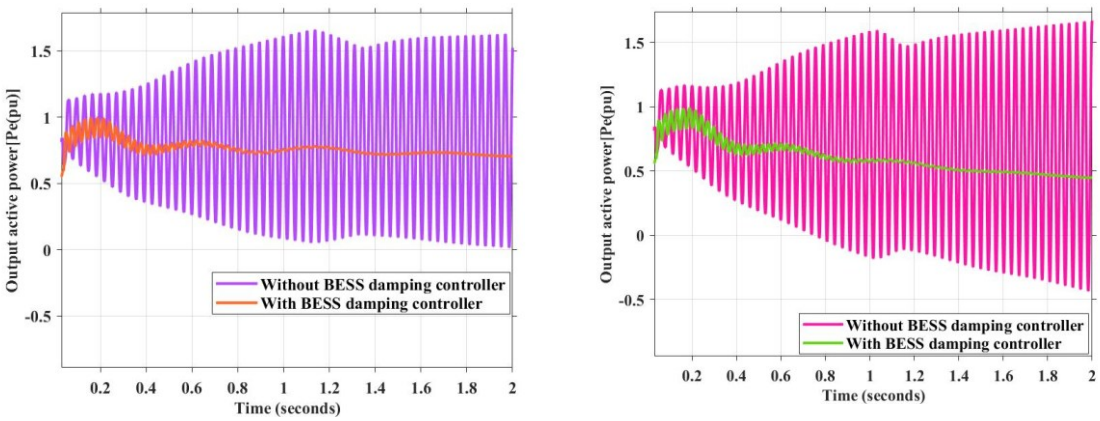

(a) (b)

Fig 4.12 The output active power of DFIG with and without BESDC at (a) 7m/s wind speed (b) 11m/s wind speed at 50% series compensation

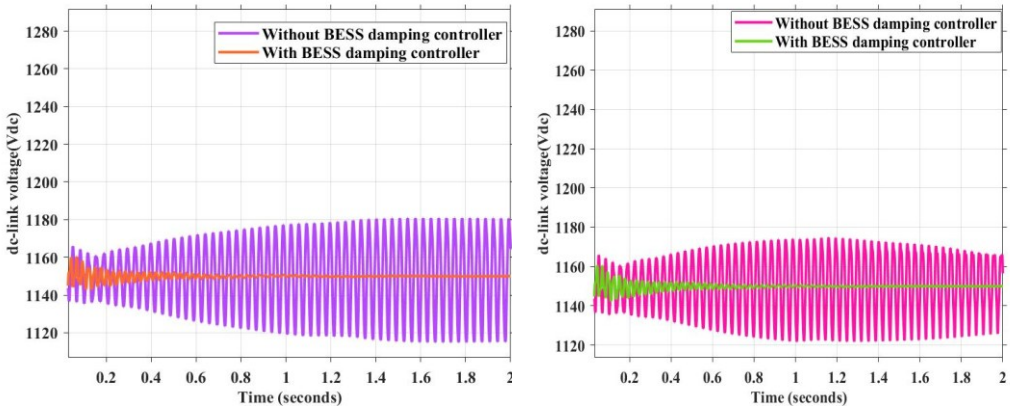

(a) (b)

Fig 4.13 DC-link voltage with and without BESDC at (a) 7m/s wind speed (b) 9m/s wind speed,50% series compensation

(c) Three-phase fault condition:

In an electrical power system, three-phase faults are a severe concern; even though it doesn't happen often, the disturbances are very intense. Consequently, it is essential to test the proposed damping controller's suppression capability.

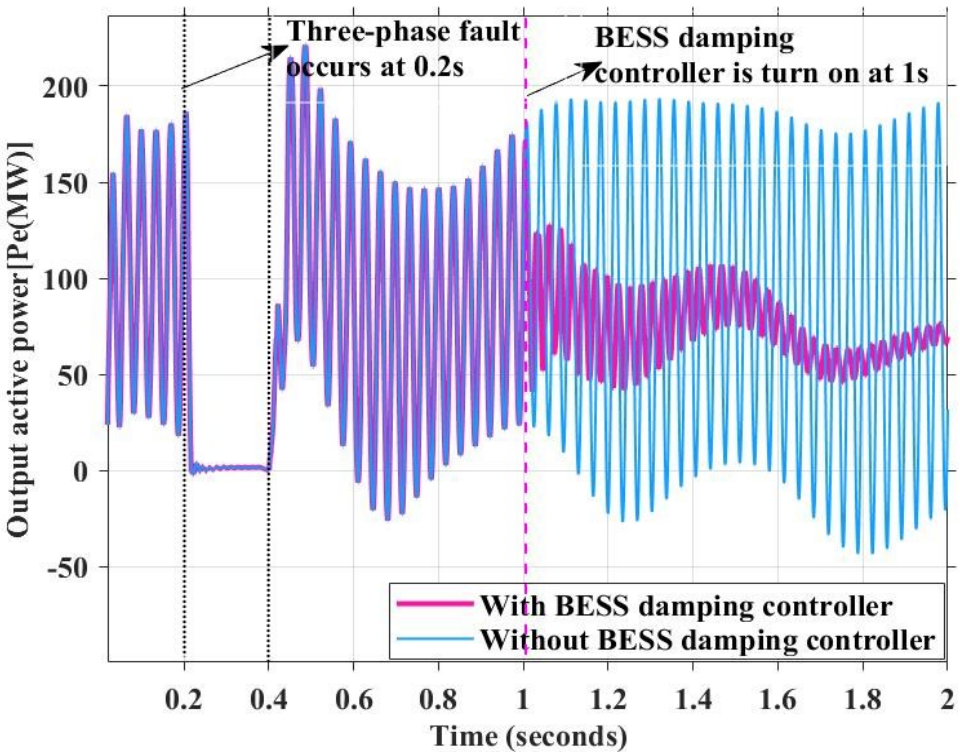

Fig 4.14 The output active power without and with BESDC under three-phase fault condition

The baseline scenario is simulated at a series compensation of 50% level and a wind speed is 9 m/s, and the series compensating capacitance is activated before the fault. The fault is introduced at time t = 0.2s and eliminated at time t = 0.4s. During the fault, the active power declined almost to zero, as depicted in Fig. 4.14. At t = 1 s, the BESDC is activated.

According to the output waveform of the active power generated by DFIG and experiences severe sub-synchronous undamped oscillation and loses stability at resultant. The oscillation converges, and the system regains stability when the BESDC is turned on. After the BESDC is turned on, as seen in Fig. 4.15, the output voltage only contains a fundamental frequency component. Fig. 4.16 shows the dc-link voltage of DFIG at the three-phase fault condition. The simulation shows that BESDC can have an excellent restraining effect even in the worst-case scenario of the three-phase fault condition.

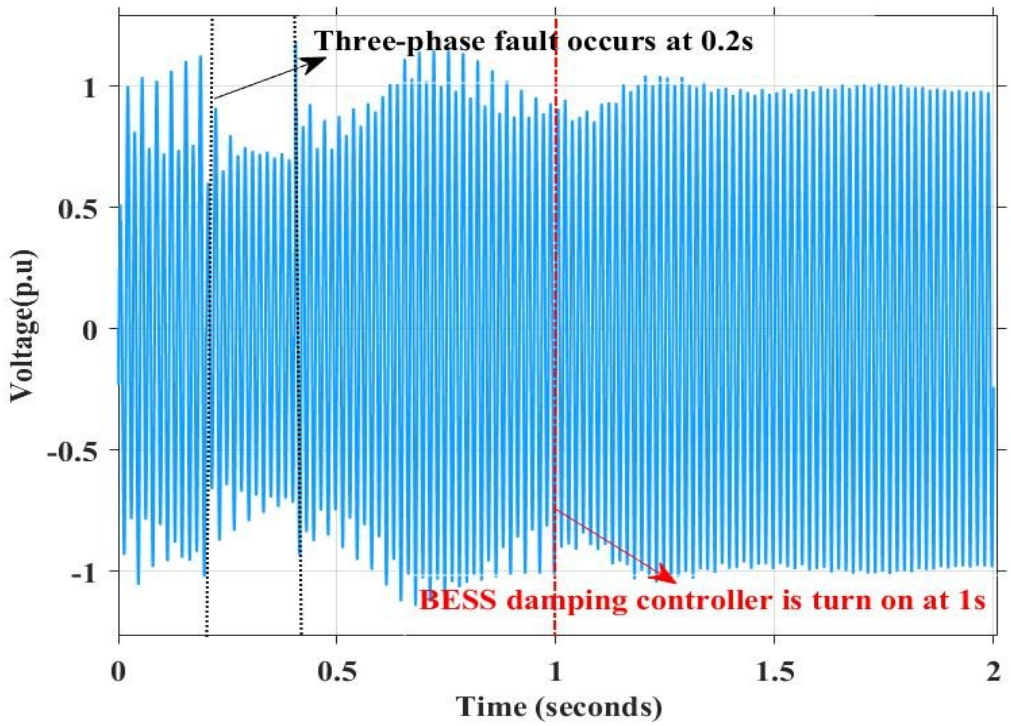

Fig 4.15 The phase output voltage of DFIG at Bus1

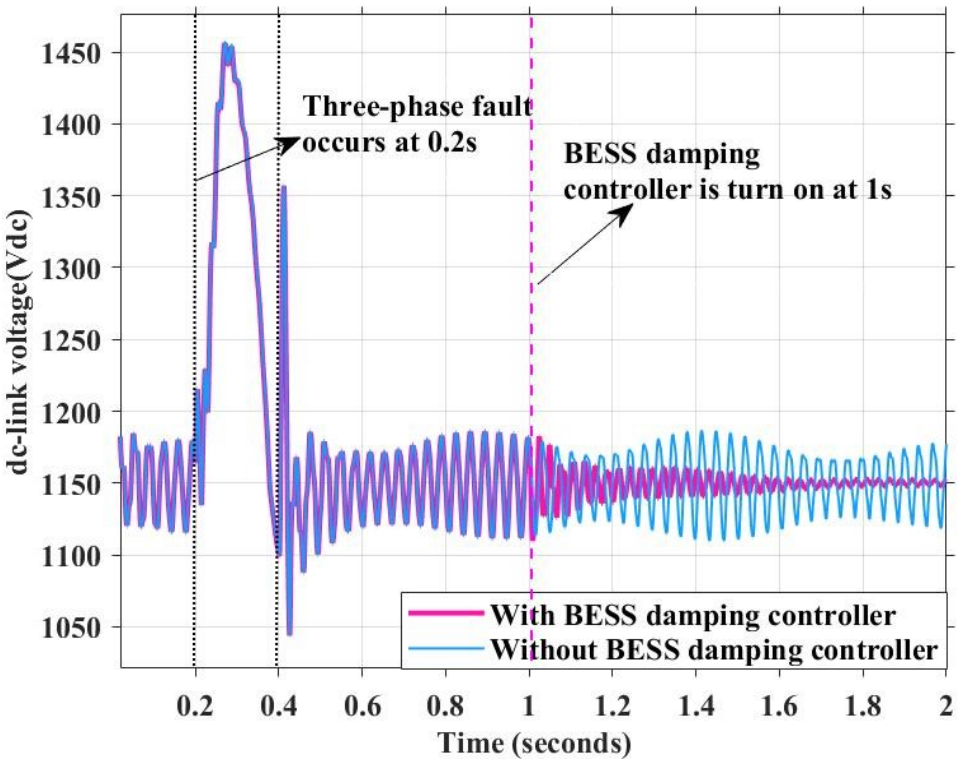

Fig 4.16 DC-link voltage without and with BESDC under three-phase fault condition

4.5 Conclusion

This chapter investigate the SSI phenomena particularly SSR a detailed mathematical model of a 100MW DFIG-based WPP interconnected to an infinite bus with an SCTL has been developed based on the IEEE FBM. With the help of eigenvalue analysis obtained, the several modes of oscillations in the overall system i.e. Electrical, electromechanical, and Torsional modes. The estimated eigenvalues of the overall study system for different operating conditions have been used to identify the stable and unstable modes of frequencies and obtain unstable SSR modes. Two cases have been investigated for the small signal stability (i) to analyze the system stability at various compensation levels and (ii) to analyze the system stability under varying wind speeds. To alleviate SSR due to SSI and enhance the power system operation, proposed a BESDC equipped with a supplementary damping signal composed of the angular speed deviations has been used to damp out oscillations in wind-integrated power grids effectively even after increasing the compensation level from 50% to 60% of series compensation. In this literature, we used WAMS data to obtain an angular speed

deviation and to overcome the challenges of considering a speed deviation as an input control signal. To validate the performance of the given proposed controller an eigenvalue analysis and a time-domain simulation have been done by using MATLAB/Simulink; the dynamic behaviors of electromagnetic torque (T_e), active power (P_e), reactive power (Q_e), and dc-link voltage (V_{dc}) of DFIG for various compensation levels, wind speeds, and three-phase fault conditions also have been investigated in this chapter. As a result, the proposed BESDC is capable of dampening out the oscillation in a very effective manner. Moreover, since the proposed BESDC-based damping controller would not need the modification of other power system controllers or the detection of harmonics, it can be easily applied to various scenarios for minimizing sub-synchronous oscillations caused by the SSR.

CHAPTER 5

INTELLIGENT BESS DAMPING CONTROLLER BASED ON UPSO

5.1 Introduction

The preceding chapter presented the design of a BESDC for mitigating SSR in DFIG-based wind power systems. Although the controller effectively improved damping performance, its robustness reduced under varying wind speeds and series compensation levels due to fixed tuning of gain and phase compensation parameters. To enhance adaptability and ensure consistent damping performance, this chapter introduces an Upgraded Particle Swarm Optimization (UPSO)-based BESDC. The standard PSO technique, widely used in nonlinear optimization, often suffers from premature convergence and limited global search capability, which restricts its effectiveness in complex, highly dynamic systems. The UPSO algorithm overcomes these drawbacks by incorporating chaotic initialization, adaptive inertia weight adjustment, and an improved velocity position update mechanism. These features enhance both global exploration and local exploitation abilities, ensuring faster convergence and avoidance of local optima. The proposed UPSO-based BESDC optimally tunes the gain and phase compensation parameters of the supplementary damping signal, thereby achieving robust SSR suppression under diverse operating conditions. Comparative eigenvalue and time-domain analyses confirm that the UPSO-based controller significantly improves damping ratios, convergence speed, and overall system stability compared to conventional BESDC approaches.

5.2 Modelling of BESDC

The proposed system of the optimized BESDC for SSR mitigation is illustrated in Fig.5.1. A battery unit is interfaced with the grid through a VSI, where the optimally tuned SDS is injected into the active power control loop to effectively suppress SSR. The energy from the battery is supplied to the grid through a three-phase VSI. As

depicted in Fig.5.2, the BESDC function depends on constant power operation and PQ (active-reactive power) control techniques. The grid voltages at the battery terminals are represented by V_{sa}, V_{sb} and V_{sc}, and their corresponding dq axis components are V_{sd}, V_{sq}. Similarly, the BESDC output voltages are V_{Ba}, V_{Bb} and V_{Bc}, with their dq components denoted as V_{Bq}, V_{Bd}. The output currents are expressed in both three-phase (i_a, i_b and i_c), and dq (i_d, i_q) reference frames. The BESDC line inductance is symbolized by L_s, and ω denotes the synchronous angular frequency. On the DC side of the system, the capacitor, current and voltage are represented as C_{dcB}, i_{dcB} and V_{dcB} respectively. For small-signal modeling, the state variables include V_{abc}, i_d, i_q, x_Q , x_P, x_{id} , x_{iq}, and x_{iq} following methodologies outlined in[148], [151], [152], [167].

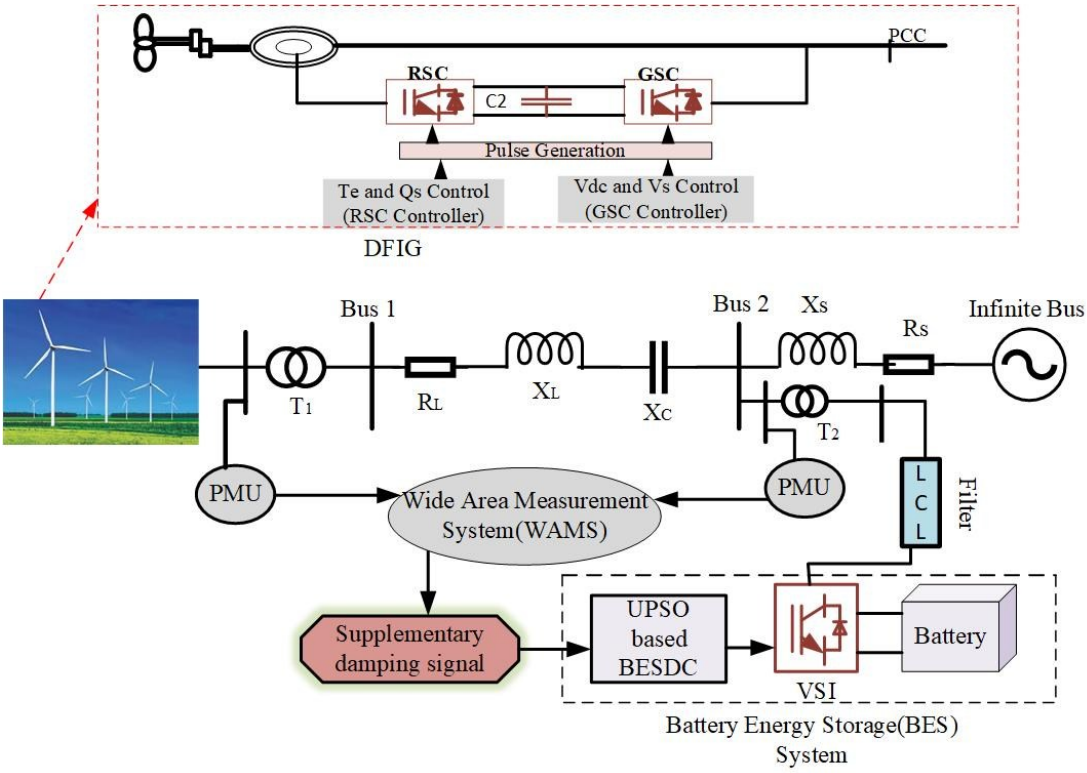

Fig 5.1 Model of the proposed system developed for SSR mitigation

The state equations governing the transmission lines, controller, and DC capacitor are defined are given below:

$$\frac{di_d}{dt} = \frac{\omega}{L_s}\left(V_{dref} + L_s i_q\right) \tag{5.1}$$

$$\frac{di_q}{dt} = \frac{\omega}{L_s}\left(V_{qref} + L_s i_d\right) \tag{5.2}$$

Controller state equation

$$\frac{dx_p}{dt} = P_{dref} - \left(V_{Sq} i_d - V_{Sd} i_q\right) \tag{5.3}$$

$$\frac{dx_{id}}{dt} = K_p\left(P_{dref} - \left(V_{Sq} i_d - V_{Sd} i_q\right) + K_{I1}\left(x_p - i_d\right)\right) \tag{5.4}$$

$$\frac{dx_Q}{dt} = Q_{dref} - \left(V_{Sd} i_d - V_{Sq} i_q\right) \tag{5.5}$$

$$\frac{dx_{iq}}{dt} = K_{p4}\left(Q_{dref} - \left(V_{Sd} i_d - V_{Sq} i_q\right) + K_{I4}\left(x_Q - i_q\right)\right) \tag{5.6}$$

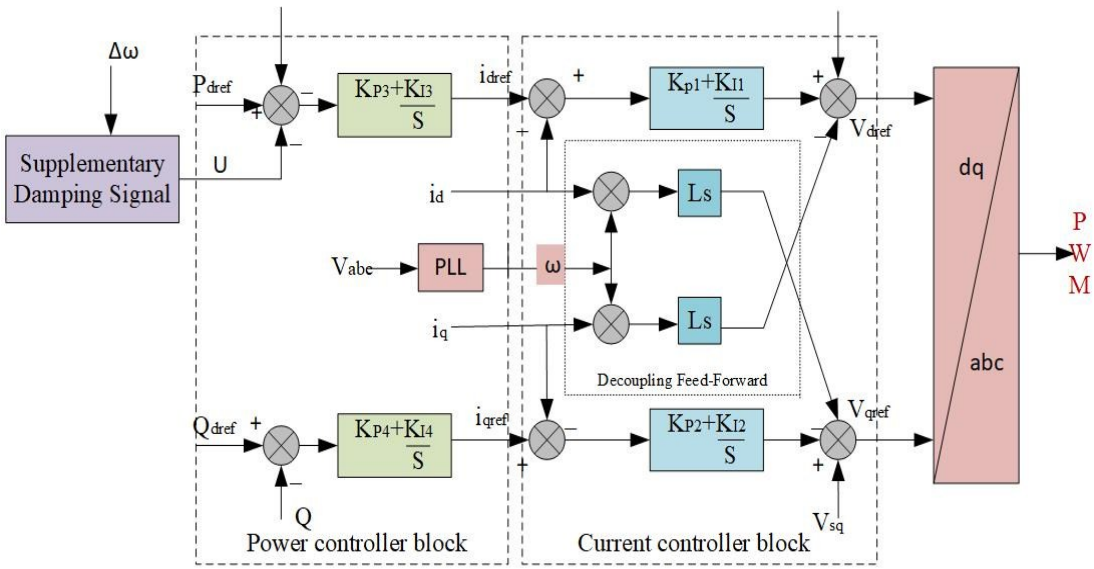

Fig 5.2 BESDC controller for SSR mitigation

DC capacitor state equation

$$\frac{dV_{dcB}}{dt} = \frac{\omega}{C_{dcB} V_{dcB}}\left(V_{Bd} i_{Bd} + V_{Bq} i_{Bq}\right) \tag{5.7}$$

For the analysis, the complete system model is represented in state-space form as:

$$\dot{X} = f\left(X, U\right) \tag{5.8}$$

where the overall state vector is defined as:

$$X = \begin{pmatrix} X_{Shaft} & X_{DFIG} & X_{TL} & X_{DC} & X_{BESS} \end{pmatrix} \tag{5.9}$$

This integrated system model is simulated using MATLAB/Simulink for eigenvalue-

based stability analysis

5.3 Optimized BESDC design

Fig. 5.3 illustrates the block diagram of SDS. The SDS consists of a limiter, Gain, n-state phase compensation and BPF blocks. Additionally, the output signal of SDS is used to modulate the damping of the SSR mode within the overall system. The small-signal representation of the complete system has been presented in the preceding section. With the help of eigenvalue model, the objective function can be formulated to determine the optimal gain coefficients $\frac{K_1}{K_2}$ for the SDS part of the BESDC.

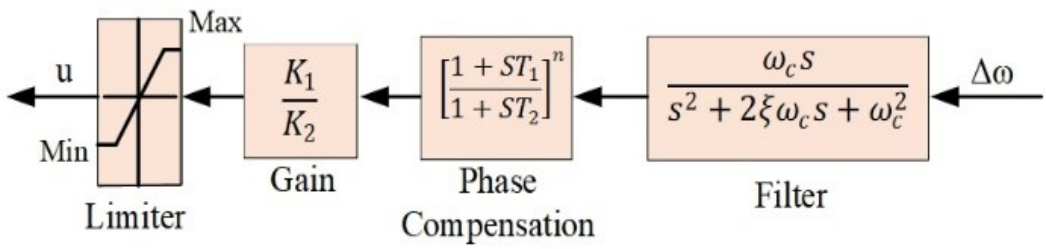

Fig 5.3 Block diagram of supplementary damping signal

Accordingly, an UPSO algorithm is applied to mitigate SSR under various operating conditions by optimally tuning the gain coefficients $\frac{K_1}{K_2}$ of the SDS. A comprehensive flowchart illustrating the enhanced BESDC design process is depicted in Fig.5.4. Based on Fig.5.4, the phases involved in the development of the enhanced BESDC can be summarized as follows:-

- Phase 1: A simulation model is developed for time-domain analysis of the entire system under varying load conditions, excluding the BESDC, to evaluate the system's SSR frequency and determine the initial parameters.
- Phase 2: Determine the transfer function between electromagnetic torque and angular speed deviation, including the band-pass filter and gain components of the SDS in BESDC. Use this transfer function to evaluate the critical phase compensation angle.
- Phase 3: The evaluation criteria is taken in different operating conditions. Using the compensation parameters from step-2, develop the small-signal model of the

entire system with the BESDC integrated , under different operating conditions. Further, determine the lead/lag correction time compensation $\frac{T_1}{T_2}$.

- Phase 4: Apply the UPSO algorithm to the small-signal models-based on DFIG wind plant configuration to optimize the SDS gain coefficients $\frac{K_1}{K_2}$, in accordance with the defined objective function and constraints.

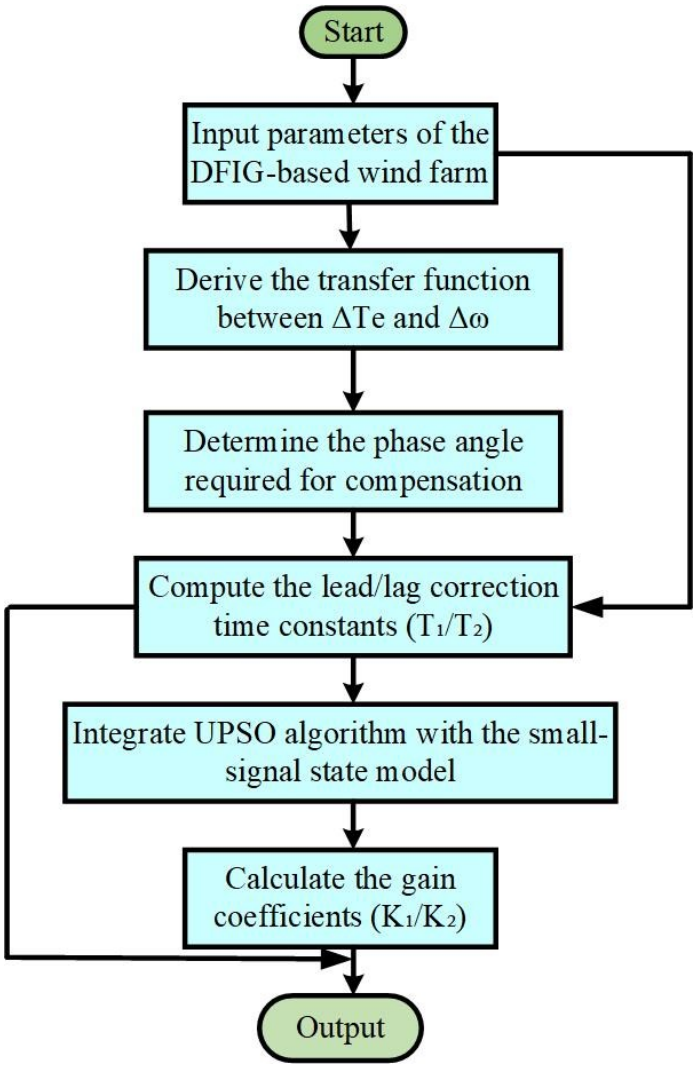

Fig 5.4 Flowchart of Enhanced BESDC layout

For damping the SSR mode, the effect of gain coefficients $\frac{K_1}{K_2}$ plays an important role. The effective alleviation of SSR under different transient operations , the gain coefficients $\frac{K_1}{K_2}$ can be used by applying UPSO algorithm.

5.4 Upgraded Particle Swarm Optimization Algorithm

There are basically three upgradations has been done in Conventional PSO algorithm to obtain UPSO algorithm [174], [175]:

(i) Chaotic Initialization using Skew Tent Map (STM):

Instead of randomly initializing the particle positions (potential solutions for K_1, K_2), we use a chaotic map to ensure a more uniform distribution across the search space. This enhances the algorithm's exploration capability. The Skew Tent Map is defined as[174]:

$$c^{(k+1)} = \begin{cases} \dfrac{c^{(k)}}{\alpha} & \text{if } 0 \leq c^{(k)} \leq \alpha \\ \dfrac{\left(1 - c^{(k)}\right)}{(1-\alpha)} & \text{if } \alpha \leq c^{(k)} \leq 1 \end{cases} \tag{5.10}$$

where $c^{(k)}$ is the chaotic variable at iteration k, and α is a control parameter set to 0.5. The sequence generated by this map is used to initialize the particle positions.

(ii) Adaptive Inertia Weight and Learning Factors:

In standard PSO, the inertia weight (ω_i) is often linearly decreased. We propose a non-linear, second-order decreasing function for a more effective search:

$$\omega_i(k) = \omega_{i,end} + \left(\omega_{i_start} - \omega_{i_end}\right) * \left[1 - \left(\frac{k}{T_{max}}\right)^2\right] \tag{5.11}$$

where k is the current iteration number and T_{max} is the maximum number of iterations. This ensures that $\omega_i(k)$ decreases smoothly from ω_{i_start} to ω_{i_end} without exceeding the intended range. Furthermore, the cognitive (c_1) and social (c_2) acceleration coefficients are dynamically adjusted based on the inertia weight to balance the influence of the particle's own experience and the swarm's best experience:

$$c_1(k) = c_{1,start} + \left(c_{1,end} - c_{1,start}\right) * \frac{k}{T_{max}} \tag{5.12}$$

$$c_2(k) = c_{2,,start} + \left(c_{2,end} - c_{2,start}\right) * \frac{k}{T_{max}} \tag{5.13}$$

where $c_{1,start}$=2.5, $c_{1,end}$=0.5, $c_{2,,start}$=0.5, $c_{2,end}$=2.5 are the initial and final values for the coefficient.

(iii) Enhanced Velocity Update with Constriction Factor:

The velocity and position update equations are modified to include a constriction factor (χ) that guarantees convergence [35]:

$$v_{ij}^{k+1} = \chi\left[v_{ij}^{k} + c_1 r_1\left(pbest_{ij}^{k} - x_{ij}^{k}\right) + c_2 r_2\left(gbest_{ij}^{k} - x_{ij}^{k}\right)\right] \tag{5.14}$$

$$x_{ij}^{k+1} = x_{ij}^{k} + v_{ij}^{k+1} \tag{5.15}$$

The constriction factor χ is calculated as:

$$\chi = \frac{2}{\left|2 - \emptyset - \sqrt{\emptyset^2 - 4\emptyset}\right|}\ , where\ \emptyset = c_1 + c_2\ and\ \emptyset > 4 \tag{5.16}$$

5.4.1 Optimization Problem Formulation

The goal of the UPSO is to find the optimal gain parameters K_1 and K_2 that maximize the damping of the critical SSR mode across a set of N predefined operating conditions (combinations of wind speed and compensation level).

Objective Function: The objective is to maximize the minimum damping ratio (ξ) among the critical oscillatory modes across all operating scenarios. The damping ratio for the ith ($\lambda_i = \sigma_i \pm j\beta_i$) eigenvalue is given by:

$$\xi_i = \frac{-\sigma_i}{\sqrt{\sigma_i^2 + \beta_i^2}} \tag{5.17}$$

A higher ξ indicates better damping. The objective function f is formulated as a minimization problem:

$$Minimize\ f = -\sum_{j=1}^{N} \delta_j \,.\, \min(\xi_{i,j}) \tag{5.18}$$

Subject to:

$$K_{1,min} \leq K_1 \leq K_{1,max} \tag{5.19}$$

$$K_{2,min} \leq K_2 \leq K_{2,max} \tag{5.20}$$

Here, $\xi_{i,j}$ is the damping ratio of the ith mode under the jth operating condition. The term $\min(\xi_{i,j})$ identifies the worst-damped (most critical) mode for that scenario. δ_j is a weighting factor assigned to each operating condition, reflecting its relative importance or likelihood of occurrence. For example, conditions with lower wind speeds and higher compensation levels (which are more prone to SSR) can be assigned a higher δ_j. The UPSO algorithm iteratively evaluates candidate solutions (K_1 , K_2) by linearizing the system model at each operating condition, calculating the eigenvalues, and computing the objective function f. The process continues until convergence is achieved.

5.5 Result and Discussion

In this study, the DFIG based wind farm operates at a wind speed of 7m/s. According to the analysis, three commonly used operating conditions are selected for evaluation, corresponding to wind speeds of 6, 7, 9, and 11 m/s. The initial weight coefficients for these conditions are set as 0.24 0.20, 0.07, and 0.02, respectively. Furthermore , the size of population is configured to 50 with maximum 100 iterations. The range of velocity from -30 to 30 m/s. Fig. 5.5 illustrate the objective function's convergence before and after the application of the UPSO algorithm. The eigenvalue result presented in Table 5.1, along with the corresponding three-dimensional surface plot shown in Fig.5.6, provide a comprehensive assessment of damping performance under varying wind speeds (6–11 m/s) and series compensation levels (40%, 50%, and 60%) for four control scenarios: (i) without BESDC, (ii) with conventional BESDC, (iii) BESDC optimized using PSO,

and (iv) BESDC optimized using UPSO.

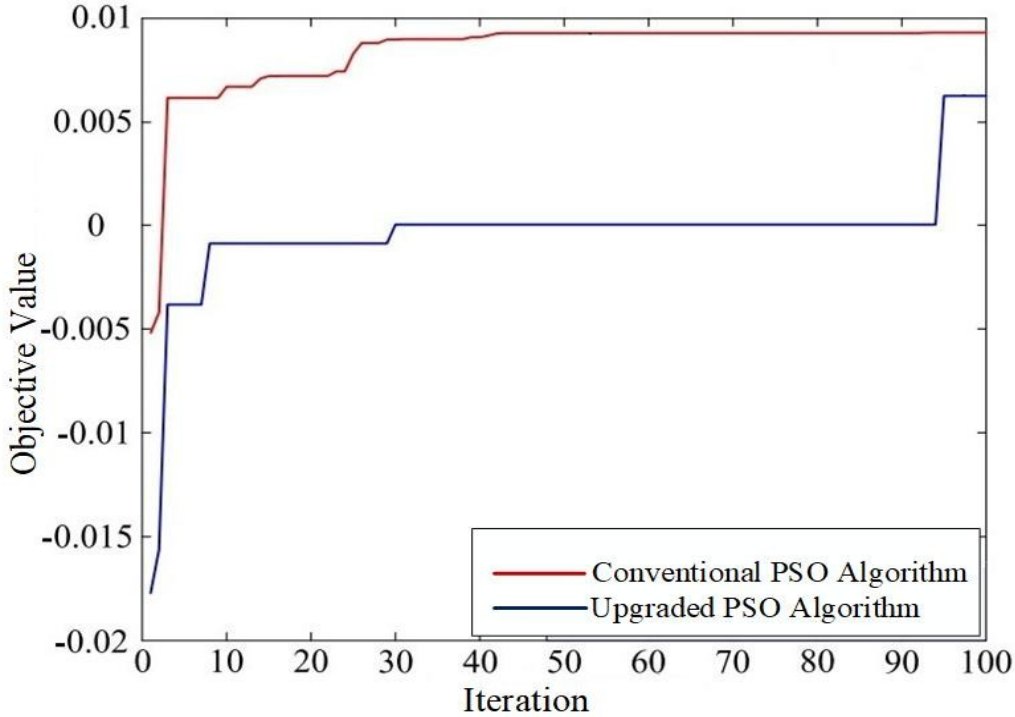

Fig 5.5 Objective function convergence comparison between conventional PSO and upgraded PSO algorithms

In the absence of any damping controller, the system exhibits weak or unstable behavior, particularly at higher compensation levels, as indicated by eigenvalues with positive real parts. The inclusion of a conventional BESDC improves damping, shifting the eigenvalues to the left-half of the complex plane; however, the resulting damping ratios remain relatively low and sensitive to operating conditions. The PSO-based BESDC demonstrates enhanced stability by producing more negative real parts, thereby improving the damping characteristics across all cases. Notably, the UPSO-based BESDC exhibits superior and consistent performance, yielding the most negative eigenvalues and the highest damping ratios for all wind speed and compensation combinations. This observation is further substantiated by Fig. 5.6, where the UPSO surface remains elevated across the entire operating domain, indicating uniformly improved damping behaviour. For example, at 60% compensation and 11 m/s wind speed, the eigenvalue shifts to $-2.16 + j207.57$, corresponding to a damping ratio of approximately 0.0104, substantially higher than those achieved with other controllers. These findings affirm that the proposed UPSO-optimized BESDC is the most effective

strategy for mitigating SSR in DFIG-based WPP under a wide range of grid conditions.

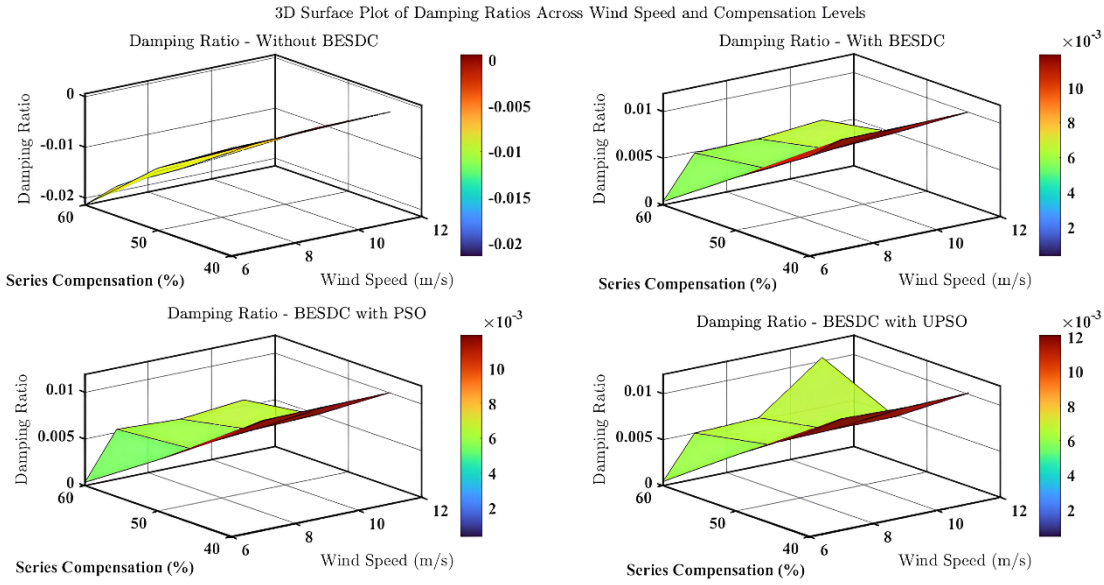

Fig 5.6 3D surface plot of damping ratio variation with wind speed and series compensation for four control strategies

Table 5.1 Eigenvalues of SSR modes under varying wind speed with and without BESDC, BESDC with PSO and BESDC with UPSO

Series Compensation	**Wind Speed (m/s)**	**Without BESDC**	**With BESDC**	**BESDC with PSO**	**BESDC with UPSO**
40%	6	**0.02±j206.8**	-2.7±j254.30	-2.75±j254.55	-2.9±j255.70
	7	**0.01±j207.0**	-3.0±j255.01	-3.0±j255.24	-3.1±j255.80
	9	-0.04±j207.4	-3.01±j255.09	-3.03±j255.32	-3.05±j255.84
	11	-0.12±j208.0	-3.04±j255.25	-3.05±j255.76	-3.09±j255.90
50%	6	**1.70±j187.5**	-1.3±j228.1	-1.25±j228.15	-1.4±j229.10
	7	**1.66±j187.9**	-1.35±j228.9	-1.38±j229.01	-1.5±j229.20
	9	**1.56±j188.7**	-1.5±j229.05	-1.51±j229.15	-1.54±j229.23
	11	**1.43±j189.5**	-1.59±j229.10	-1.56±j229.14	-1.6±j229.25
60%	6	**3.66±j170.8**	-0.07±j206.04	-0.07±j206.16	-0.09±j207.07
	7	**3.26±j171.4**	-1.0±j206.09	-1.01±j206.10	-1.04±j207.25
	9	**3.15±j172.7**	-1.03±j207.05	-1.04±j207.09	-1.09±j207.35
	11	**2.95±j173.4**	-1.16±j207.10	-1.18±j207.28	-2.16±j207.57

Following the implementation of the BESDC, all SSR mode eigenvalues exhibit real parts

in the left half of the complex plane, demonstrating effective mitigation of the SSR. Additionally, as shown in Table 5.1, severe SSR modes is observed at lower wind speeds, while higher wind speeds significantly help in suppressing SSR. For example, the system remains stable at a wind speed of approx. 11m/s without using BESDC. Hence, the operating conditions with wind speed higher than 11m/s may not be considered. In comparison to the conventional PSO based-BESDC, the enhanced BESDC employing the UPSO algorithm offers significantly improves SSR damping at lower wind speeds, while achieving enhancement at higher wind speeds more than 11 m/s. As a result, for system damping at lower speeds, the above proposed with of using BESDC with UPSO algorithm is used globally for optimization of the damping design by redistributing damping across multiple operating conditions. In summary, the enhanced BESDC with UPSO algorithm not only effectively mitigates SSR but also achieves optimal damping redistribution across various operating conditions. Further as shown in Fig.5.5 the UPSO algorithm converges better than the conventional PSO algorithm.

5.5.1 Empirical Case Studies and Simulation-Based Validation

To authenticate the effectiveness of the proposed improved SSR alleviation technique, a detailed time-domain simulation model is designed in MATLAB/Simulink. The base case is analyzed using the IEEE FBM at a wind speed of 9 m/s with 50% SCTL to evaluate the performance of the damping controller. Fig.5.8. illustrates the dynamic response of the system, including DFIG active power, electromagnetic torque, and DC-link voltage, under three conditions: without BESDC, with BESDC, and with enhanced BESDC controller. As observed, the system achieves an active power of 0.54 pu for a wind speed of 9 m/s, while maintaining a power factor of 1 at both the stator as well as grid-side terminals. This verifies that the DFIG's reactive power demand remains zero under steady-state conditions. The reference value for the DC-link voltage is defined as 1150 V. As shown in Fig.5.8, the application of the BESDC effectively reduces oscillations due to the FSC. Besides, the enhanced BESDC technique provides superior damping performance by expediting the decay of oscillation amplitude and minimizing settling time. This results in a more stable and resilient system response, significantly enhancing overall dynamic performance and robustness against disturbances. In contrast, without BESDC-based

damping control leads to adverse interactions between the rotor circuit and SSR, resulting in insufficient damping. Consequently, this causes undamped oscillations in the DFIG response, ultimately compromising system stability. The efficacy of the proposed scheme is evaluated through simulations under two distinct use cases: varying wind speeds, and different levels of series compensation. Moreover, the performance of the proposed scheme is systematically compared against both the conventional PSO method and the UPSO approach to assess its relative efficiency and robustness.

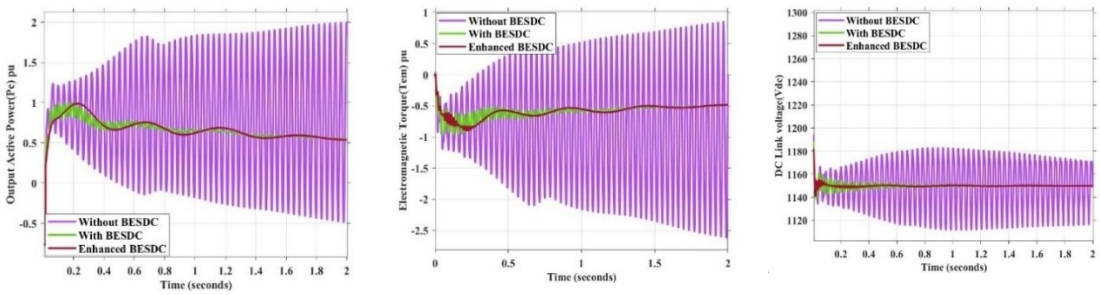

(a) (b) (c)

Fig 5.7 Output response of DFIG at 50% SCTL and 9 m/s wind speed for with, without BESDC and Enhanced BESDC (a) Active power output (b) Electromagnetic torque, (c) DC-link voltage of DFIG

(i) Impact of Varying Series Compensation level

The base case is simulated at 40% and 60% SCTL while maintaining all other system parameters constant. Since the level of SCTL significantly impacts system damping, the efficacy of the proposed Enhanced BESDC is assessed under different series compensation conditions. This evaluation is analogous to analyses the BESDC's performance across various damping conditions. As illustrated in Fig.5.7, an increase in SCTL level, the amplitude of undamped oscillations driving the system toward instability. However, adopting a proposed damping controller significantly mitigates output power oscillations, even with SCTL level from 40% to 60%. Fig.5.8 illustrates the active power response of the DFIG under three conditions: without BESDC, with BESDC, and with the Enhanced BESDC techniques. Similarly, Fig.5.9 shows the corresponding DC-link voltage dynamics. Without BESDC, the system shows undamped behavior, with sustained oscillations without the amplitude decay. This indicates an inherently unstable or weakly controlled system without usage of required damping techniques. The standard BESDC technique helps to reduce oscillations by gradually decreasing their amplitude,

resulting in improved system stability compared to the undamped case.

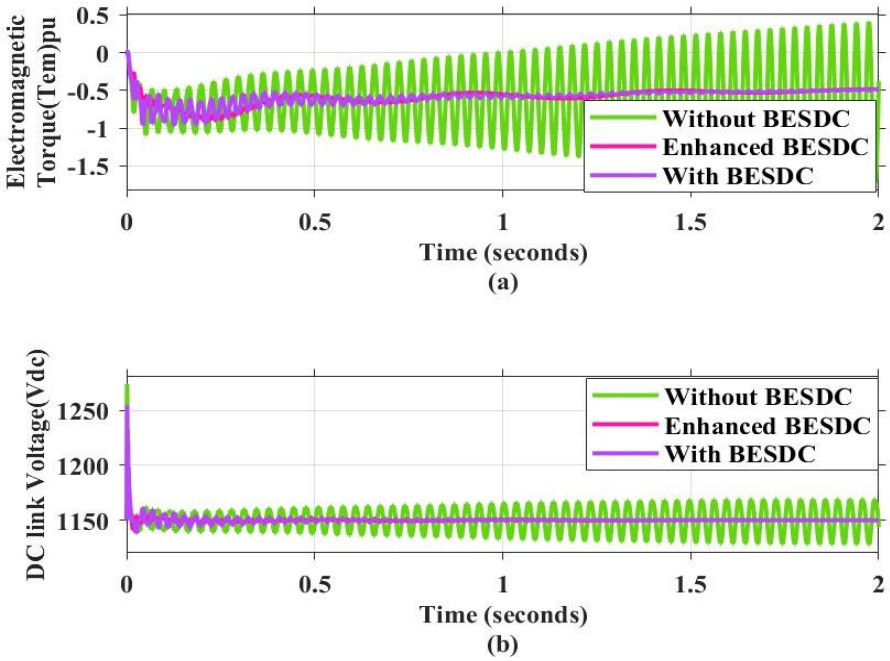

Fig 5.8 The output response of with, without and enhanced BESDC at 40% series compensation of (a) Electromagnetic torque(pu) (b) DC link voltage of DFIG

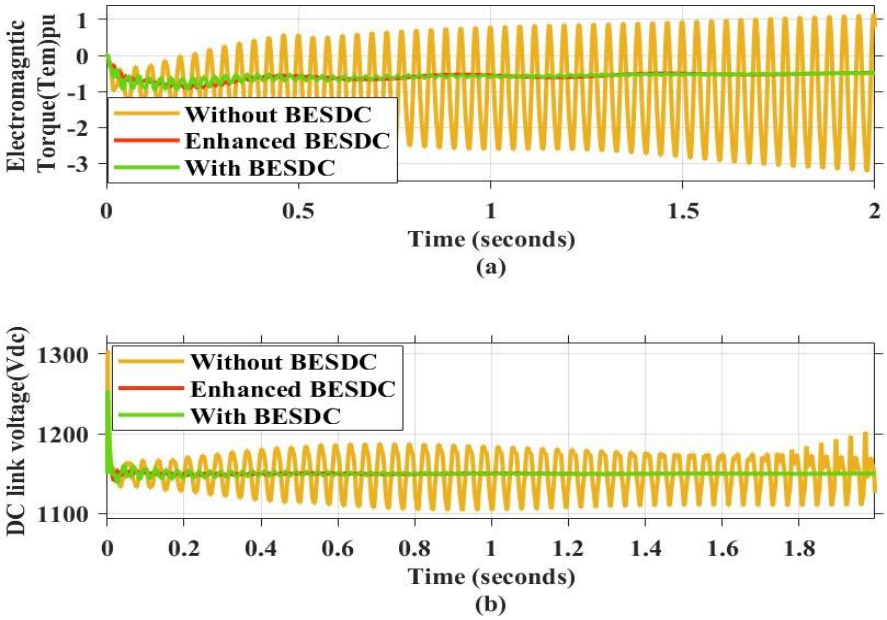

Fig 5.9 The output response of with, without and enhanced BESDC at 60% series compensation of (a) Electromagnetic torque(pu) (b) DC link voltage of DFIG

The enhanced BESDC further improves damping, allowing oscillations with faster time constant, reducing steady state time, and providing even better system stability. These results validate the effectiveness of the enhanced BESDC in improving damping

performance and ensuring stable system operation under different SCTL level conditions.

(ii) Impact of Wind Speed Variations

The base case is simulated at wind speeds of 7 m/s and 11 m/s, with all other parameters held constant. As wind speed increases, the damping coefficient improves accordingly. This case study considers a transmission line with 50% SCTL, where undamped oscillations are observed.

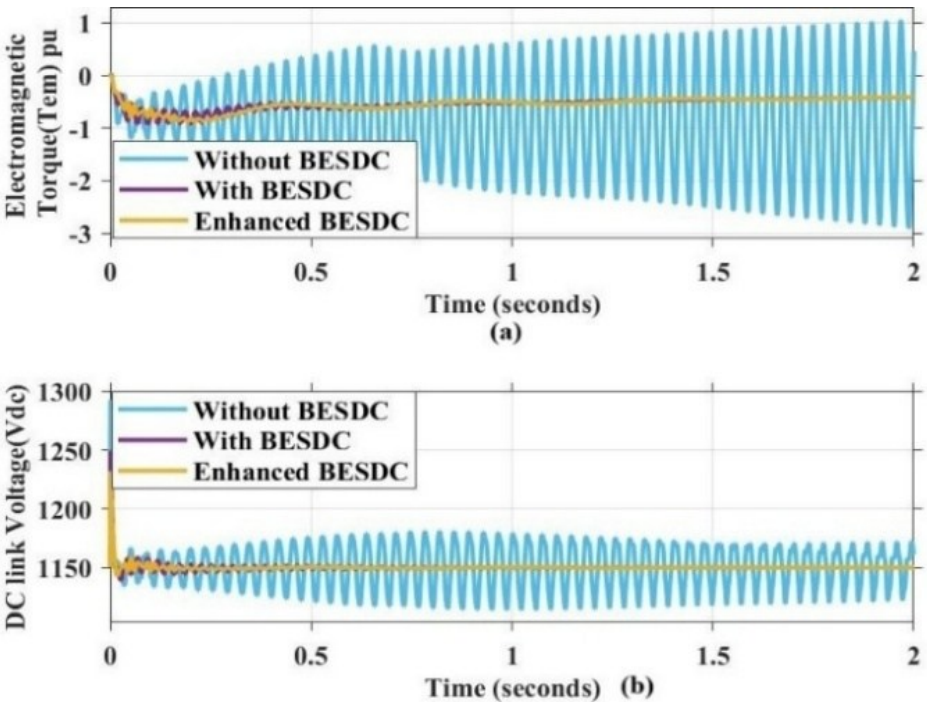

Fig 5.10 The output response of with, without and enhanced BESDC at 7m/s wind speed and 50% SCTL (a) Electromagnetic torque(pu) (b) DC link voltage of DFIG

The proposed enhanced BESDC technique effectively mitigates these oscillations, as demonstrated in Fig.5.10 and 5.11. Fig.5.10 illustrates the electromagnetic torque response of the DFIG under three distinct scenarios: without BESDC, with BESDC, and with the enhanced BESDC. Similarly, Fig.5.11 presents the DC-link voltage response of the DFIG for the same cases. The results confirm that the proposed damping controller effectively suppresses oscillations across varying wind speeds, ensuring improved system stability.

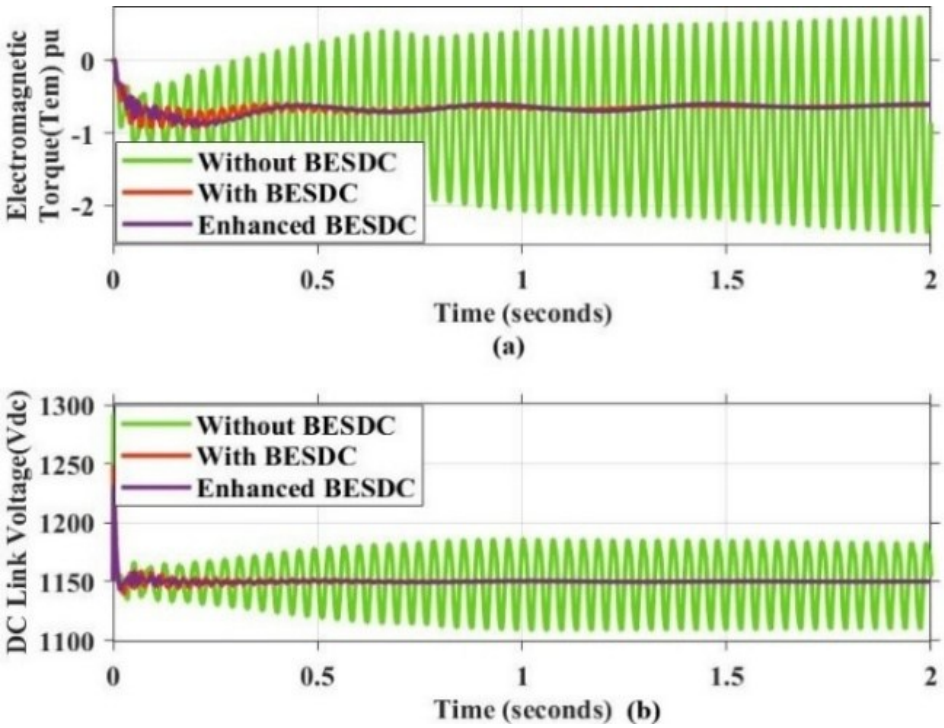

Fig 5.11 The output response of with, without and enhanced BESDC at 11m/s wind speed and 50% SCTL (a) Electromagnetic torque(pu) (b) DC link voltage of DFIG

5.6 Comparison with PSO and UPSO

A comparative analysis is conducted between the conventional PSO and the proposed UPSO techniques for tuning the enhanced BESDC, aimed at alleviating SSR. This evaluation is based on conditions where the wind speed is 9 m/s and SCTL is set to 50%. The dynamic behavior of the DFIG active power and the DC link voltage is illustrated in Fig. 5.12. It confirms that the system retains stability under both PSO and UPSO-based BESDC configurations in the IEEE First Benchmark Model. However, the BESDC tuned with UPSO exhibits improved damping characteristics and a faster transient response compared to the conventional PSO. The results demonstrate the superior performance of the proposed UPSO-based controller in mitigating SSR and enhancing dynamic performance of the overall system.

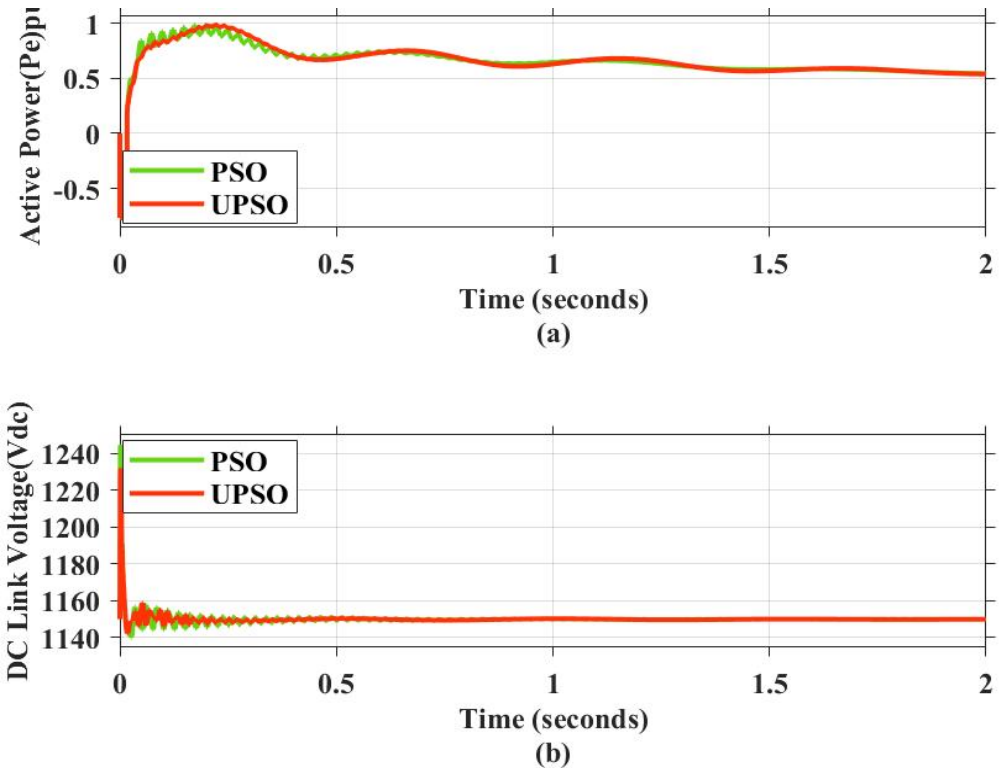

Fig 5.12 Simulation result of PSO and UPSO at 50% SCTL, 9m/s wind speed of (a) Active output power (b) DC-link voltage

Table 5.2 Quantitative Performance Comparison of PSO vs. UPSO for BESDC Tuning

Performance Metric	**PSO**	**UPSO**	**Improvement**
Avg. Convergence Iterations	83	48	42.2% faster convergence
Min Damping Ratio (Critical Mode)	0.067	0.091	+35.8% improvement
Max. Peak Overshoot (Torque, 55% SCTL)	17.2%	12.9%	–24.6%
DC-link Voltage Oscillation Reduction	Baseline	–18.9%	Compared to PSO
Objective Function (Fitness Value)	0.318	0.204	–35.8%
Robustness to Wind Speed Variation	Moderate	High	Qualitative improvement

To further quantify the advantages of UPSO, Table 5.2 presents a comparative evaluation of convergence characteristics, damping performance, and control effectiveness under identical operating conditions. UPSO not only achieves global convergence

approximately 42% faster than PSO but also improves the minimum damping ratio of critical electromechanical modes by 35.8%. Time-domain simulations further reveal that UPSO reduces peak overshoot in electromagnetic torque and DC-link voltage oscillations by 24.6% and 18.9% respectively, demonstrating enhanced dynamic response and reduced control effort. These findings support the potential of UPSO for real-time deployment in intelligent grid-connected systems, with future work exploring its implementation on hardware-in-the-loop (HIL) platforms for validation in practical scenarios.

5.7 Conclusion

In comparison with the controllers developed in earlier chapters, a clear and systematic progression of research outcomes can be observed. The conventional BESDC designed in Chapter 4 provided an important baseline solution, offering noticeable improvement in damping performance under nominal wind speeds and moderate levels of series compensation. However, its tuning process was manual and fixed, making it less effective when system parameters such as wind speed, grid strength, or compensation level varied significantly. This limitation highlighted the need for an optimization-based design framework.

Building on this foundation, introduced the PSO-optimized BESDC, which significantly enhanced the robustness of parameter tuning. By employing a global optimization strategy, the PSO-based controller improved damping ratios, shifted critical eigenvalues further into the stable region, and reduced oscillation amplitudes in nonlinear time-domain simulations. Nevertheless, the PSO technique exhibited certain drawbacks, such as the risk of premature convergence and dependency on initial population settings, which could restrict its capability to consistently deliver optimal results across highly nonlinear operating scenarios.

To overcome these challenges, Chapter 5 developed the UPSO-optimized BESDC, which incorporates chaotic initialization, adaptive inertia weight adjustment, and improved velocity–position update mechanisms. These enhancements not only strengthen the global search ability of the optimization process but also ensure faster convergence and avoidance of local minima. The UPSO-based controller consistently

demonstrated superior performance compared to both the conventional BESDC and the PSO-optimized design, achieving higher damping ratios, faster oscillation decay, reduced overshoot, and improved stability margins across all operating conditions considered. This stepwise development—progressing from a fixed-parameter conventional BESDC, to a PSO-based intelligent controller, and finally to an UPSO-based advanced controller—clearly illustrates the effectiveness of intelligent optimization algorithms in addressing the nonlinear, time-varying, and uncertain dynamics of DFIG-based wind power systems. The comparative findings not only validate the superiority of the UPSO-based approach but also establish a framework for the design of future adaptive damping controllers in renewable-rich, low-inertia power grids.

CHAPTER 6

STUDY OF TRANSFORMER SATURATION UNDER SSI

6.1 Introduction

SSI has emerged as a critical stability concern in modern power systems dominated by inverter-based renewable generation and series-compensated transmission networks. While extensive research has focused on the electromechanical and control-driven mechanisms of SSI—particularly SSR, SSCCI, and SSTCI—the influence of these oscillations on power transformers remains significantly underexplored. This oversight is notable because transformers possess inherently nonlinear magnetic characteristics, making them highly susceptible to low-frequency disturbances that accompany SSI events. In a series-compensated network, subsynchronous frequency components (typically 10–40 Hz) can resonate with the electrical system and propagate into transformer windings. When these components superimpose on the fundamental grid voltage, they alter the voltage–flux trajectory, causing cumulative flux build-up within the core. As a result, the transformer may enter deep saturation, even under otherwise normal operating conditions. Core saturation leads to distorted magnetizing currents, generation of intermodulation sidebands, harmonic pollution, and potential maloperation of protective devices. Such distortions not only degrade power quality but also pose a risk of thermal stress, excessive vibration, and compromised insulation life. Given the increasing deployment of series compensation and the high penetration of DFIG-based wind farms, understanding SSI-induced transformer behaviour is vital for grid reliability. This chapter develops a detailed nonlinear transformer model capable of capturing saturation dynamics under sub-synchronous excitation. Through impedance-frequency analysis and time-domain simulations, the study identifies resonant conditions, flux overshoot patterns, harmonic signatures, and stability thresholds. These findings provide essential insights for equipment protection, system planning, and defining safe compensation limits in SSI-prone corridors.

6.2 Study System

For a more detailed analysis, this study focuses on a long transmission line equipped with series compensation to boost the power transfer capacity of the existing network. The system under investigation is inspired by the real-world Hydro-Quebec network. As shown in Fig.6.1, the study system is represented by a single-line diagram of a 3-phase, 60 Hz, 735 kV transmission line operating under weak load conditions.

The transmission line spans 600 km and delivers power from a generating station equipped with six generators, each rated at 350 MVA, to the receiving system. The 600 km line is divided into two segments of 300 km each, interconnected through buses B1, B2, and B3. Each segment is a series compensated line with 30% of the line's reactance compensated to enhance power transfer capability. Additionally, a 330 Mvar shunt reactor is for shunt compensation on both lines.

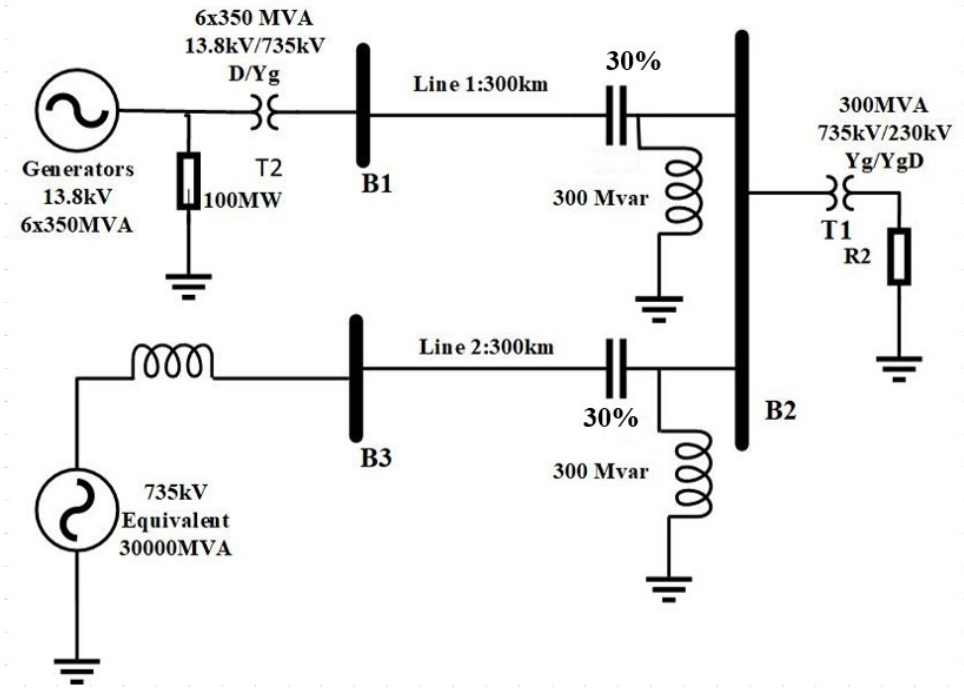

Fig 6.1 Single line diagram of considering power system

6.3 Mathematical Modeling

6.3.1 Transformer flux dynamics and saturation condition

The core flux $\phi(t)$ is governed by Faraday's law of induction, integrating the terminal voltage $v(t)$[176], [177]:

$$\phi(t) = \frac{1}{N}\int v(t)dt \tag{6.1}$$

For a voltage comprising fundamental (f_s=60 Hz) and subsynchronous components[18]:

$$v(t) = \sqrt{2}V_S \sin(2\pi f_s t) + \sqrt{2}V_{SSR} \sin(2\pi f_{SSR} t) \tag{6.2}$$

The flux becomes:

$$\phi(t) = \underbrace{\frac{V_S}{2\pi f_s}[1 - \cos(2\pi f_s t)]}_{\phi_{fund(t)}} + \underbrace{\frac{V_{SSR}}{2\pi f_{SSR}}[1 - \cos(2\pi f_{SSR} t)]}_{\phi_{SSR(t)}} \tag{6.3}$$

The worst-case peak flux occurs when fundamental and SSR components align in phase:

$$\phi_{peak} = \frac{V_S}{2\pi f_s} + \frac{V_{SSR}}{2\pi f_{SSR}} \tag{6.4}$$

Expressed in per-unit (pu) relative to nominal flux ($\phi_{base} = \frac{V_{base}}{2\pi f_s}$)

$$\phi_{peak} = V_S^{pu} + V_{SSR}^{pu} \cdot \frac{f_s}{f_{SSR}} \tag{6.5}$$

Transformer saturation occurs when the magnetic flux $\phi(t)$ exceeds the material-specific knee-point flux ϕ_{sat}, beyond which the magnetizing inductance sharply reduces. The saturation condition is mathematically expressed as[178]:

$$\phi_{peak} > \phi_{sat} \tag{6.6}$$

Where ϕ_{sat} is the saturation knee point (typically 1.15–1.28 pu). The saturation severity is quantified by the excess flux ratio:

$$\gamma = \frac{\phi_{peak}}{\phi_{sat}} - 1 \tag{6.7}$$

Under saturation, magnetizing current $i_m(t)$ exhibits piecewise behaviour[177]:

$$i_m(\phi) = \begin{cases} \dfrac{\phi}{L_m}, & \phi \le \phi_{sat} \\ \dfrac{\phi_{sat}}{L_m} + k(\phi - \phi_{sat})^7, & \phi > \phi_{sat} \end{cases} \tag{6.8}$$

Where k is the saturation coefficient (0.1–0.3 pu) and L_m is the unsaturated inductance. This model captures the essential features of both linear magnetization and the nonlinear saturation region, and is implemented using a piecewise or lookup-table-based core characteristic. Fig.6.2 illustrates the detailed computational workflow for

saturation assessment.

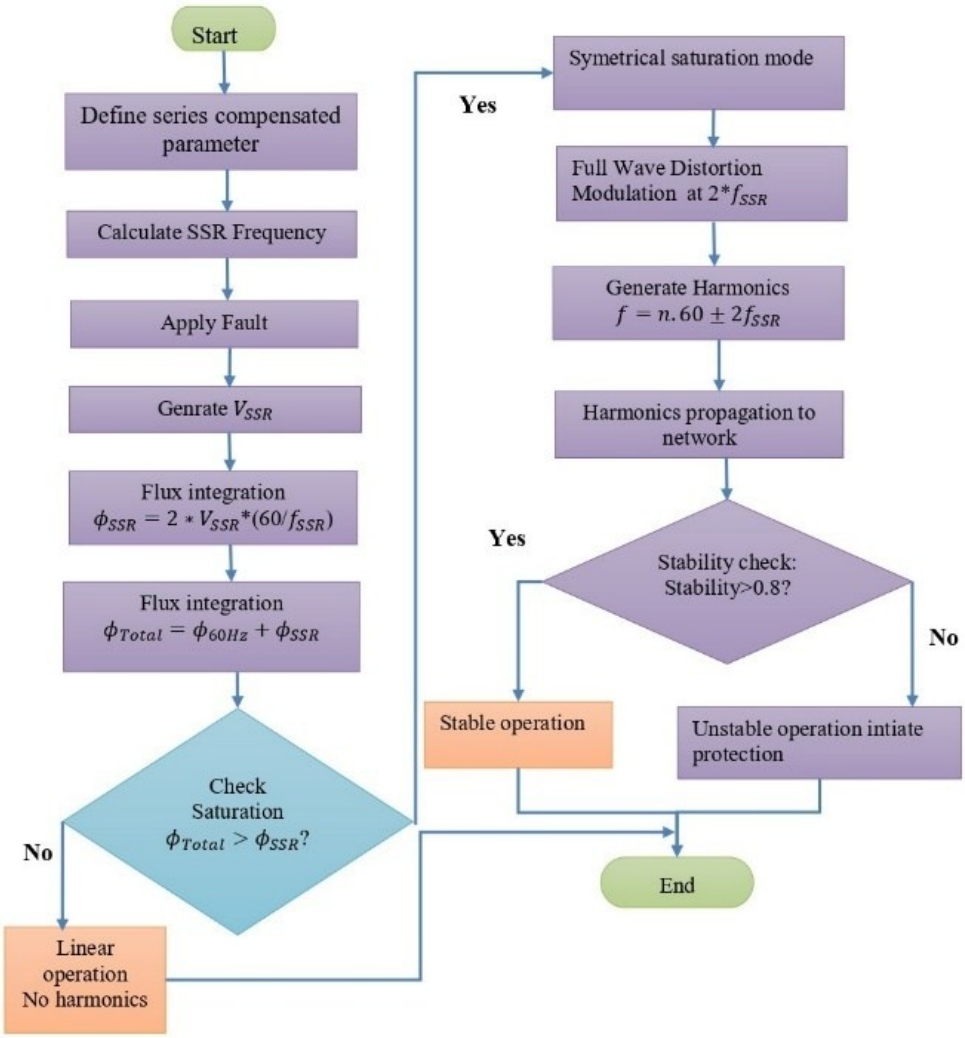

Fig 6.2 Workflow for transformer saturation and stability assessment during faults

6.4 Demodulation due to transformer saturation

The flux waveform enters the saturation region when its magnitude exceeds the saturation threshold ϕ_{sat}. Beyond this point, the magnetizing current becomes nonlinear[179].

Let $i_m(t)$ represent the magnetizing current, which under saturation becomes a nonlinear function of flux, $i_m = f_{NL}(\phi)$. For analytical approximation, consider a Taylor series expansion:

$$i_m(t) = a_1\phi(t) + a_2\phi^2(t) + a_3\phi^3(t) + \cdots \tag{6.9}$$

Here, the nonlinear terms (quadratic and cubic) introduce harmonic and intermodulation components due to trigonometric product identities. We now analyze how frequency components mix under square and cube of $\phi(t)$. [179]

$$\phi(t) \approx Acos(2\pi f_1 t) + Bcos(2\pi f_{SSR} t) \tag{6.10}$$

Squaring equation(6.10), we get

$$\phi^2(t) = A^2 cos^2(2\pi f_1 t) + 2ABcos(2\pi f_1 t)\cos(2\pi f_{SSR} t) + B^2 cos^2(2\pi f_{SSR} t) \tag{6.11}$$

Using formula,

$$\cos(a)\cos(b) = \frac{1}{2}[\cos(a+b) + \cos(a-b)] \tag{6.12}$$

and

$$cos^2(x) = \frac{1}{2}[1 + \cos(2x)] \tag{6.13}$$

Substituting, we get terms in $\phi^2(t)$ at the following frequencies: (i) DC(0 Hz), $2f_1$, (ii) $2f_{SSR}$ and, (iii) $f_1 + f_{SSR}$, $f_1 - f_{SSR}$.

Thus, the quadratic term introduces sidebands at $f_1 \pm f_{SSR}$. Similarly, the cubic term $\phi^3(t)$ introduces the following terms: $f_1 \pm 2f_{SSR}$, $3f_1$, $3f_{SSR}$, etc.

Hence, the full spectrum of the magnetizing current contains:

- Fundamental: $f_1 = 60\ Hz$
- Sidebands: $f_1 \pm f_{SSR}$, $f_1 \pm 2f_{SSR}$
- Harmonics: $2f_1$, $3f_1$,….
- Modulated harmonics: $2f_1 \pm f_{SSR}$, $3f_1 \pm f_{SSR}$,…

This phenomenon is mathematically analogous to amplitude modulation in communications, where a high-frequency carrier f_1 is modulated by a low-frequency signal f_{SSR}[180]. The transformer saturation acts as a nonlinear demodulator, converting low-frequency SSR oscillations into amplitude variations in the magnetizing current and its harmonics. Thus, transformer saturation under SSR acts as a nonlinear frequency mixer, producing sidebands and spreading energy across a wider spectrum.

These sidebands can degrade power quality, interfere with protection schemes, or trigger maloperation of relays sensitive to harmonic content. They also violate the assumptions of sinusoidal steady-state used in many control designs and impedance-based models[181]

6.5 Simulation results and case studies

6.5.1 Frequency response analysis of the system model

Impedance versus frequency analysis is a vital tool for evaluating the dynamic severity of a power system. It helps identify critical factors such as line losses, generation characteristics, and load impacts by analyzing the location and magnitude of resonance points. A defining feature of series-compensated transmission systems is the presence of subsynchronous modes, with impedance zeros and poles appearing below the nominal power frequency. Severe resonance can occur if the mechanical torsional mode of the turbo-generator shaft closely aligns with a system impedance zero.

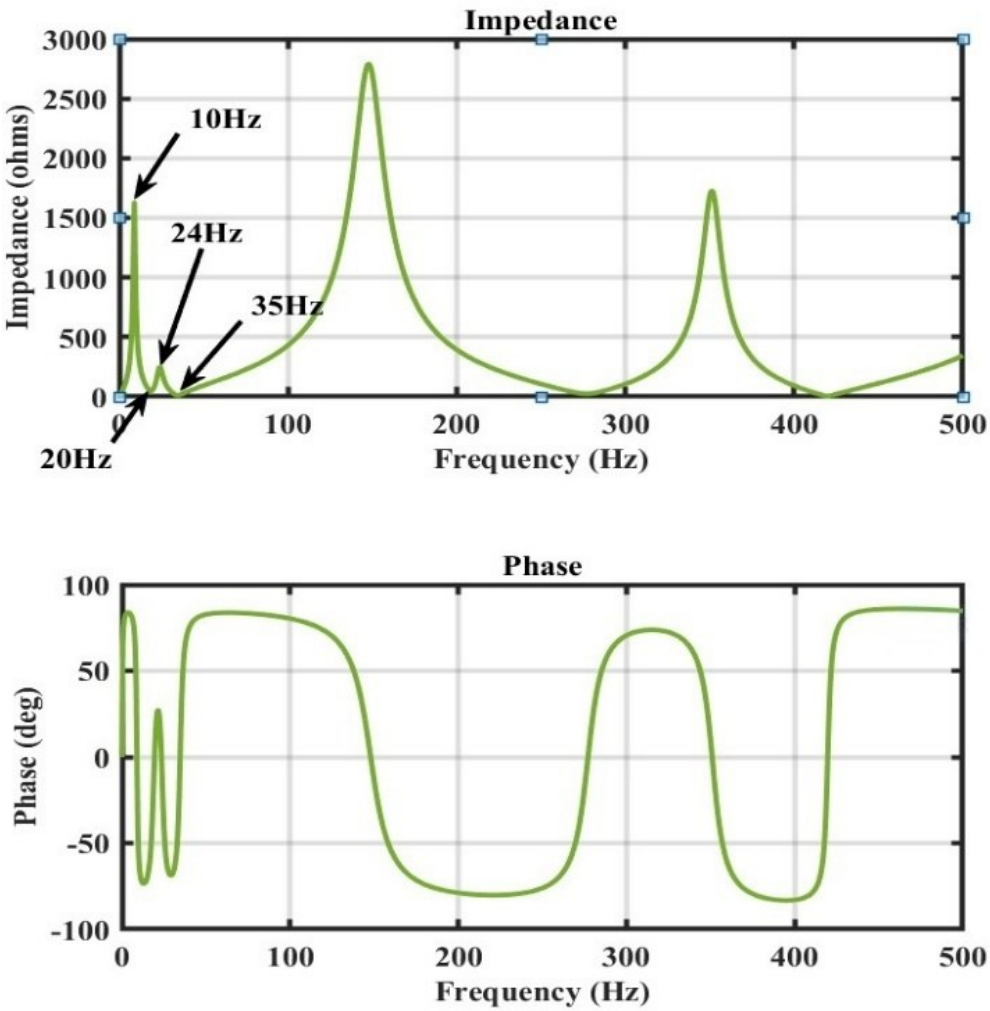

Fig 6.3 Positive sequence impedance versus frequency characteristics of a series compensated power system at 30% of series compensation

In such cases, the corresponding impedance pole at the subsynchronous frequency can amplify voltage magnitudes, potentially leading to transformer core saturation.
The Thevenin positive impedance at bus 2 is illustrated in Fig. 6.3, along with the positive sequence magnitude and phase of the system model. The types of resonance that occur in the system are detailed as follows:

- *Series Resonance (20 Hz):* Occurs due to the interaction between the series capacitor and line inductance. Its frequency shifts with the degree of series compensation.
- *Parallel Resonance (10 Hz):* Results from the combined effect of shunt reactors and series compensation, leading to a peak in system impedance.
- *Distributed Parameter Resonance:* Caused by the 600 km line's series inductance and shunt capacitance, often excited during fault clearing.

These resonance modes critically affect system performance under fault conditions, especially in relation to SSR and transformer saturation.

6.5.2 Time-domain simulations

To evaluate the impact of SSR on transformer saturation and voltage modulation, a detailed simulation study is conducted. The test system includes a 300 MVA, 735/230 kV transformer (T_1) energized from the high-voltage side through a 13.8 kV, 300 km transmission line, consisting of two parallel circuits, each with 30% fixed series compensation. A three-phase symmetrical fault is applied on line 2 at bus B_2, lasting three cycles (0.05 s). The objective is to assess the transformer's flux and magnetizing current response under subsynchronous excitation triggered during and after fault clearing.

Case 1: saturation of transformer

Fig. 6.4(a) shows the fault current waveform I_a, with a sudden increase during the fault and a complex recovery phase post-clearance. When examining the A-phase voltage at bus B_2 [Fig. 6.4(b)], a 10 Hz subsynchronous oscillation becomes evident immediately following the fault. This is further confirmed in the frequency spectrum [Fig.6.4(c)], which exhibits a sharp component at 10 Hz. This 10 Hz component superimposed on the 60 Hz fundamental results in cumulative flux build-up in the transformer core. After fault clearing, the voltage magnitude recovers; however, due to the presence of this low-

frequency oscillation, the magnetic flux overshoots the linear region and enters the saturation domain. As shown in Fig.6.5(a), the flux rises to 1.89 pu, well beyond the saturation knee point (1.28 pu). The resulting magnetizing current waveform in Fig.6.5(b) displays symmetrical pulses, which confirms symmetrical saturation—i.e., the core saturates in both positive and negative directions of the flux swing.

Case 2: voltage modulation

The symmetrical saturation induces significant modulation effects in the magnetizing current and terminal voltage. Fig.6.6(a) shows the frequency spectrum of the magnetizing current, which contains:

- Sidebands at 40 Hz and 80 Hz, resulting from 20 Hz modulation of the 60 Hz waveform. These originate from the half-period pulse trains caused by the 10 Hz flux oscillation.
- Odd harmonics (e.g., 3rd, 5th, 7th) are also modulated at 20 Hz, introducing amplitude-modulated spectral features.
- Even harmonics emerge due to residual waveform asymmetries and are modulated at 10 Hz, as evidenced by new components at: 110 Hz = 120 − 10 Hz and 130 Hz = 120 + 10 Hz.

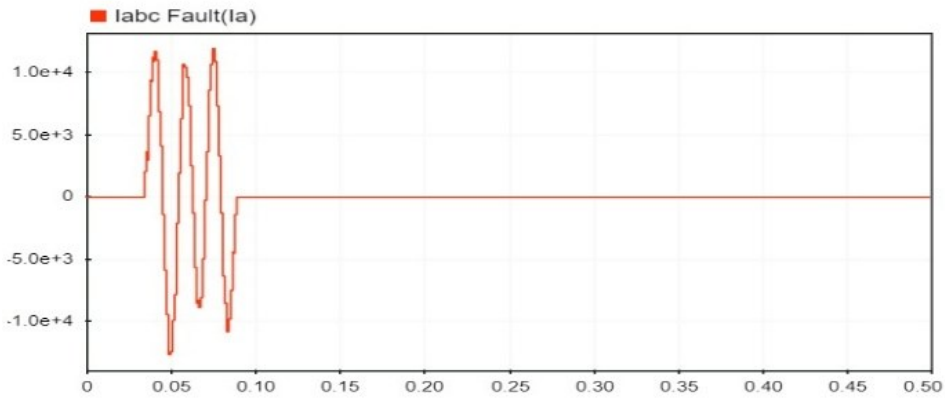

(a)

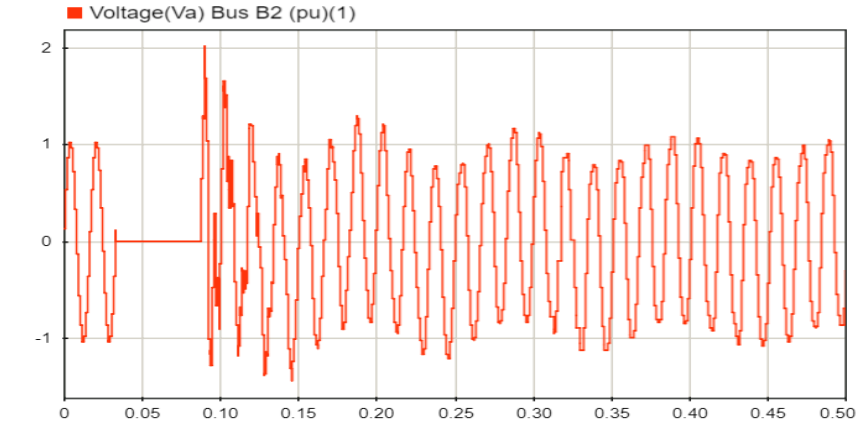

(b)

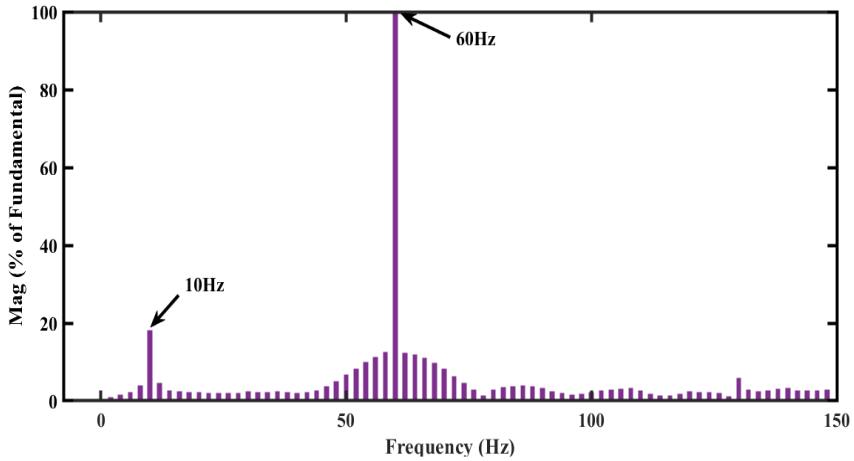

(c)

Fig 6.4 (a)Three-phase line to ground fault current at line 2. (b) Bus voltage at B2. (c) Frequency spectrum of bus voltage of phase A.

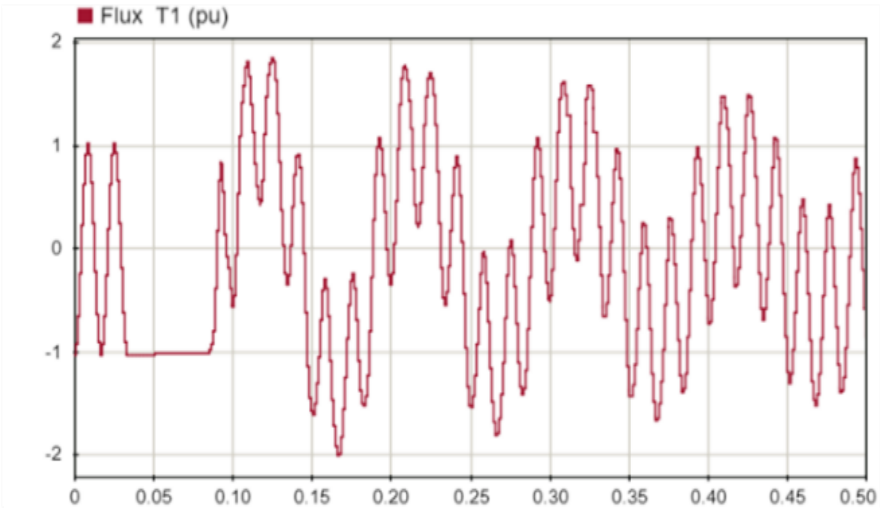

(a)

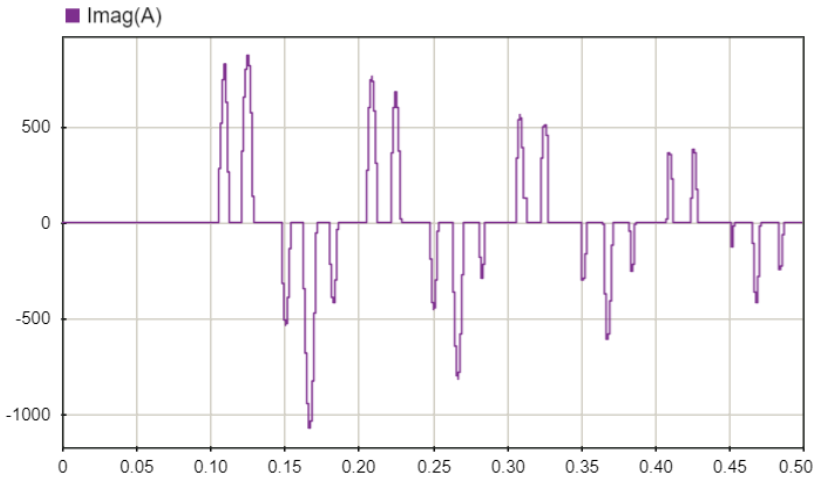

(b)

Fig 6.5 Impact of transformer saturation at a subsynchronous frequency:(a) Transformer core flux (b) Transformer magnetizing current

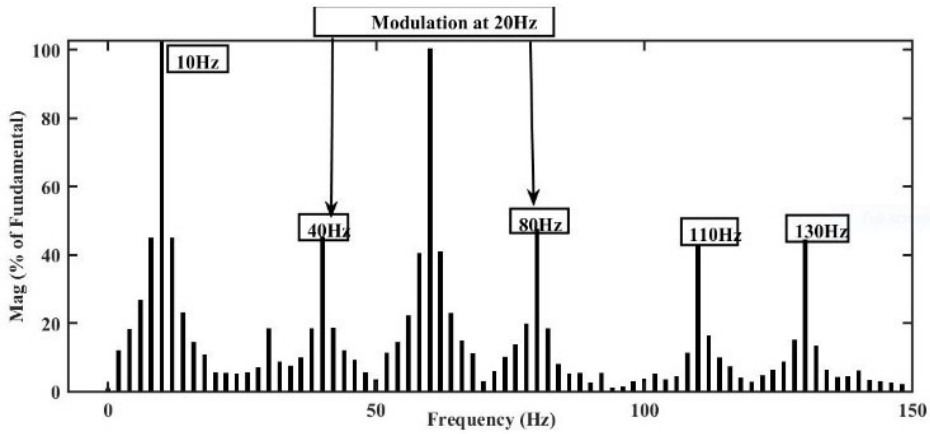

(a)

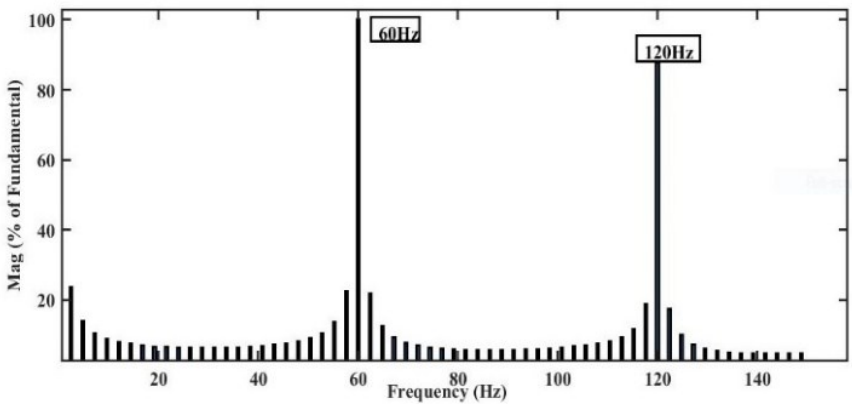

(b)

Fig 6.6 Impact of transformer saturation at a subsynchronous frequency (a)Frequency spectrum of magnetizing current with series compensated (b)Without series compensation

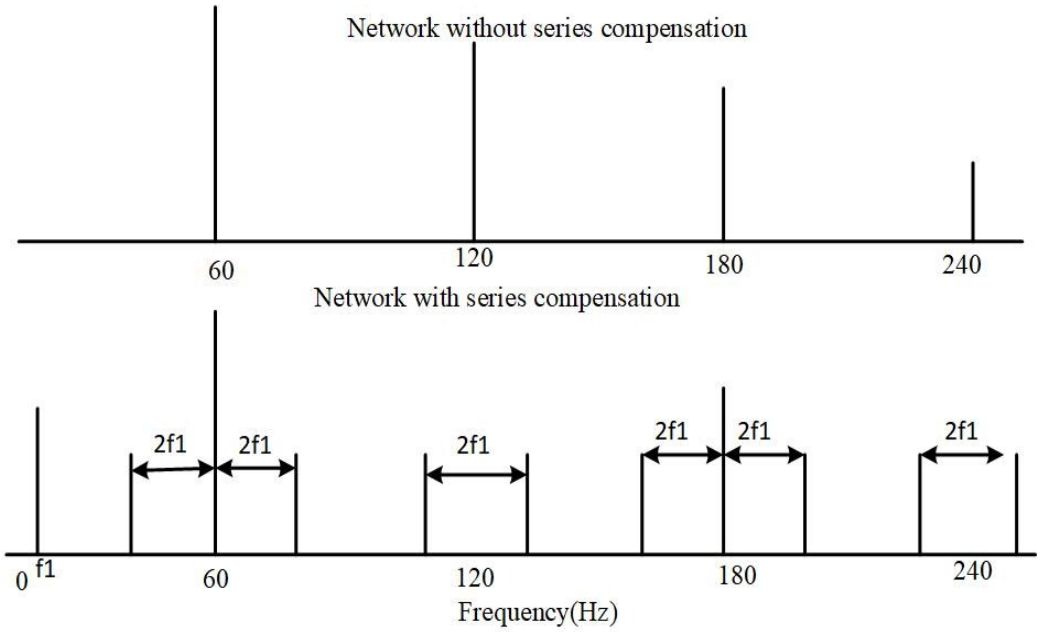

Fig 6.7 Magnetizing current spectrum of the transformer during fault clearing, with and without series compensation(SSR at f1)

This demonstrates the complex harmonic and intermodulation behaviour resulting from transformer saturation under subsynchronous excitation. In contrast, Fig.6.6(b) shows the magnetizing current spectrum without series compensation. While harmonics are still present, no sidebands are observed, confirming that series compensation intensifies the nonlinear response and introduces spectral broadening through modulation. Fig.6.7 offers a direct comparison between both cases, emphasizing that series-compensated networks are more prone to deep saturation and spectral distortion, increasing the potential for operational instability and insulation stress due to harmonic propagation.

Case 3: effect of series compensation level

The comprehensive analysis of series compensation levels (0-80%) reveals a critical trade-off between power transfer enhancement and SSR risks. As compensation increases from 20% to 80%, the series resonance frequency decreases from 25.3 Hz to 14.1 Hz following the relationship $f_{series} = 60\sqrt{K_c}$, while shunt resonance declines from 12.7 Hz to 7.1 Hz according to $f_{shunt} = 10/\sqrt{K_c}$ illustrates in Fig.6.8. This frequency reduction triggers two destabilizing mechanisms: First, the flux gain factor

$G_\phi = 1/\sqrt{K_c}$ increases exponentially, amplifying transformer saturation vulnerability – at 40% compensation, a 0.014 pu SSR voltage generates 34% more flux than at 20% compensation. Second, the damping ratio decays linearly ($\zeta = 0.08 - 0.015K_c$), dropping below the 0.05 stability threshold at 33% compensation.

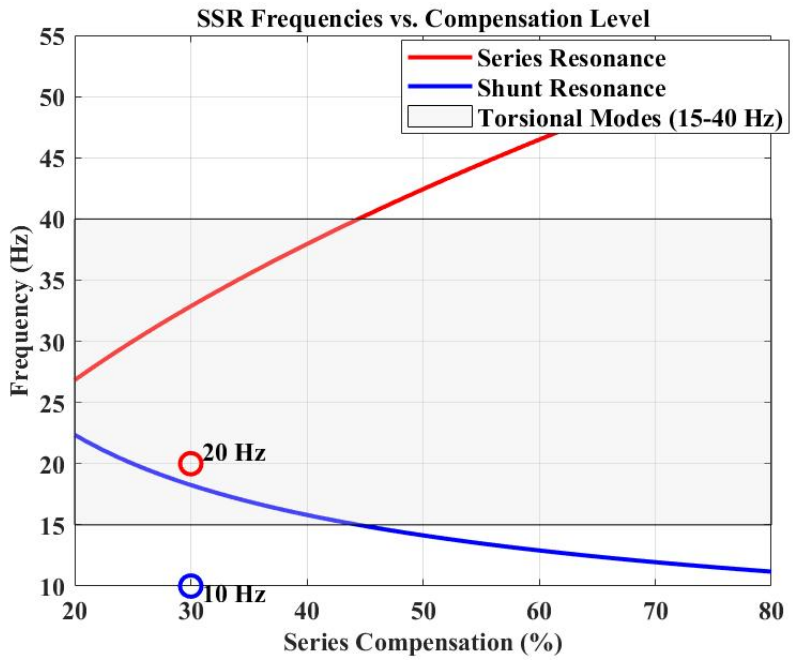

Fig 6.8 SSR frequencies vs. compensation showing dangerous 20 Hz/10 Hz resonances at 30% compensation (torsional zone: gray).

The stability index ($\zeta \times f_{series} \times G_\phi$), delineates three operational regions as shown in Fig.6.9: (i) Safe zone($K_c < 0.28, index > 1.0$)where frequencies remain above 25 Hz, avoiding torsional mode overlaps; (ii) Marginal zone ($0.28 \leq K_c \leq 0.35, index < 0.8 - 1.0$) characterized by 20-25 Hz resonances where transformer saturation occurs during severe disturbances; and (iii) Unstable zone ($K_c < 0.35, index < 0.8$) where frequencies below 20 Hz cause uncontrolled oscillation growth. For the 30% compensation case study (K_C=0.3,index=0.86), the 20 Hz series resonance coincides with turbo-generator Mode 2 (18-22 Hz), while the 10 Hz shunt resonance induces saturation at remarkably low disturbance voltages (0.014 pu). This configuration exhibits only 14% stability margin, with fault clearing events generating flux peaks up to 3.4 pu (266% above saturation knee).

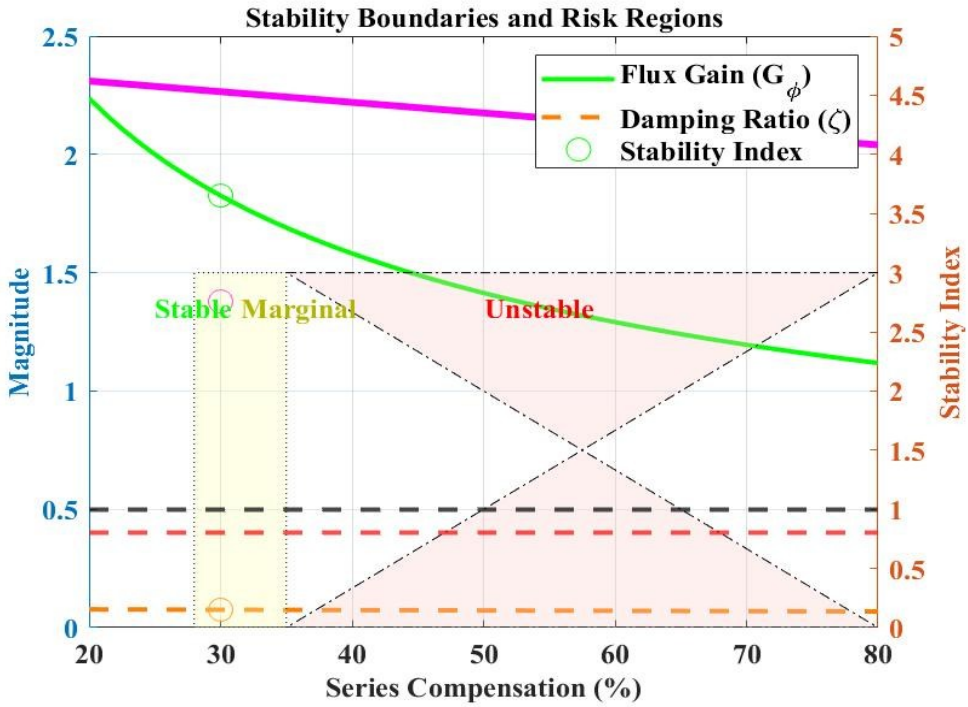

Fig 6.9 Stability thresholds vs. compensation. 30% case (marked) in marginal zone with flux gain >1.25 and damping ratio near instability limit

Critically, the SSR-stability relationship exhibits strong nonlinearity: Beyond 35% compensation, every 1% increase reduces the stability index by 8.2% while boosting flux gain by 1.4%. To ensure secure operation, compensation should be limited to 28% (K_C=0.28), maintaining frequencies above 25 Hz and damping ratio ζ > 0.05. For existing 30% compensated systems, mitigation requires 20 Hz notch filtering and flux-based control interventions at $\phi > 1.20\phi_{sat}$. These findings establish 35% compensation as an absolute upper limit – beyond which SSR-induced saturation causes uncontrollable voltage collapse regardless of control system enhancements.

6.6 Conclusion

This chapter has provided a comprehensive analysis of transformer saturation dynamics under subsynchronous resonance in series-compensated transmission systems, highlighting a critical nonlinear phenomenon that is often neglected in classical SSR stability studies. The major conclusions drawn are as follows:

- Subsynchronous resonance at frequencies as low as 5–15 Hz can lead to

transformer core saturation, even when SSR voltage components are of relatively low magnitude. The interaction of these frequencies with the 60 Hz fundamental waveform causes substantial flux excursions.

- Series compensation significantly lowers the SSR frequency, thereby increasing the overlap with transformer dynamic sensitivities. Higher compensation levels are directly correlated with deeper and more persistent saturation conditions.
- Transformer saturation leads to complex voltage and current waveforms, characterized by pulse-like magnetizing currents, subharmonic oscillations, and intermodulation sidebands. These include spectral components at 40 Hz, 80 Hz, 110 Hz, and 130 Hz, which may degrade system power quality and affect protective devices.

These findings emphasize the importance of considering nonlinear transformer behaviour in SSR assessments, particularly as future grids adopt more series compensation and long-distance transmission. Future research may explore real-time SSR detection, hardware-based saturation control, and integration of damping support using grid-scale energy storage systems.

CHAPTER 7

CONCLUSION, FUTURE SCOPE AND SOCIAL IMPACT

7.1 Conclusion

The research presented in this thesis has addressed the critical problem of SSI in DFIG-based WPP integrated with SCTL networks. The increasing penetration of renewable energy, while essential for meeting global decarbonization and sustainability goals, has introduced dynamic challenges that are significantly different from those encountered in conventional synchronous generator-dominated grids. Among these, SSI remains one of the most severe concerns, capable of causing catastrophic equipment failures, widespread outages, and long-term degradation of system reliability if not effectively mitigated.

At the outset, a comprehensive review and classification of SSI phenomena was conducted. Traditional SSI classifications such as SSR were expanded to encompass more recent developments like Sub-Synchronous Converter Control Interaction and Sub-Synchronous Torsional Control Interaction. This extended framework provided a holistic view of the multiple interaction pathways that arise in converter-dominated renewable energy systems. Several historical incidents, including those in the U.S., China, and Europe, were analyzed to highlight the severity of the issue and to establish the real-world significance of the problem.

The key contribution of this research has been the design, optimization, and validation of advanced damping controllers to mitigate SSI. Starting with conventional BESDC, the study introduced optimization techniques based on UPSO. Comparative analysis through eigenvalue studies and nonlinear time-domain simulations confirmed that the proposed UPSO-based BESDC delivers:

- Enhanced damping ratios for critical SSI modes,
- Reduced overshoot in transient responses,

- Faster stabilization following disturbances,
- Robust performance across a wide range of wind speeds and series compensation levels, and
- Superior adaptability compared to conventional and PSO-based controllers.

This establishes the UPSO-based BESDC as a promising and scalable solution for ensuring stable integration of large-scale wind energy into existing grids. Furthermore, the modular and flexible nature of BESS ensures easier deployment, relatively low maintenance requirements, and multipurpose use for grid services beyond SSI mitigation.

The second major contribution of this thesis lies in highlighting the impact of SSI on transformer saturation. While much of the literature traditionally focused on turbine-generator shaft dynamics, this work demonstrated that transformers are equally vulnerable components, particularly under post-fault SSR conditions. By developing a nonlinear flux–voltage integral model, it was shown that subsynchronous voltage components, especially during fault-clearing scenarios, can drive transformers into deep nonlinear regions, causing core saturation, flux overshoot, magnetizing current distortion, harmonic generation, and spectral sideband formation. These effects are unique compared to other known causes of transformer saturation such as DC bias, geomagnetically induced currents, or inrush currents, thereby representing a distinct risk mechanism for modern grids. Time-domain simulations confirmed that higher levels of series compensation exacerbate these nonlinear effects, reducing stability margins and increasing the likelihood of saturation-induced protection malfunctions.

From a broader perspective, the thesis demonstrates that a combined approach of nonlinear equipment modeling and advanced damping controller design is essential for realistic SSI studies in renewable-dominated systems. By explicitly considering transformer nonlinearities and adopting optimization-driven control methods, the research bridges a critical gap between theoretical models and real-world operational challenges.

In summary, the conclusions drawn from this thesis can be encapsulated as follows:

1. **Extended SSI Framework:** An expanded classification of SSI phenomena has been established, covering electromechanical, control-based, and converter-based interactions in both conventional and renewable-integrated grids.
2. **Transformer Vulnerability:** Transformers, often neglected in SSR studies, are shown to be highly susceptible to post-fault SSR-induced saturation, leading to harmonic distortion, protection issues, and potential insulation failures.
3. **Nonlinear Flux Modeling:** A nonlinear flux–voltage integral model successfully captured the dynamics of transformer saturation under subsynchronous excitation, offering new insights into harmonic propagation and sideband formation.
4. **Series Compensation Risks:** Higher levels of series compensation significantly lower resonance frequencies, magnify flux overshoot, and shrink stability margins, identifying safe operating zones and dangerous instability thresholds.
5. **Optimized Damping Control:** Among various control approaches, the UPSO-based BESDC outperformed conventional and PSO-based designs, proving its capability as a flexible, adaptive, and reliable mitigation strategy for SSI.
6. **Bridging Theory and Practice:** The findings highlight the necessity of integrating nonlinear transformer dynamics and optimization-driven damping control into future SSI studies for realistic risk assessment and robust mitigation.

Collectively, these contributions provide a strong foundation for enhancing grid stability, asset protection, and renewable energy integration**,** thereby addressing one of the most critical challenges facing modern power systems.

7.2 Future Scope

Although this thesis has achieved significant progress, there remain several avenues for further investigation and refinement. Some of the most promising directions for future research are outlined below:

- **Experimental Validation and Hardware-in-the-Loop (HIL) Studies:** While this research has relied on MATLAB/Simulink-based modeling and simulations, experimental verification using Real-Time Digital Simulators (RTDS) and HIL platforms is necessary for practical validation. Scaled laboratory prototypes incorporating DFIGs, series-compensated networks, and energy storage systems can provide valuable insights into controller performance under real operating conditions.
- **Hybrid Energy Storage Integration:** The present work focused on BESS-based damping. Future studies can explore hybrid systems that combine batteries with Superconducting Magnetic Energy Storage (SMES), flywheels, or ultracapacitors. Such combinations can exploit the complementary advantages of fast response and high energy density, thereby enhancing damping effectiveness.
- **Transformer-Oriented Mitigation and Protection**: Since this thesis highlighted the vulnerability of transformers under SSI, future research may focus on flux-based relays, adaptive saturation detection, and transformer-friendly damping strategies. Developing early warning schemes for flux excursions can prevent catastrophic insulation failures.
- **Artificial Intelligence and Machine Learning Approaches**: Beyond PSO and UPSO, advanced AI techniques such as reinforcement learning, neural networks, and fuzzy-logic-based adaptive controllers could be employed to design next-generation damping strategies. These methods could offer self-learning and predictive capabilities for highly uncertain renewable grids.
- **Grid Code Integration and Policy Implications**: With the growing penetration of renewable energy, grid codes may eventually mandate SSI damping requirements. Embedding optimized damping strategies, such as

UPSO-BESDC, into standard DFIG control architectures could ensure compliance and accelerate deployment in real-world networks.

- **Impact of Multi-Energy Systems and Sector Coupling**: The role of SSI in future integrated energy systems—such as wind-hydrogen, wind-solar hybrid plants, and microgrids—remains largely unexplored. These coupled systems present new interaction pathways and potential resonance risks that demand further analysis.

7.3 Social Impact

The societal implications of this research are significant, particularly in the context of the global transition to sustainable energy systems:

- **Reliable Grid Operation**: By mitigating SSI, the proposed damping strategies enhance the stability of renewable-dominated power systems, reducing the risk of blackouts and large-scale disruptions. This ensures secure electricity supply to industries, businesses, and households.
- **Asset Protection and Economic Savings**: Transformer saturation, shaft fatigue, and converter damage can lead to costly equipment failures. The proposed solutions help protect high-value infrastructure, extend equipment lifespans, and reduce operational and maintenance costs for utilities.
- **Environmental Sustainability**: Effective SSI mitigation facilitates the integration of higher levels of wind energy into the grid. This reduces reliance on fossil-fuel-based generation, contributing directly to carbon reduction goals and environmental protection.
- **Economic Growth and Energy Security**: Stable renewable integration lowers the cost of outages and improves investor confidence in clean energy projects. In countries with growing electricity demand, such solutions contribute to energy security, job creation, and economic development.
- **Public Trust in Renewable Energy**: Ensuring power quality and stability increases public confidence in renewable integration. A reliable, clean energy supply strengthens societal acceptance of large-scale wind farms and other renewable projects, accelerating the global energy transition.

Reference

[1] C.-C. Chu, S.-H. Lee, K. L. Lian, J.-H. Liu, and Y.-J. Lin, "A Survey of Global Revisions to Grid Codes on System Inertia and Frequency Stability in Power Grids with High Renewable Energy Integration," in *2025 IEEE Industry Applications Society Annual Meeting (IAS)*, 2025, pp. 1–8.

[2] M. A. Basit, S. Dilshad, R. Badar, and S. M. Sami ur Rehman, "Limitations, challenges, and solution approaches in grid-connected renewable energy systems," *Int. J. Energy Res.*, vol. 44, no. 6, pp. 4132–4162, 2020.

[3] K. Gu, F. Wu, and X. P. Zhang, "Sub-synchronous interactions in power systems with wind turbines: A review," *IET Renew. Power Gener.*, vol. 13, no. 1, pp. 4–15, 2019.

[4] C. Jung, D. Schindler, and J. Laible, "National and global wind resource assessment under six wind turbine installation scenarios," *Energy Convers. Manag.*, vol. 156, pp. 403–415, 2018.

[5] M. Arshad and B. O'Kelly, "Global status of wind power generation: theory, practice, and challenges," *International Journal of Green Energy*, vol. 16, no. 14. pp. 1073–1090, 2019.

[6] N. Verma, N. Singh, S. Yadav, and S. Gupta, "Reactive power compensation of solid state transformer for WECS," in *2018 2nd International Conference on Electronics, Materials Engineering and Nano-Technology, IEMENTech 2018*, 2018.

[7] L. Yunhong, L. Hui, N. Wenyuan, and X. Xiaorong, "Impact on SSR of wind farms connected to series-compensated lines from the different structures of power grid," *J. Eng.*, vol. 2017, no. 13, pp. 2158–2163, 2017.

[8] F. M. Albatsh, S. Mekhilef, S. Ahmad, H. Mokhlis, and M. A. Hassan, "Enhancing power transfer capability through flexible AC transmission system devices: a review," *Front. Inf. Technol. Electron. Eng.*, vol. 16, no. 8, pp. 658–678, 2015.

[9] Y. Zhang, C. Klabunde, and M. Wolter, "Study of resonance issues between DFIG-based offshore wind farm and HVDC transmission," *Electr. Power Syst. Res.*, vol. 190, p. 106767, 2021.

[10] A. S. Trevisan *et al.*, "Analysis of low frequency interactions of DFIG wind turbine systems in series compensated grids," *Electr. Power Syst. Res.*, vol. 191, p. 106845, 2021.

[11] A. Kunwar and R. C. Bansal, "Effect of high-voltage direct current link on small signal stability of a power system with different penetration level of doubly fed induction generator and direct drive synchronous generator based wind farms," *International Journal of Green Energy*, vol. 13, no. 4. International Journal of Green Energy, pp. 335–343, 2016.

[12] A. Aziz, A. Than Oo, and A. Stojcevski, "Frequency regulation capabilities in wind power plant," *Sustain. Energy Technol. Assessments*, vol. 26, no. September, pp. 47–76, 2018.

[13] L. Wang, X. Xie, H. Liu, Y. Zhan, J. He, and C. Wang, "Review of emerging SSR / SSO issues and their classi fi cations," *J. Eng.*, vol. 2017, no. October, pp. 1666–1670, 2017.

[14] J. Li and X. Zhang, "Impact of increased wind power generation on subsynchronous resonance of turbine-generator units," *J. Mod. Power Syst. Clean Energy*, vol. 4, pp. 219–228, 2016.

[15] X. Zhu, Q. Zhou, N. Zhang, Z. Chen, J. Zhao, and M. Jin, "SSO of DFIG-based wind farm integrated by a hybrid series compensator," *J. Eng.*, vol. 2019, no. 16, pp. 798–801, 2019.

[16] W. Du, Z. Zhen, and H. Wang, "The Subsynchronous Oscillations Caused by an LCC HVDC Line in a Power System under the Condition of Near Strong Modal Resonance," *IEEE Trans. Power Deliv.*, vol. 34, no. 1, pp. 231–240, 2019.

[17] J. Samanes, E. Gubia, J. Lopez, and R. Burgos, "Sub-Synchronous Resonance Damping Control Strategy for DFIG Wind Turbines," *IEEE Access*, vol. 8, no. 1, pp. 223359–223372, 2020.

[18] K. R. Padiyar, *Analysis of Subsynchronous Resonance in Power Systems*. Springer US, 1999.

[19] J. Shair, X. Xie, L. Yuan, Y. Wang, and Y. Luo, "Monitoring of subsynchronous oscillation in a series-compensated wind power system using an adaptive extended Kalman filter," pp. 4193–4203, 2021.

[20] J. Shair, X. Xie, L. Wang, W. Liu, J. He, and H. Liu, "Overview of emerging subsynchronous oscillations in practical wind power systems," *Renew. Sustain. Energy Rev.*, vol. 99, pp. 159–168, 2019.

[21] L. Fan, S. Member, C. Zhu, and S. Member, "Modal Analysis of a DFIG-Based Wind Farm Interfaced With a Series Compensated Network," *IEEE Trans. Energy Convers.*, vol. 26, no. 4, pp. 1010–1020, 2011.

[22] H. Liu, X. Xie, C. Zhang, Y. Li, H. Liu, and Y. Hu, "Quantitative SSR Analysis of Series-Compensated DFIG-Based Wind Farms Using Aggregated RLC Circuit Model," *IEEE Trans. Power Syst.*, vol. 32, no. 1, pp. 474–483, 2017.

[23] M. Mokhtari, J. Khazaei, and D. Nazarpour, "Sub-synchronous resonance damping via doubly fed induction generator," *Int. J. Electr. Power Energy Syst.*, vol. 53, pp. 876–883, 2013.

[24] J. Li, X. Yuan, M. Zhang, and Z. Liu, "Analysis on SSR frequency components by studying two-dimensional modulation of synchronous generator ' s flux linkage," *J. Eng.*, vol. 2019, no. 16, pp. 1313–1318, 2019.

[25] J. A. Member *et al.*, "ERCOT Experience with Sub-Synchronous Control Interaction and Proposed Remediation," *PES T&D 2012*, pp. 1–5, 2012.

[26] J. Adams, V. A. Pappu, and A. Dixit, "ERCOT experience screening for Sub-Synchronous Control Interaction in the vicinity of series capacitor banks," *IEEE Trans. Power Syst.*, pp. 1–5, 2015.

[27] Y. Cheng, M. Sahni, D. Muthumuni, and B. Badrzadeh, "Reactance Scan Crossover-Based Approach for Investigating SSCI Concerns for DFIG-Based," *EEE Tmmaaions Power Deliv.*, vol. 28, no. 2, pp. 742–751, 2013.

[28] B. Badrzadeh *et al.*, "Sub-synchronous Interaction in Wind Power Plants- Part I : Study Tools and Techniques," *EEE Power Energy Soc. Gen. Meet.*, pp. 1–9, 2012.

[29] H. A. Mohammadpour, A. Ghaderi, and E. Santi, "Analysis of sub-synchronous resonance in doubly-fed induction generator-based wind farms interfaced with gate – controlled series capacitor," *IET Gener. Transm. Distrib.*, vol. 8, no. May, pp. 1998–2011, 2014.

[30] K. Gu, F. Wu, and X. Zhang, "Sub-synchronous interactions in power systems with wind turbines : a review," *IET Renew. Power Gener. Spec.*, 2018.

[31] R. K. Varma, S. Auddy, and Y. Semsedini, "Mitigation of Subsynchronous Resonance in a Series-Compensated Wind Farm Using FACTS Controllers," *IEEE Trans. Power Deliv.*, vol. 23, no. 3, pp. 1645–1654, 2008.

[32] M. Sahni *et al.*, "Sub-synchronous interaction in wind power plants- part II: An ercot case study," *IEEE Power Energy Soc. Gen. Meet.*, pp. 1–9, 2012.

[33] H. Liu *et al.*, "Subsynchronous Interaction between Direct-Drive PMSG Based Wind Farms and Weak AC Networks," *IEEE Trans. Power Syst.*, vol. 32, no. 6, pp. 4708–4720, 2017.

[34] X. Xie, S. Member, W. Liu, H. Liu, Y. Du, and Y. Li, "A System-Wide Protection Against Unstable SSCI in Series-Compensated Wind Power Systems," *IEEE Trans. Power Deliv.*, vol. 33, no. 6, pp. 3095–3104, 2018.

[35] R. Langella, A. Testa, and A. E. Emanuel, "On the effects of subsynchronous interharmonic voltages on power transformers: Three phase units," *2009 IEEE Power Energy Soc. Gen. Meet. PES '09*, vol. 23, no. 4, pp. 2480–2487, 2009.

[36] S. Rezaei, "An Adaptive Algorithm Based on Subharmonic and Time Domain Analysis to Prevent Mal Operation of Overcurrent Relay During Subsynchronous Resonance," *IEEE Trans. Ind. Appl.*, vol. 54, no. 3, pp. 2085–2096, 2018.

[37] M. Wu, L. Xie, L. Cheng, and R. Sun, "A Study on the Impact of Wind Farm Spatial Distribution on Power System Sub-Synchronous Oscillations," *IEEE Trans. Power Syst.*, vol. 31, no. 3, pp. 2154–2162, 2016.

[38] H. Liu and X. Xie, "Impedance network modeling and quantitative stability analysis of sub-/super-synchronous oscillations for large-scale wind power systems," *IEEE Access*, vol. 6, pp. 34431–34438, 2018.

[39] X. Xie *et al.*, "Characteristic Analysis of Subsynchronous Resonance in Practical Wind Farms Connected to Series-Compensated Transmissions," *IEEE Trans. Energy Convers.*, vol. 32, no. 3, pp. 1117–1126, 2017.

[40] D. A. H. Walker, D.N., C.E.J. Bowler, R.L. Jackson, "Results of subsynchronous resonance test at Mohave," *IEEE Trans. Power Appar. Syst.*, 1975.

[41] J. W. Butler and C. Concordia, "Analysis of: Series Capacitor Application Problems,"

Trans. Am. Inst. Electr. Eng., vol. 56, no. 8, pp. 975–988, 1937.

[42] D. N. E. and C. C. C. E. J. Bowler, "Self Excited Torsional Frequency Oscillations with Series Capacitors," *IEEE Trans. Power Appar. Syst.*, vol. PAS-92, no, pp. 1688–1695, 1973.

[43] X. Xie, H. Liu, H. Liu, and Q. Jiang, "A two-level SSR protection system and its application at the Shangdu Power Plant," *Int. J. Electr. Power Energy Syst.*, vol. 64, pp. 1229–1236, 2015.

[44] W. Watson and M. E. Coultes, "Static Exciter Stabilizing Signals on Large Generators - Mechanical Problems," *IEEE Trans. Power Appar. Syst.*, 1972.

[45] E. R. Taylor and R. B. Starnes, "A bibliography for the study of subsynchronous resonance between rotating machines and power systems: IEEE Committee Report," *IEEE Trans. Power Appar. Syst.*, vol. 95, no. 1, pp. 216–218, 1976.

[46] M. Bahrman *et al.*, "Experience with HVDC - Turbine-Generator Torsional Interaction at Square Butte," *IEEE Trans. Power Appar. Syst.*, no. 3, pp. 966–975, 1980.

[47] R. G. Farmer, A. L. Schwalb, and E. Katz, "Navajo Project Report on Subsynchronous Resonance Analysis and Solutions.," *IEEE Trans. Power Syst.*, no. 4, 1977.

[48] M. C. H. L.A. Kilgore, D.G. Ramey, "Simplified transmission and generation system analysis procedures for subsynchronous resonance problems," *IEEE Trans. Power Appar. Syst.*, pp. 1840–1846, 1977.

[49] I. C. Report, "First Supplement To a Bibliography for the Study of Subsynchronous Resonance Between Rotating Machines and Power Systems.," *IEEE Trans. Power Appar. Syst.*, no. 6, pp. 1872–1875, 1979.

[50] I. C. Reports, "Supplement Study Bibliography Subsynchronous Rotating Systems," *IEEE Power Eng. Rev.*, no. February, p. 34, 1985.

[51] R. E. Beaulieu, "Effects of Governor Characteristics on Turbo-Generator Shaft Torsionals," *IEEE Trans. Power Appar. Syst.*

[52] I. C. Report, "Reader's guide to subsynchronous resonance," *IEEE Trans. Power Syst.*, vol. 7, no. 1, pp. 150–157, 1992.

[53] M. R. I. et Al, "Fourth supplement to a bibliography for the study of subsynchronous resonance between rotating machines and power systems," *IEEE Trans. Power Syst.*, vol. 12, no. 3, 1997.

[54] Anon, "Proposed Terms and Definitions for Subsynchronous Oscillations.," *IEEE Trans. Power Appar. Syst.*, no. 2, pp. 506–511, 1979.

[55] R. A. Hedin, S. Member, and L. E. Eilts, "SSR characteristics of alternative types of series compensation schemes," *IEEE Trans. Power Syst.*, vol. 10, no. 2, 1995.

[56] S. Chernet, M. Beza, and M. Bongiorno, "Investigation of subsynchronous control interaction in DFIG-based wind farms connected to a series compensated transmission line," *Electr. Power Energy Syst.*, vol. 105, pp. 765–774, 2019.

[57] R. K. Varma and A. Moharana, "SSR in Double-Cage Induction Generator-Based

Wind Farm Connected to Series-Compensated Transmission Line," vol. 28, no. 3, pp. 2573–2583, 2013.

[58] A. Moharana, Member, and R. K. Varma, "Modal Analysis of Type-1 Wind Farm Connected to Series Compensated Transmission," *IEEE Electr. Power Energy Conf. Modal*, pp. 202–209, 2012.

[59] F. Blaabjerg, K. Ma, and Y. Yang, "Power electronics for renewable energy systems – Status and trends," *CIPS 2014; 8th Int. Conf. Integr. Power Electron. Syst.*, pp. 25–27, 2014.

[60] J. Adams, C. Carter, and S. H. Huang, "ERCOT experience with Sub-synchronous Control Interaction and proposed remediation," *Proc. IEEE Power Eng. Soc. Transm. Distrib. Conf.*, pp. 1–5, 2012.

[61] F. Salehi, I. B. M. Matsuo, and W. J. Lee, "Detection of Sub-Synchronous Control Interaction (SSCI) Using Modal Identification Analysis and FFT," *2018 North Am. Power Symp. NAPS 2018*, pp. 1–5, 2018.

[62] S. Velpula, R. Thirumalaivasan, and M. Janaki, "A review on SubSynchronous Resonance and its mitigation techniques in DFIG based wind farms," *Int. J. Renew. Energy Res.*, vol. 8, no. 4, pp. 2275–2288, 2018.

[63] L. Fan, R. Kavasseri, Z. L. Miao, and C. Zhu, "Modeling of DFIG-based wind farms for SSR analysis," *IEEE Trans. Power Deliv.*, vol. 25, no. 4, pp. 2073–2082, 2010.

[64] N. Verma and N. Kumar, "DFIG - Based Wind Plant Coupled Series Compensated Transmission Line : Modeling and SSR Stability Analysis," *J. Inst. Eng. Ser. B*, 2022.

[65] X. Xie, X. Guo, Y. Han, and S. Member, "Mitigation of Multimodal SSR Using SEDC in the Shangdu Series-Compensated Power System," *IEEE Trans. Power Syst.*, vol. 26, no. 1, pp. 384–391, 2011.

[66] Y. Cheng *et al.*, "Real-World Subsynchronous Oscillation Events in Power Grids with High Penetrations of Inverter-Based Resources," *IEEE Trans. Power Syst.*, vol. 8950, no. c, pp. 1–15, 2022.

[67] H. A. Mohammadpour, E. Santi, and S. Member, "Analysis of Subsynchronous Control Interactions in DFIG-based Wind Farms : ERCOT Case Study," *IEEE Energy Convers. Congr. Expo.*, pp. 500–505, 2015.

[68] J. Sun and I. Vieto, "Development and Application of Type-III Turbine Impedance Models Including DC Bus Dynamics," *IEEE Open J. Power Electron.*, vol. 1, pp. 513–528, 2020.

[69] Y. Li, L. Fan, and Z. Miao, "Replicating Real-World Wind Farm SSR Events," *IEEE Trans. Power Deliv.*, vol. 35, no. 1, pp. 339–348, 2020.

[70] National Grid ESO, "Technical Report on the events of 9 August 2019," *Tech. Rep.*, no. September, pp. 2–38, 2019.

[71] J. Shair, X. Xie, W. Liu, X. Li, and H. Li, "Modeling and stability analysis methods for investigating subsynchronous control interaction in large-scale wind power systems," *Renew. Sustain. Energy Rev.*, vol. 135, p. 110420, 2021.

[72] S. Member, L. Harnefors, and F. B. Fellow, "Analysis and Mitigation of SSCI in DFIG Systems With Experimental Validation," *IEEE Trans. Energy Convers.*, vol. PP, no. c, p. 1, 2019.

[73] L. Wang, X. Xie, Q. Jiang, H. Liu, Y. Li, and H. Liu, "Investigation of SSR in Practical DFIG-Based Wind Farms Connected to a Series-Compensated Power System," *IEEE Trans. Power Syst.*, vol. 30, no. 5, pp. 2772–2779, 2015.

[74] W. Du, Q. Fu, and H. Wang, "Subsynchronous Oscillations Caused by Open-Loop Modal Coupling between VSC-Based HVDC Line and Power System," *IEEE Trans. Power Syst.*, vol. 33, no. 4, pp. 3664–3677, 2018.

[75] M. A. M. and A. E. P. N. Rostamkolai, R. J. Piwko, E. V. Larsen, D. A. Fisher, "Subsynchronous torsional interactions with static var compensators-in fluence of hvdc," *IEEE Trans. Power Syst.*, no. 1, pp. 255–261, 1991.

[76] W. Du, C. Chen, and H. Wang, "Subsynchronous Interactions Induced by DFIGs in Power Systems Without Series Compensated Lines," *IEEE Trans. Sustain. Energy*, vol. 9, no. 3, pp. 1275–1284, 2018.

[77] Y. Liu, J. Zheng, Q. Chen, Z. Duan, Y. Tian, and M. Ban, "MMC-STATCOM supplementary wide-band damping control to mitigate subsynchronous control interaction in wind farms," *Int. J. Electr. Power Energy Syst.*, vol. 141, no. April, p. 108171, 2022.

[78] A. E. Leon, S. Member, J. M. Mauricio, and S. Member, "Mitigation of Subsynchronous Control Interactions Using Multi-Terminal DC Systems," *IEEE Trans. Sustain. Energy*, vol. 12, no. 1, pp. 420–429, 2021.

[79] N. Prabhu and K. R. Padiyar, "Investigation of subsynchronous resonance with VSC-based HVDC transmission systems," *IEEE Trans. Power Deliv.*, vol. 24, no. 1, pp. 433–440, 2009.

[80] R. J. P. and H. S. P. M. Bahrman, E. V. Larsen, "Experience with HVDC - Turbine-Generator Torsional Interaction at Square Butte," *IEEE Trans. Power Appar. Syst.*, no. 3, pp. 966–975, 1980.

[81] L. Wang, "Modal control of an HV DC system for the damping of subsynchronous oscillations," *IEE Proc. C (Generation, Transm. Distrib.*, vol. 136, no. 2, pp. 78–86, 1989.

[82] E. Larsen and D. Fisher, "Design of a supplementary modulation control function for the Chester SVC," *IEEE Trans. Power Deliv.*, vol. 8, no. 2, pp. 719–724, 1993.

[83] S. Zhao, N. Wang, R. Li, B. Gao, B. Shao, and S. Song, "Sub-synchronous control interaction between direct-drive PMSG-based wind farms and compensated grids," *Int. J. Electr. Power Energy Syst.*, vol. 109, no. January, pp. 609–617, 2019.

[84] T. Rauhala, "On effect of HVDC on subsynchronous damping," *8th IEE Int. Conf. AC DC Power Transm.*, no. 3, pp. 125–129, 2006.

[85] M. Du, Buyang and Zhu, Jianhang and Hu, Jiabing and Guo, Zeren and Shao, Dejun and Xu, Youping and Shi, "Subsynchronous Oscillation Research of LCC-HVDC

Receiving End System with Large-scale Renewable Power Generation," *2022 IEEE 5th Int. Electr. Energy Conf.*, pp. 3374–3379, 2022.

[86] S. Kovacevic, D. Jovcic, P. Rault, and O. Despouys, "Three-way Subsynchronous Torsional Interactions Between LCC HVDC , MMC HVDC and a Thermal Generator," *J. Mod. Power Syst. Clean Energy*, vol. XX, no. Xx, pp. 1–10, 2022.

[87] H. Xia, X. Zhou, L. Hong, J. Guo, Y. Liu, and H. Yin, "Interactions analysis and quadrature voltage compensation control for stabilizing LCC-HVDC system with multiple STATCOMs," *Int. J. Electr. Power Energy Syst.*, vol. 142, no. PA, p. 108251, 2022.

[88] B. Gao, P. Deng, Y. Wang, H. Yu, and B. Ren, "Evaluation of damping of subsynchronous interaction between direct-drive wind farm and LCC-HVDC based on the damping path analysis," *Int. J. Electr. Power Energy Syst.*, vol. 144, p. 108532, 2022.

[89] V. B. Virulkar and G. V Gotmare, "Sub-synchronous resonance in series compensated wind farm : A review," *Renew. Sustain. Energy Rev.*, vol. 55, pp. 1010–1029, 2016.

[90] X. Xie, X. Guo, Y. Han, and S. Member, "Mitigation of Multimodal SSR Using SEDC in the Shangdu Series-Compensated Power System," *IEEE Trans. Power Syst.*, vol. 26, no. 1, pp. 384–391, 2011.

[91] X. Xie, L. Wang, X. Guo, Q. Jiang, Q. Liu, and Y. Zhao, "Development and Field Experiments of a Generator Terminal Subsynchronous Damper," *IEEE Trans. Power Electron.*, vol. 29, no. 4, pp. 1693–1701, 2014.

[92] P. Systems, W. H. Renewables, and H. Liu, "An Oscillatory Stability Criterion Based on the Unified dq -Frame Impedance Network Model for," *IEEE Trans. Power Syst.*, vol. 33, no. 3, pp. 3472–3485, 2018.

[93] H. Liu, S. Member, X. Xie, S. Member, and C. Zhang, "Quantitative SSR Analysis of Series-Compensated DFIG-Based Wind Farms Using Aggregated RLC Circuit Model," *IEEE Trans. Power Syst.*, vol. 32, no. 1, pp. 474–483, 2017.

[94] K. Dey, M. Kumar, and A. M. Kulkarni, "Comparison of dynamic phasor , discrete-time and frequency scanning based SSR models of a TCSC ☆," *Electr. Power Syst. Res.*, vol. 196, no. February, p. 107237, 2021.

[95] N. Johansson, S. Member, and L. Ängquist, "A Comparison of Different Frequency Scanning Methods for Study of Subsynchronous Resonance," *IEEE Trans. Power Syst.*, vol. 26, no. 1, pp. 356–363, 2011.

[96] I. M. Canay, "A novel approach to the torsional interaction and electrical damping of the synchronous machine: Part II: Application to an arbitrary network," *IEEE Trans. Power Appar. Syst.*, vol. PAS-101, no. 10, pp. 3639–3647, 1982.

[97] W. Zhai, Q. Jia, and G. Yan, "Analysis of sub synchronous oscillation characteristics from a direct drive wind farm based on the complex torque coefficient method," *CSEE J. Power Energy Syst. Power Energy Syst.*, pp. 1–10, 2021.

[98] X. Peng, R. Chen, J. Zhou, S. Qin, R. Bi, and H. Sun, "Research on Mechanism and

Damping Control Strategy of DFIG-Based Wind Farm Grid-Connected System SSR Based on the Complex Torque Method," *Electonics*, vol. 10, no. 14, 2021.

[99] N. Verma and N. Kumar, "SSR Stability Analysis and Modeling for DFIG Connected to Series Compensated Transmission Line," *IEI Conf.*, no. 2021: 36.IEC.

[100] M. Abdeen *et al.*, "A Recent Analytical Approach for Analysis of Sub-Synchronous Resonance in Doubly-Fed Induction Generator-Based Wind Farm," *IEEE Access*, vol. 9, pp. 68888–68897, 2021.

[101] Z. Din *et al.*, "Recent development and future trends of resonance in doubly fed induction generator system under weak grid," *IET Renew. Power Gener.*, vol. 16, no. 5, pp. 807–834, 2022.

[102] H. Li, J. Shair, J. Zhang, and X. Xie, "Investigation of Subsynchronous Oscillation in a DFIG-based Wind Power Plant Connected to MTDC Grid," *IEEE Trans. Power Syst.*, 2022.

[103] M. A. Chowdhury, M. A. Mahmud, W. Shen, and H. R. Pota, "Nonlinear Controller Design for Series-Compensated DFIG-Based Wind Farms to Mitigate Subsynchronous Control Interaction," *IEEE Trans. Energy Convers.*, vol. 32, no. 2, pp. 707–719, 2017.

[104] C. Z. M. H. Z. Wu, "Parameters impact on the performance of a double-fed induction generator-based wind turbine for subsynchronous resonance control," *IET Renew. Power Gener.*, vol. 6, pp. 92–98, 2012.

[105] L. Zhang, L. Harnefors, and H. P. Nee, "Interconnection of two very weak AC systems by VSC-HVDC links using power-synchronization control," *IEEE Trans. Power Syst.*, vol. 26, no. 1, pp. 344–355, 2011.

[106] Z. Lidong, H. Lennart, and H. Nee, "Power-Synchronization Control of Grid-Connected," *IEEE Trans. Power Syst.*, vol. 25, no. 2, pp. 809–820, 2010.

[107] H. Xie, B. Li, C. Heyman, M. M. De Oliveira, and M. Monge, "Subsynchronous resonance characteristics in presence of doubly-fed induction generator and series compensation and mitigation of subsynchronous resonance by proper control of series capacitor," *IET Renew. Power Gener.*, vol. 8, no. 4, pp. 411–421, 2014.

[108] M. Sahraei-ardakani and S. A. Blumsack, "Market-Based Operation of Series FACTS Devices," *IEEE Trans. Power Syst.*, vol. 31, no. 5, pp. 3702–3714, 2016.

[109] H. A. Mohammadpour, M. Islam, E. Santi, and Y. Shin, "SSR Damping in Fixed-Speed Wind Farms Using Series FACTS Controllers," *IEEE Trans. Power Deliv.*, vol. 31, no. 1, pp. 76–86, 2016.

[110] A. Ghorbani, B. Mozaffari, and A. M. Ranjbar, "Application of subsynchronous damping controller (SSDC) to STATCOM," *Int. J. Electr. Power Energy Syst.*, vol. 43, no. 1, pp. 418–426, 2012.

[111] N. Kumar and M. P. Dave, "Application of an auxiliary controlled static var system for damping subsynchronous resonance in power systems iLd en," *Electr. Power Syst. Res.*, vol. 37, pp. 189–201, 1996.

[112] R. P. Carpanen and B. S. Rigby, "Electrical Power and Energy Systems An improved

SSSC-based power flow controller design method and its impact on torsional interaction," *Int. J. Electr. Power Energy Syst.*, vol. 43, no. 1, pp. 194–209, 2012.

[113] X. Zhang, X. Xie, H. Liu, and Y. Li, "Robust subsynchronous damping control to stabilise SSR in series-compensated wind power systems," *IET Gener. Transm. Distrib.*, vol. 13, no. 3, pp. 337–344, 2019.

[114] L. Wang, X. Xie, Q. Jiang, and X. Liu, "Centralised solution for subsynchronous control interaction of doubly fed induction generators using voltage-sourced converter," *IET Gener. Transm. Distrib.*, vol. 9, no. 16, pp. 2751–2759, 2015.

[115] X. Zhang, X. Xie, H. Liu, H. Liu, Y. Li, and C. Zhang, "Mitigation of Sub-Synchronous Control Interaction in Wind Power systems with GA-SA tuned Damping Controller," *IFAC-PapersOnLine*, vol. 50, no. 1, pp. 8740–8745, 2017.

[116] R. K. Varma, S. Member, R. Salehi, and S. Member, "SSR Mitigation With a New Control of PV Solar Farm as STATCOM (PV-STATCOM)," *IEEE Trans. Sustain. Energy*, vol. 8, no. 4, pp. 1473–1483, 2017.

[117] K. Li, M. Liu, W. Zheng, Y. Li, and X. Wang, "The research of SSR which can be restrained by photovoltaic grid connected," *IOP Conf. Ser. Earth Environ. Sci.*, vol. 121, no. 4, 2018.

[118] M. Khayyatzadeh and R. Kazemzadeh, "Sub-synchronous resonance damping using high penetration PV plant," *Mech. Syst. Signal Process.*, vol. 84, pp. 431–444, 2017.

[119] M. Janaki, N. Prabhu, R. Thirumalaivasan, and D. P. Kothari, "Mitigation of SSR by subsynchronous current injection with VSC HVDC," *Int. J. Electr. Power Energy Syst.*, vol. 57, pp. 287–297, 2014.

[120] J. Lyu, X. Cai, M. Amin, and M. Molinas, "Sub-synchronous oscillation mechanism and its suppression in MMC-based HVDC connected wind farms," *IET Gener. Transm. Distrib.*, vol. 12, no. 4, pp. 1021–1029, 2018.

[121] N. Perera, R. Midence, and V. Liyanage, "Protection for sub synchronous torsional interaction conditions using an industrial sub-harmonic relay," *71st Annu. Conf. Prot. Relay Eng. CPRE 2018*, vol. 2018-Janua, pp. 1–6, 2018.

[122] W. Shin, M. Ko, H.-K. Ku, J. Song, and K. Hur, "Estimation of Structural Mechanical Damping in Multi-mass of Turbine Generator for SSTI Study," *J. Electr. Eng. Technol.*, vol. 17, no. 3, pp. 1639–1650, 2022.

[123] B. Gao, P. Deng, Y. Wang, Y. Liu, and B. Ren, "Evaluation of Damping of Subsynchronous Interaction between Direct-Drive Wind Farm and Lcc-Hvdc Based on the Damping Path Analysis," *SSRN Electron. J.*, vol. 144, p. 108532, 2022.

[124] W. Chen, X. Xie, D. Wang, H. Liu, and H. Liu, "Probabilistic stability analysis of subsynchronous resonance for series-compensated DFIG-based wind farms," *IEEE Trans. Sustain. Energy*, vol. 9, no. 1, pp. 400–409, 2018.

[125] Z. An, C. Shen, Z. Zheng, F. Liu, X. Chang, and W. Wei, "Scenario-based analysis and probability assessment of sub-synchronous oscillation caused by wind farms with direct-driven wind generators," *J. Mod. Power Syst. Clean Energy*, vol. 7, no. 2, pp.

243–253, 2019.

[126] G. Li *et al.*, "Analysis and Mitigation of Subsynchronous Resonance in Series-Compensated Grid-Connected System Controlled by a Virtual Synchronous Generator," *IEEE Trans. Power Electron.*, vol. 35, no. 10, pp. 11096–11107, 2020.

[127] Z. Chai, H. Li, X. Xie, M. Abdeen, T. Yang, and K. Wang, "Output impedance modeling and grid-connected stability study of virtual synchronous control-based doubly-fed induction generator wind turbines in weak grids," *Int. J. Electr. Power Energy Syst.*, vol. 126, p. 106601, Mar. 2021.

[128] H. Khalilinia and J. Ghaisari, "Sub-synchronous resonance damping in series compensated transmission lines using a STATCOM in the common bus," *2009 IEEE Power Energy Soc. Gen. Meet. PES '09*, pp. 1–7, 2009.

[129] M. S. El-moursi, B. Bak-jensen, and M. H. Abdel-rahman, "Novel STATCOM Controller for Mitigating SSR and Damping Power System Oscillations in a Series Compensated Wind Park," *IEEE Trans. power e*, vol. 25, no. 2, pp. 429–441, 2010.

[130] X. Bian, Y. Ding, Q. Jia, L. Shi, X. P. Zhang, and K. L. Lo, "Mitigation of sub-synchronous control interaction of a power system with DFIG-based wind farm under multi-operating points," *IET Gener. Transm. Distrib.*, vol. 12, no. 21, pp. 5834–5842, 2018.

[131] H. A. Mohammadpour, A. Ghaderi, H. Mohammadpour, and E. Santi, "SSR damping in wind farms using observed-state feedback control of DFIG converters," *Electr. Power Syst. Res.*, vol. 123, pp. 57–66, 2015.

[132] S. O. Faried, I. Unal, D. Rai, and J. Mahseredjian, "Utilizing DFIG-based wind farms for damping subsynchronous resonance in nearby turbine-generators," *IEEE Trans. Power Syst.*, vol. 28, no. 1, pp. 452–459, 2013.

[133] D. Dickmander, D. Osborn, and D. Fisher, "Control system design and performance verification for the Chester, Maine static VAr compensator," *EEE Tmmaaions Power Deliv.*, no. 3, 2000.

[134] P. Li, L. Xiong, F. Wu, M. Ma, and J. Wang, "Systems Sliding mode controller based on feedback linearization for damping of sub- synchronous control interaction in DFIG-based wind power plants," *Electr. Power Energy Syst.*, vol. 107, pp. 239–250, 2019.

[135] M. A. Chowdhury and G. M. Shafiullah, "SSR Mitigation of Series-Compensated DFIG Wind Farms by a Nonlinear Damping Controller Using Partial Feedback Linearization," *IEEE Trans. Power Syst.*, vol. 33, no. 3, pp. 2528–2538, 2018.

[136] S. Chernet, M. Beza, and M. Bongiorno, "Investigation of subsynchronous control interaction in DFIG-based wind farms connected to a series compensated transmission line," *Int. J. Electr. Power Energy Syst.*, vol. 105, pp. 765–774, 2019.

[137] M. Ghafouri, U. Karaagac, H. Karimi, S. Jensen, J. Mahseredjian, and S. O. Faried, "An LQR Controller for Damping of Subsynchronous Interaction in DFIG-Based Wind Farms," *IEEE Trans. Power Syst.*, vol. 32, no. 6, pp. 4934–4942, 2017.

[138] P. H. Huang, M. S. El Moursi, W. Xiao, and J. L. Kirtley, "Subsynchronous resonance mitigation for series-compensated dfig-based wind farm by using two-degree-of-freedom control strategy," *IEEE Trans. Power Syst.*, vol. 30, no. 3, pp. 1442–1454, 2015.

[139] K. Gu, F. Wu, and X. Zhang, "Sub-synchronous Interactions in Power Systems with Wind Turbines : A Review," *IET Renew. Power Gener.*, pp. 2–18, 2018.

[140] Y. Wang, Q. Wu, R. Yang, G. Tao, and Z. Liu, "H∞ current damping control of DFIG based wind farm for sub-synchronous control interaction mitigation," *Int. J. Electr. Power Energy Syst.*, vol. 98, pp. 509–519, 2018.

[141] H. Liu, X. Xie, S. Member, Y. Li, H. Liu, and Y. Li, "Damping DFIG-associated SSR with subsynchronous suppression filters: a case study on a practical wind farm system," *IET Conf. Proc.*, 2015.

[142] S. D. Wind, J. Yao, X. Wang, J. Li, R. Liu, and H. Zhang, "Sub-Synchronous Resonance Damping Control Farm With Improved Particle Swarm Optimization Algorithm," *IEEE Trans. Energy Convers.*, vol. 34, no. 2, pp. 849–859, 2019.

[143] H. Liu, X. Xie, Y. Li, H. Liu, and Y. Hu, "Mitigation of SSR by embedding subsynchronous notch filters into DFIG converter controllers," *IET Gener. Transm. Distrib.*, vol. 11, no. 11, pp. 2888–2896, 2017.

[144] A. E. Leon, "Integration of DFIG-Based Wind Farms into Series-Compensated Transmission Systems," *IEEE Trans. Sustain. Energy*, vol. 7, no. 2, pp. 451–460, 2016.

[145] P. Li, J. Wang, L. Xiong, and F. Wu, "Nonlinear controllers based on exact feedback linearization for series-compensated DFIG-based wind parks to mitigate sub-synchronous control interaction," *Energies*, vol. 10, no. 8, 2017.

[146] W. Gil-González, O. D. Montoya, and A. Garces, "Control of a SMES for mitigating subsynchronous oscillations in power systems: A PBC-PI approach," *J. Energy Storage*, vol. 20, no. June, pp. 163–172, 2018.

[147] R. Hemmati, H. Faraji, and N. Y. Beigvand, "Multi objective control scheme on DFIG wind turbine integrated with energy storage system and FACTS devices: Steady-state and transient operation improvement," *Int. J. Electr. Power Energy Syst.*, vol. 135, no. June 2021, p. 107519, 2022.

[148] M. W. Tsang and D. Sutanto, "Damping inter-area oscillation using a battery energy storage system," *IEE Conf. Publ.*, no. 450, pp. 409–414, 1998.

[149] Y. Zhu, C. Liu, K. Sun, D. Shi, and Z. Wang, "Optimization of battery energy storage to improve power system oscillation damping," *IEEE Trans. Sustain. Energy*, vol. 10, no. 3, pp. 1015–1024, 2019.

[150] Z. Moradi-Shahrbabak, "A genetic approach to design an SSR damping controller in a hybrid photovoltaic-battery system by considering the state of charge," *J. Energy Storage*, vol. 108, no. August 2024, 2025.

[151] G. Li, Y. Chen, A. Luo, and H. Wang, "An Enhancing Grid Stiffness Control Strategy of STATCOM/BESS for Damping Sub-Synchronous Resonance in Wind Farm

Connected to Weak Grid," *IEEE Trans. Ind. Informatics*, vol. 16, no. 9, pp. 5835–5845, 2020.

[152] M. F. Ahmed, M. A. Mandor, M. El-Hadidy, and F. M. Bendary, "Fuzzy based battery energy storage system and braking resistor for mitigation of shaft-torsional oscillations," *J. King Saud Univ. - Eng. Sci.*, vol. 33, no. 8, pp. 589–600, 2021.

[153] V. Jain and N. Kumar, "Designing of Supplementary Controller for STATCOM for Damping of Oscillations in Power System," *J. Inst. Eng. Ser. B*, vol. 99, no. 5, pp. 419–429, 2018.

[154] H. A. Mohammadpour and E. Santi, "Modeling and control of gate-controlled series capacitor interfaced with a DFIG-based wind farm," *IEEE Trans. Ind. Electron.*, vol. 62, no. 2, pp. 1022–1033, 2015.

[155] J. Shair, X. Xie, S. Member, J. Yang, J. Li, and H. Li, "Adaptive Damping Control of Subsynchronous Oscillation in DFIG-based Wind Farms Connected to Series-Compensated Network," vol. 8977, no. c, pp. 1–13, 2021.

[156] G. Li, Y. Chen, S. Member, A. Luo, S. Member, and Y. Wang, "An Inertia Phase Locked Loop for Suppressing Sub-synchronous Resonance of Renewable Energy Generation System under Weak Grid," *IEEE Trans. Power Syst.*, vol. 36, no. 5, pp. 4621–4631, 2021.

[157] A. Adrees, *Risk Based Assessment of Subsynchronous Resonance in AC/DC Systems*. 2017.

[158] Y. Lei, A. Mullane, G. Lightbody, and R. Yacamini, "Modeling of the wind turbine with a doubly fed induction generator for grid integration studies," *IEEE Trans. Energy Convers.*, vol. 21, no. 1, pp. 257–264, 2006.

[159] P. S. E. C. IEEE, "IEEE Subsynchronous Resonance Task Force of the Dynamic System Performance Working Group Power System Engineering," *IEEE Trans. Power Appar. Syst.*, vol. PAS-96, no. 5, pp. 1565–1572, 1977.

[160] Y. Lei, A. Mullane, G. Lightbody, and R. Yacamini, "Modeling of the Wind Turbine With a Doubly Fed Induction Generator for Grid Integration Studies," vol. 21, no. 1, pp. 257–264, 2006.

[161] F. and B. P. Mei, "Modal Analysis of Grid-Connected Doubly Fed Induction Generators," *IEEE Trans. Energy Convers.*, vol. 22, no. 3, pp. 1278–1283, 2007.

[162] Y. Cheng, J. Rose, V. A. Pappu, and J. Conto, "Subsynchronous resonance assessment for a large system with multiple series compensated transmission circuits," *IET Renew. Power Gener.*, vol. 13, no. 1, pp. 27–32, 2018.

[163] C. Karunanayake, J. Ravishankar, and Z. Y. Dong, "Nonlinear SSR Damping Controller for DFIG Based Wind Generators Interfaced to Series Compensated Transmission Systems," *IEEE Trans. Power Syst.*, vol. 35, no. 2, pp. 1156–1165, 2020.

[164] L. Piyasinghe, Z. Miao, S. Member, J. Khazaei, L. Fan, and S. Member, "Impedance Model-Based SSR Analysis for TCSC Compensated Type-3 Wind Energy Delivery Systems," vol. 6, no. 1, pp. 179–187, 2015.

[165] M. Eskandari, A. Rajabi, A. V. Savkin, M. H. Moradi, and Z. Y. Dong, "Battery energy storage systems (BESSs) and the economy-dynamics of microgrids: Review, analysis, and classification for standardization of BESSs applications," *J. Energy Storage*, vol. 55, no. PB, p. 105627, 2022.

[166] M. Chen, S. Member, and G. A. Rinc, "Accurate Electrical Battery Model Capable of Predicting Runtime and I – V Performance," *IEEE Trans. Energy Convers.*, vol. 21, no. 2, pp. 504–511, 2006.

[167] M. Beza and M. Bongiorno, "An adaptive power oscillation damping controller by STATCOM with energy storage," *IEEE Trans. Power Syst.*, vol. 30, no. 1, pp. 484–493, 2015.

[168] T. Wu, Y. J. Zhang, and X. Tang, "A VSC-Based BESS Model for Multi-Objective OPF Using Mixed Integer SOCP," *IEEE Trans. Power Syst.*, vol. 34, no. 4, pp. 2541–2552, 2019.

[169] J. L. Agorreta, M. Borrega, J. López, and L. Marroyo, "Modeling and control of N-paralleled grid-connected inverters with LCL filter coupled due to grid impedance in PV plants," *IEEE Trans. Power Electron.*, vol. 26, no. 3, pp. 770–785, 2011.

[170] K. R. Padiar, "Analysis of subsynchronous resonance in power systems," *Springer Sci. \& Bus. Media*, 2012.

[171] K. S. Shim, S. T. Kim, J. H. Lee, E. J. Choi, and J. H. Choi, "Detection of low-frequency oscillation using synchrophasor in wide-area rolling blackouts," *Int. J. Electr. Power Energy Syst.*, vol. 63, pp. 1015–1022, 2014.

[172] T. Rauhala, A. M. Gole, and P. Jarventausta, "Detection of Subsynchronous Torsional Oscillation Frequencies Using Phasor Measurement," *IEEE Trans. Power Deliv.*, vol. 31, no. 1, pp. 11–19, 2016.

[173] P. M. Joshi and H. K. Verma, "Synchrophasor measurement applications and optimal PMU placement: A review," *Electr. Power Syst. Res.*, vol. 199, p. 107428, 2021.

[174] S. Liu *et al.*, "An Improved Particle Swarm Optimization Method for Nonlinear Optimization," *Int. J. Intell. Syst.*, vol. 2024, no. 1, p. 6628110, 2024.

[175] J. Gou, Y.-X. Lei, W.-P. Guo, C. Wang, Y.-Q. Cai, and W. Luo, "A novel improved particle swarm optimization algorithm based on individual difference evolution," *Appl. Soft Comput.*, vol. 57, pp. 468–481, 2017.

[176] C.-M. GHEORGHE, I.-A. Macinic, and A.-G. GHEORGHE, "Oblong core cross-section impact on power transformer characteristics," *Rev. Roum. DES Sci. Tech. ÉLECTROTECHNIQUE ÉNERGÉTIQUE*, vol. 67, no. 3, pp. 281–286, 2022.

[177] S. Abdulsalam, X. Wilsun, W. L. A. Neves, and L. Xian, "Estimation of transformer saturation characteristics from inrush current waveforms," *2006 IEEE Power Eng. Soc. Gen. Meet. PES*, vol. 21, no. 1, pp. 170–177, 2006.

[178] M. Dolinar, D. Dolinar, Š. Gorazd, B. Polajžer, and J. Ritonja, "A three-phase core-type transformer iron core model with included magnetic cross saturation," *IEEE Trans. Magn.*, vol. 42, no. 10, pp. 2849–2851, 2006.

[179] I. Daut, S. Hasan, and S. Taib, “Magnetizing current, harmonic content and power factor as the indicators of transformer core saturation,” *J. Clean Energy Technol.*, vol. 1, no. 4, pp. 304–307, 2013.

[180] J. Berge and R. K. Varma, “Determination of the spectrum of frequencies generated by a saturated transformer,” in *2011 24th Canadian Conference on Electrical and Computer Engineering (CCECE)*, 2011, pp. 1272–1277.

[181] M. Fritsch and M. Wolter, “Saturation of High-Frequency Current Transformers: Challenges and Solutions,” *IEEE Trans. Instrum. Meas.*, vol. 72, pp. 1–10, 2023.

Appendix

I. DFIG Parameters

Parameter	Rating	
	Individual	**Aggregated**
Rated power	1.5MW	100MW
Rated Voltage	575V	575V
Rated Frequency	60Hz	60Hz
R_S	0.023	0.023
X_{lS}	0.18	0.18
R_r	0.016	0.016
X_{lr}	0.16	0.16
X_M	2.9	2.9
DC-link voltage	1150V	1150V
DC-link capacitor	10000μF	67*10000μF

II. Transmission Line Parameters

Parameter	Rating
Transformer Ratio	575V/161kV
Base power	100MVA
R_l	0.02
X_l	0.5
X_C at 50% of series compensated line	64.8 Ω
X_T	0.14
X_{sys}	0.06

III. Drive Train Parameters

Parameter	Rating
H_t	4.32 sec
H_g	0.685 sec
D_t	0
D_g	0
D_{tg}	1.5 p. u
K_{tg}	1.11

IV. PI Parameters of DFIG Converter

Parameter	Rating	Parameter	Rating
K_{P1}	0.2	K_{i1}	0.4
K_{P2}	4	K_{i2}	100
K_{P3}	0.01	K_{i3}	0.04
K_{P4}	4	K_{i4}	100
K_{P5}	0.1	K_{i5}	2
K_{P6}	0.08	K_{i6}	0.5
K_{P7}	0.1	K_{i7}	2
K_{P8}	0.08	K_{i8}	0.5

DELHI TECHNOLOGICAL UNIVERSITY

(Formerly Delhi College of Engineering)

Shahbad Daulatpur, Main Bawana Road, Delhi-42

PLAGIARISM VERIFICATION

Title of the Thesis **"Analysis of Subsynchronous Interaction and Its Mitigation for Improving Power System Performance"** Total Pages **167**

Name of the Scholar: **Neevatika Verma**

Supervisor (s)

Narendra Kumar-I

Department **Electrical Engineering**

This is to report that the above thesis was scanned for similarity detection. Process and outcome is given below:

Software used: **Turnitin** Similarity Index: **6%** , Total Word Count: **36,862**

Date: _____

Candidate's Signature **Signature of Supervisor(s)**

List of Publications

Journals (SCIE):

1) Verma, N., N. Kumar and R. Kumar. "Enhanced Battery Energy Storage Damping Controller for Alleviation Sub-Synchronous Resonance in Wind Power Plants" (Accepted)

2) Verma, N., & Kumar, N. "Nonlinear Dynamic Analysis of Transformer Saturation Induced by Subsynchronous Resonance". Revue Roumaine Des Sciences Techniques—série Électrotechnique Et Énergétique, 71(2), 241-246 (2026). https://doi.org/10.59277/RRST-EE.2026.2.12 **(I.F=1.9)**

3) Verma, N., Kumar, N. "Intelligent Control for Sub-Synchronous Resonance Mitigation: A UPSO-Optimized Battery Storage Approach for Future Wind Power Systems". J. Electr. Eng. Technol. (2025). https://doi.org/10.1007/s42835-025-02423-y. **(I.F=1.6)**

4) N. Verma, N. Kumar and R. Kumar, "Battery energy storage-based system damping controller for alleviating sub-synchronous oscillations in a DFIG-based wind power plant," in Protection and Control of Modern Power Systems, vol. 8, no. 2, pp. 1-18, April 2023, https://doi.org/10.1007/s40031-022-00807-6 . **(I.F=11.9)**

5) N. Verma, N. Kumar, S. Gupta, H. Malik and F. P. García Márquez, "Review of sub-synchronous interaction in wind integrated power systems: classification, challenges, and mitigation techniques," in Protection and Control of Modern Power Systems, vol. 8, no. 2, pp. 1-26, April 2023, https://doi.org/10.1186/s41601-023-00291-0 **(I.F=11.9)**

Journals (SCOPUS):

6) Verma, N., Kumar, N. "DFIG-Based Wind Plant Coupled Series Compensated Transmission Line: Modeling and SSR Stability Analysis." *J. Inst. Eng. India Ser. B* 103, 1917–1926 (2022). https://doi.org/10.1007/s40031-022-00807-6.

International/ National Conferences:

1) N. Verma, N. Kumar, "Impact of Subsynchronous Resonance on Power Transformer," *International Electrical and Electronics Engineering Conference*. Oct-2021.

2) Verma, N. & Kumar, N. (2021). SSR Stability Analysis and Modeling for DFIG Connected to Series Compensated Transmission Line. In *PREPARE@ u®| IEI Conferences*. https://doi.org/10.36375/prepare_u.iei.a221

3) Verma, N., & Kumar, N. (2024). A Comprehensive Analysis of Subsynchronous Resonance in Wind Power System: Effects of Series Compensation, Wind Speed, and Modes. In *International Conference on Signal, Machines, Automation, and Algorithm* (pp. 697-711). Springer, Singapore. https://doi.org/10.1007/978-981-97-6349-8_49

Proof of Publication

Rev. Roum. Sci. Techn.– Électrotechn. et Énerg.
Vol. **71**, *2*, pp. 241–246, Bucarest, 2026

NONLINEAR DYNAMIC ANALYSIS OF TRANSFORMER SATURATION INDUCED BY SUBSYNCHRONOUS RESONANCE

NEEVATIKA VERMA[1,2], NARENDRA KUMAR [1]

Keywords: Subsynchronous Resonance (SSR); Transformer saturation; Series compensation; Flux dynamics; Magnetizing current; Post-fault transients.

This paper presents a novel investigation into the influence of post-fault subsynchronous resonance (SSR) on transformer flux dynamics and saturation behavior. A theoretical framework is established to examine resonance conditions in fixed-series-compensated transmission lines using frequency-domain impedance analysis, identifying electrical resonance points that can induce subsynchronous excitation. A nonlinear flux-voltage integral model is developed and implemented in MATLAB/Simulink to simulate transformer response under fault-clearing scenarios. Results reveal that the SSR-induced voltage recovery—particularly at 10 Hz—can drive the core flux well beyond the saturation knee, reaching up to 1.89 pu. The corresponding magnetizing current exhibits 20 Hz modulation, generating intermodulation sidebands at 40 Hz, 80 Hz, 110 Hz, and 130 Hz. Comparative analysis shows that series compensation significantly amplifies flux excursions and spectral distortion, confirming the role of transformer saturation as a nonlinear resonance amplifier. These findings underscore the importance of incorporating nonlinear transformer modeling into SSR studies for accurate assessment and mitigation in modern compensated power systems.

1. INTRODUCTION

With rising electricity demand, integrating renewable energy into existing grids has become essential. To enhance power transfer and stability, compensation techniques such as shunt capacitors, STATCOM, and series capacitors (FSC, TCSC) are widely used [1,2]. However, series compensation can introduce Subsynchronous Resonance (SSR), where energy exchange between the network and rotating machinery at subsynchronous frequencies leads to oscillations, causing stability issues and potential damage to turbine-generator shafts and other equipment [3].

Since the 1970s, SSR has been extensively studied, especially for its impact on turbine-generator torsional modes and more recently, on inverter-based renewable energy systems [3,4]. However, the effect of SSR on power transformers, particularly magnetic core saturation during SSR conditions, remains underexplored.

Subsynchronous voltage and current oscillations caused by SSR can drive power transformers into their nonlinear operating region, resulting in magnetic core saturation [5]. This phenomenon is especially critical during fault-clearing events or transient operating conditions, where sharp voltage excursions coincide with subsynchronous frequencies. Saturation of the transformer core under such conditions can lead to waveform distortion, harmonic injection, flux demodulation, and maloperation of protection devices [6]. Yet, most SSR-focused studies continue to model transformers as linear components, thereby neglecting their nonlinear magnetic behavior and its potential feedback into the SSR dynamics.

Existing studies on transformer saturation mainly address mechanisms unrelated to SSR. Some focus on DC bias and harmonic instability in HVDC systems, where core saturation arises from unidirectional currents [7]. Others examine current transformer saturation due to decaying DC components during faults, which differs from SSR-induced effects [8]. Additional work considers geomagnetically induced currents (GICs) during solar storms, which introduce low-frequency quasi-DC components that saturate cores [9], but under conditions unlike those in series-compensated AC systems. Similarly, studies on flux walking in high-frequency transformers (*e.g.*, dual-active-bridge converters) operate in entirely different frequency domains [10]. Moreover, impedance-based SSR analyses rarely account for transformer saturation [11].

This paper addresses the gap by investigating transformer core saturation under SSR in a series-compensated system. A nonlinear transformer model is developed and analyzed in a time-domain framework using MATLAB/Simulink. The main contributions are:

- Identification of resonance frequencies that increase the risk of transformer core saturation in series-compensated systems.
- Modeling and simulation of nonlinear transformer behavior during SSR events using MATLAB/Simulink.
- Spectral analysis reveals sidebands and harmonic intermodulation due to 20 Hz modulation of magnetizing current.
- Demonstration that series compensation amplifies flux excursions and nonlinear distortion after faults.

The paper is organized as follows: Section 2 reviews SSR theory; Section 3 describes the study system; Section 4 presents the system modeling; Section 5 discusses the results; and Section 6 concludes with key contributions.

2. SSR MECHANISM AND ITS IMPACT ON NETWORK COMPONENTS

Theoretical aspects of SSR are described in [12]. Assuming negligible line resistance, the power transfer capability can be expressed as:

$$P = \frac{V_S . V_T}{X_T} \sin\delta. \quad (1)$$

Here, P is the transmitted power, V_S and V_T are the sending end and receiving end voltages, X_T is the net reactance, and X_S is the transfer reactance of the uncompensated line transmission line. Power transfer capability can be increased by adding a series capacitor, followed by a reduction in total reactance X_T [12].

Therefore, net reactance would be

$$X_T = (X_S - X_C), \quad (2)$$

where X_C is the capacitive reactance of the series capacitor.

If the percentage of compensation is K_C, then

$$X_T = (1 - K_C)X_S. \quad (3)$$

[1] Department of Electrical Engineering, Delhi Technological University, India.
[2] Department of Electrical Engineering, Government Engineering College, Siwan, India.

Journal of Electrical Engineering & Technology
https://doi.org/10.1007/s42835-025-02423-y

ORIGINAL ARTICLE

Intelligent Control for Sub-Synchronous Resonance Mitigation: A UPSO-Optimized Battery Storage Approach for Future Wind Power Systems

Neevatika Verma[1,2] · Narendra Kumar[1]

Received: 23 July 2025 / Revised: 13 August 2025 / Accepted: 25 August 2025
© The Author(s) under exclusive licence to The Korean Institute of Electrical Engineers 2025

Abstract

This paper proposes an enhanced Battery Energy Storage Damping Controller (BESDC) as a novel intelligent solution for mitigating Sub-Synchronous Resonance (SSR) in Fixed Series Compensated Transmission Lines (FSCTL) connected to Doubly Fed Induction Generator (DFIG)-based wind power system. Addressing the growing complexity and stability challenges of modern power systems, the controller integrates a Supplementary Damping Signal (SDS) into the d–q axis control structure of the BESDC. This SDS utilizes real-time angular speed deviation data acquired via a Wide Area Measurement System (WAMS), enabling system-wide observability and dynamic response. To ensure robust damping across varying operating conditions, an Upgraded Particle Swarm Optimization (UPSO) algorithm, guided by eigenvalue sensitivity analysis, is employed to optimally tune the controller gain. The study accounts for the intermittency of wind speeds and variability in FSCTL levels, representing practical grid scenarios. Time-domain simulations conducted in MATLAB/Simulink demonstrate that the proposed intelligent BESDC consistently stabilizes critical modes at wind speeds of 6 m/s, 7 m/s, 9 m/s, and 11 m/s and compensation levels of 40%, 50%, and 60%. Compared to conventional BESDC designs, the proposed framework achieves superior damping performance and improved system resilience. These results underscore the potential of intelligent, optimization-based damping strategies in developing stable, future-ready electrical infrastructures.

Keywords Sub-Synchronous Resonance (SSR) · Battery energy storage systems · Series compensation · DFIG · Damping controller

1 Introduction

In recent years, global wind power capacity has experienced significant and accelerating growth, largely driven by the urgent global push toward decarbonization and the integration of renewable energy sources into modern power systems. In 2023 alone, approximately 117 GW of new wind energy capacity was installed, positioning global cumulative capacity on track to exceed the 1,000 GW milestone by 2025. Offshore wind installations reached 75 GW, reflecting increased investment in deep-sea renewable projects, while onshore developments contributed over 106 GW [1].

China remains the global leader in wind deployment, with substantial contributions from the United States, Brazil, Germany, and India. A key enabling technology behind this rapid expansion is the DFIG, which has been extensively adopted due to its capability for variable-speed operation, independent control of active and reactive power, and superior cost-effectiveness [2]. DFIGs are particularly well-suited for grid-connected wind power systems and are integral to modern power network architectures. Given the remote location of most wind farms, long-distance transmission to load centres typically relies on Fixed Series Compensated Transmission Lines (FSCTLs), which offer a cost-effective alternative to high-cost Flexible AC Transmission Systems (FACTS) [3]. While FSCTLs enhance power

✉ Neevatika Verma
nivetikaverma2311@gmail.com

Narendra Kumar
narendra.kumar@dtu.ac.in

1 Department of Electrical Engineering, Delhi Technological University, Delhi, India

2 Department of Electrical Engineering, Government Engineering College Siwan, Bihar, India

Published online: 02 September 2025

Verma et al.
Protection and Control of Modern Power Systems (2023) 8:32
https://doi.org/10.1186/s41601-023-00309-7

Protection and Control of
Modern Power Systems

ORIGINAL RESEARCH Open Access

Battery energy storage-based system damping controller for alleviating sub-synchronous oscillations in a DFIG-based wind power plant

Neevatika Verma[1], Narendra Kumar[1] and Rajeev Kumar[2,3*]

Abstract

This paper presents the issue of the Sub-synchronous resonance (SSR) phenomenon in a series compensated DFIG-based wind power plant and its alleviation using a Battery Energy Storage-based Damping Controller ($BESSDC_L$). A supplementary damping signal is developed considering the angular speed deviation and is incorporated into the BESS control system. Wide-area Measurement System data is used to determine the angular speed deviation. A linearized system model is developed to perform eigenvalue analysis, and to detect and examine unstable SSR modes. The variation of wind speed and three-phase fault are also taken into consideration to validate the robustness of the controller. To further verify the efficacy of the proposed damping controller, time-domain simulations are performed using MATLAB/Simulink. The application of the proposed $BESSDC_L$ stabilizes all the unstable system modes effectively at wind speeds of 7 m/s, 9 m/s, and 11 m/s, and at 40%, 50%, and 60% series compensation levels, as well three-phase fault conditions.

Keywords Battery energy storage system, Damping controller, Doubly-fed induction generator (DFIG), Series compensation, Sub-synchronous resonance (SSR)

1 Introduction

The world is now focusing on renewable energy sources. One of the best-paying and most accessible sources of energy is wind. The areas where wind energy is abundant are generally very remote to power-demand areas. Thus, new wind energy power plants can be integrated into the existing national grid through dedicated or existing transmission lines by increasing the power transfer capability using fixed series compensation (FSC) or FACT devices [1]. Installing FSC in a long transmission line is an inexpensive and efficient way to improve the capability of power transfer of an existing transmission line [2]. However, the problem that may arise because of FSC in a long transmission line is Sub-synchronous resonance (SSR), which can lead to shaft failure and power system instability [3, 4]. Various historical events have already been reported in which the undamped SSR outcomes caused the complete failure of generator rotor shafts. The first two incidents happened in the Mohave power plant, in Nevada, USA, in 1970 and 1971, [5], and the first event occurred in the wind plant in October 2009 at Zorillo Gulf Wind Farm, Texas [6]. Following these incidents, the research community has focused on finding ways to deal with the SSR problem.

*Correspondence:
Rajeev Kumar
rajeev.rakshit@gmail.com
[1] Department of Electrical Engineering, Delhi Technological University, New Delhi, India
[2] Electrical Engineering Department, Jamia Millia Islamia, New Delhi, India
[3] Electrical and Electronics Engineering Department, KIET Group of Institutions, Ghaziabad, India

Springer Open

© The Author(s) 2023. **Open Access** This article is licensed under a Creative Commons Attribution 4.0 International License, which permits use, sharing, adaptation, distribution and reproduction in any medium or format, as long as you give appropriate credit to the original author(s) and the source, provide a link to the Creative Commons licence, and indicate if changes were made. The images or other third party material in this article are included in the article's Creative Commons licence, unless indicated otherwise in a credit line to the material. If material is not included in the article's Creative Commons licence and your intended use is not permitted by statutory regulation or exceeds the permitted use, you will need to obtain permission directly from the copyright holder. To view a copy of this licence, visit http://creativecommons.org/licenses/by/4.0/.

Verma et al.
Protection and Control of Modern Power Systems (2023) 8:17
https://doi.org/10.1186/s41601-023-00291-0

Protection and Control of Modern Power Systems

REVIEW **Open Access**

Review of sub-synchronous interaction in wind integrated power systems: classification, challenges, and mitigation techniques

Neevatika Verma[1], Narendra Kumar[1], Saket Gupta[1,5], Hasmat Malik[2,4] and Fausto Pedro García Márquez[3*]

Abstract

Emerging sub-synchronous interactions (SSI) in wind-integrated power systems have added intense attention after numerous incidents in the US and China due to the involvement of series compensated transmission lines and power electronics devices. SSI phenomenon occurs when two power system elements exchange energy below the synchronous frequency. SSI phenomenon related to wind power plants is one of the most significant challenges to maintaining stability, while SSI phenomenon in practical wind farms, which has been observed recently, has not yet been described on the source of conventional SSI literature. This paper first explains the traditional development of SSI and its classification as given by the IEEE, and then it proposes a classification of SSI according to the current research status, reviews several mitigation techniques and challenges, and discusses analysis techniques for SSI. The paper also describes the effect of the active damping controllers, control scheme parameters, degree of series compensation, and various techniques used in wind power plants (WPPs). In particular, a supplementary damping controller with converter controllers in Doubly Fed Induction Generator based WPPs is briefly pronounced. This paper provides a realistic viewpoint and a potential outlook for the readers to properly deal with SSI and its mitigation techniques, which can help power engineers for the planning, economical operation, and future expansion of sustainable development.

Keywords Damping controller, Doubly fed induction generator (DFIG), Series compensations, Sub-synchronous interactions (SSI), Sub-synchronous resonance (SSR)

1 Introduction

In order to meet the enormous electricity demand, renewable energy sources are aiding in the current power system. Wind energy is one of the leading renewable sources, and it is projected that if all countries were to build wind farms on 2% of their land area, their energy needs could be met [1, 2]. Wind energy resources are free of cost provided by nature, are abundant and eco-friendly, while the only cost is the conversion of energy [3]. With so many different technologies available, the DFIG-based wind energy conversion system stands out because of its variable speed operation, ability to operate in both sub-synchronous and super-synchronous modes, low cost, and high power density [4].

1.1 Background

Electricity generated from wind energy can easily be integrated into the existing power grid either by commissioning new dedicated transmission lines or improving existing transmission lines' power transfer

*Correspondence:
Fausto Pedro García Márquez
faustopedro.garcia@uclm.es
[1] Department of Electrical Engineering, Delhi Technological University, Delhi 110042, India
[2] Department of Electrical Power Engineering, Faculty of Electrical Engineering, Universiti Teknologi Malaysia (UTM), 81310 Johor, Malaysia
[3] Ingenium Research Group, Department, Universidad Castilla-La Mancha, 13071 Ciudad Real, Spain
[4] Department of Electrical Engineering, Graphic Era Deemed to be University, Dehradun 248002, India
[5] Instrumentation and Control Engineering Department, Bharati Vidyapeeth's College of Engineering, New Delhi 110056, India

Springer Open

© The Author(s) 2023. **Open Access** This article is licensed under a Creative Commons Attribution 4.0 International License, which permits use, sharing, adaptation, distribution and reproduction in any medium or format, as long as you give appropriate credit to the original author(s) and the source, provide a link to the Creative Commons licence, and indicate if changes were made. The images or other third party material in this article are included in the article's Creative Commons licence, unless indicated otherwise in a credit line to the material. If material is not included in the article's Creative Commons licence and your intended use is not permitted by statutory regulation or exceeds the permitted use, you will need to obtain permission directly from the copyright holder. To view a copy of this licence, visit http://creativecommons.org/licenses/by/4.0/.

J. Inst. Eng. India Ser. B
https://doi.org/10.1007/s40031-022-00807-6

ORIGINAL CONTRIBUTION

DFIG-Based Wind Plant Coupled Series Compensated Transmission Line: Modeling and SSR Stability Analysis

Neevatika Verma[1] · **Narendra Kumar**[1]

Received: 3 January 2022 / Accepted: 12 September 2022
© The Institution of Engineers (India) 2022

Abstract Wind energy production is expanding and has become a terrific source of renewable energy. The installed capacity of wind energy has nearly doubled every 3 years during the past two decades of the twenty-first century. Wind farms typically are not close to the grid, so a series compensated transmission lines are required to improve the transfer capability of extant power transmission lines economically. Sub-synchronous resonance (SSR), which can cause torsional interactions that result in T-G shaft fatigue and a related protective mechanism, is always a risk with series compensation. A modified IEEE first benchmark model is employed for SSR analysis in this paper. Power transmission via a series compensated transmission line from a wind generator with a doubly fed induction generator (DFIG) base has been investigated. In this paper, the dynamics of the grid side converter (GSC) as well as rotor side converter (RSC) has utilized to model the DFIG. As a result, system dynamics may be greatly impacted. However, in previous paper for RSC and GSC, a constant voltage source model has been taken into consideration. Consequently, for some important parameters, these models are unable to replicate the dynamic effect of SSR. More accurate dynamics are reflected in the analysis by using GSC and RSC modeling. The effect of SSR under various operating conditions, such as wind speed changes and altering the series compensation, has been investigated using the eigenvalue analysis. Time-domain simulations have been conducted using MATLAB to verify the analysis.

✉ Neevatika Verma
nivetikaverma2311@gmail.com

[1] Department of Electrical Engineering, Delhi Technological University, New Delhi 110042, India

Keywords Eigenvalue · Series compensation · Sub-synchronous resonance (SSR)

Abbreviations

SSR	Sub-synchronous resonance
DFIG	Doubly fed induction generator
GSC	Grid side converter
RSC	Rotor side converter
WPP	Wind power plant

List of Symbols

ρ	Air density (kgm^{-3})
V_{wi}	Wind speed (m/s)
R	Rotor radius (m) of wind turbine
A	Blade sweep area (m^2)
C_f	Design constant of wind turbine blades
λ	Tip speed ratio
Ω_m	Mechanical angular velocity
ω_t	Shaft speed of wind turbine
ω_r	Shaft speed of DFIG
T_g	Internal torque of the system
T_m	Electromagnetic torque of the generator
D_t	Damping coefficient of wind turbine
H_t	Inertia constant of wind turbine
H_g	Inertia constant of wind generator
D_{tg}	Damping coefficient of wind generator
K_{tg}	Shaft stiffness of the coupling between two masses
ω_e	Synchronous reference speed
ψ_{qm}, ψ_{dm}	Quadrature and direct axes air gap flux linkage
i_{qr}, i_{dr}	Quadrature and direct axes DFIG rotor current component
i_{qs}, i_{ds}	Quadrature and direct axes DFIG stator current component

Published online: 28 October 2022

SPRINGER NATURE Link

Log in

Find a journal Publish with us Track your research Search Cart

A Comprehensive Analysis of Subsynchronous Resonance in Wind Power System: Effects of Series Compensation, Wind Speed, and Modes

Conference paper | First Online: 14 December 2024

pp 697–711 | Cite this conference paper

International Conference on Signal, Machines, Automation, and Algorithm

(SIGMAA 2023)

Neevatika Verma & Narendra Kumar

Part of the book series: Advances in Intelligent Systems and Computing ((AISC, volume 1460))

Included in the following conference series:
International Conference on Signal, Machines, Automation, and Algorithm

337 Accesses 1 Citation

Abstract

This article explains the detailed effect of the subsynchronous resonance (SSR) phenomenon in the doubly fed induction generator (DFIG)-based wind power system (WPS) using the IEEE First Benchmark Model (FBM) as the studied system. SSR poses a serious risk to system stability in power systems adopting renewable energy sources. The primary goals of this novel investigation encompass the identification of distinctive frequency modes associated with SSR in DFIG-based WPS and to investigate the effects of varying series compensation levels and wind speeds on various system modes, such as supersynchronous, subsynchronous, electromechanical, shaft, and system modes. It is found that electromechanical modes usually react to changes in wind speed, while subsynchronous modes are sensitive to both compensation and wind speed changes. Moreover, this paper studies the influence of variations in series compensation levels and wind speed on the stability of the system. The findings indicate that system stability is achieved when series compensation is below 50%, whereas instability ensues when the compensation exceeds 50% at 8 m/s wind speed. Moreover, this study offers a new understanding of the SSR behavior of DFIG-based WPS, specifically within the context of the IEEE FBM. IEEE First Benchmark Mode ensures the applicability and comparability of the findings in a standardized framework. These findings can help grid operators, power system engineers, and wind farm developers establish strategies to improve system stability and reliability when integrating renewable energy sources.

Access this chapter

Log in via an institution

Subscribe and save

Springer+ from €37.37 /Month

- Starting from 10 chapters or articles per month
- Access and download chapters and articles from more than 300k books and 2,500 journals
- Cancel anytime

View plans

Buy Now

Chapter EUR 29.95
Price includes VAT (India)

- Available as PDF
- Read on any device
- Instant download
- Own it forever

Buy Chapter

eBook EUR 213.99

Softcover Book EUR 219.99

Tax calculation will be finalised at checkout

Impact of Subsynchronous Resonance on Power Transformer

Neevatika Verma[1], Narendra Kumar[2]

[1]Department of Electrical Engineering,
Delhi Technological University, India,
Nivetikaverma2311@gmail.com

[2]Department of Electrical Engineering
Delhi Technological University, India
Dnk_1963@yahoo.com

Abstract*: Under certain operating conditions, a series compensated power system may experience a very strange phenomenon known as Subsynchronous Resonance (SSR), which degrades the power system stability and may result in a breakdown of the turbine generator shafts and damage various operating equipment due to generation of undamped oscillations. This paper investigates the theoretical approach of Subsynchronous Resonance and characteristics of resonance condition of fixed series compensation of transmission line by adding frequency domain analysis of line impedance to observe where the electrical resonance points occur and excite subsynchronous resonance and led to transformer undergoes saturation condition. Detail study would be performed through MATLAB/SIMULINK, and the expected result is that SSR can excite the transformer to saturation. The SSR cause modulates voltage and current at the subsynchronous frequency and increases voltage reason behind the saturation of the transformer's core.

***Keywords*: Subsynchronous Resonance(SSR), transformer saturation, series compensation**

I. Introduction

As per capita, electrical energy consumption is increasing day by day, power generation from different sources is required to meet this increased demand. However, due to environmental, economic impact, and regulatory policies, there is an infrastructural limit to install various power generation projects. Further, there is a decentralization policy for the generation of electrical power; more renewable energy sources are being integrated day by day in the existing power grid network[1]. Therefore, recent developments in large electrical network systems involve the addition of compensation equipment for AC transmission lines which enhances the typical power system stability as well as the power transfer capability. [2]. Passive shunt compensation, STATCOM, and series compensation with series capacitors(FSC & TCSC) are some of the most widely used reactive power control techniques[3]. However, there is a certain limitation to use these types of compensation techniques as the system will be inherent to sub-synchronous resonance (SSR). Series compensation capacitors and passive shunt compensation inductors interact to produce sub-synchronous resonances[4]. After the Mohave power station incident in 1970-71, the effects of SSR were visualized. Several phenomena effects can be attributed to SSR after decades of research. The possible impacts of SSR in the typical power system are Induction generator effects, torsional interactions phenomenon, and torque amplification are all possible [5]

Furthermore, SSR causes an increase oscillating current and voltage magnitude, and these increased oscillating voltages due to subsynchronous frequency, which causes the transformer saturation, resulting in damage to the power system equipment due to oscillating output waveform[6][7]. The magnetic saturation of the power transformers is not considered in previous literature[8]. Therefore, to validate the conclusions of these studies, analytical simulations were used in this paper to verify and

In this paper, a transient electromagnetic study for transformer energization and its unexcepted voltage waveform is obtained at a nearby bus with oscillatory voltage waveform. It indicates the occurrence of network resonance frequency and analyses the characteristics of resonance frequency and transformer saturation. This paper explains the induction generation effect, torsional interactions, and torque amplification phenomenon caused to the addition of series compensation by FSCs/TCSCs or by passive shunt compensator

The sections are structured as follows: the theoretical aspects of SSR discuss in section 2. Section 3 presented modelling of the power system which is used for the case study. Simulation and case study and its analysis are presented in section 4, and in the last section, 5, presented conclusions.

II. SSR-Theoretical Aspects

Theoretical aspects of subsynchronous resonance are described in the power system:

Considering negligible resistance of line, the power transfer capability can be related as[9];-

$$P=(V_S \times V_T/X_T)\sin\delta \quad (1)$$

Where X_T is net reactance & X_s is transfer reactance of the uncompensated line.

Power transfer capability can be increased by adding a series capacitor, followed by a reduction in total reactance X_T.

https://doi.org/10.36375/prepare_u.iei.a221

SSR Stability Analysis and Modeling for DFIG Connected to Series Compensated Transmission Line

Neevatika Verma, Narendra Kumar
Department of Electrical Engineering
(Delhi Technological University)
(New Delhi-110042)
{nivetikaverma2311@gmail.com,}

Abstract - Due to the massive increase in electrical energy demand, wind power penetration into electric networks is increasing. Usually, the wind farms are located away from the grid, necessitating a series compensated transmission system. Series compensation is always prone to sub-synchronous resonance (SSR), which may lead to the torsional interactions resulting T-G shaft fatigue and associated protection system. In this paper, a modified IEEE first Benchmark Model is used for SSR analysis. A doubly-fed induction generator (DFIG) has been considered supplying power to the grid through a series compensated transmission line. The dynamics of the Rotor Side Converter (RSC) and the Grid Side Converter (GSC) is used to model the DFIG. Thus, it can generate a significant impact in system dynamics. However, previous works have considered a constant voltage source model for RSC and GSC. Therefore, consequently these models are not capable of replicating the dynamic impact of SSR for some critical factors. The inclusion of GSC and RSC modeling in analysis reflects dynamics that are more accurate. The eigenvalue analysis has been used to study the impact of SSR under different operating situations, for instance, wind speed fluctuations and varying the series compensation. To validate the analysis, time-domain simulations have been carried out by using MATLAB.

Keywords – Doubly Fed induction Generator (DFIG), Series Compensation, Sub-synchronous Resonance (SSR), Stability

INTRODUCTION

As renewable energy is the current requirement to meet the global power need without much impact on the environment. Wind power plays a significant role in fulfilling the power requirement. To accommodate the additional power, transmission infrastructural changes are frequently required for wind farms located far from load centers. From the economic considerations, series capacitor compensation of existing lines is typically recommended, over constructing new lines, to boost power transmission capacity and stability margin[1]. On the other hand, fixed series capacitor compensation is a source of SSR phenomenon not only in new power plants but also in existing generating power systems and power electronic equipment[2]. The primary source of the SSR phenomenon is the electrical resonance frequency, which is smaller in amplitude to the natural system frequency. It usually occurs if the natural mechanical frequency of the turbine matches with the electrical resonance frequency—the SSR oscillation results in the slip voltage of SSR frequency at the rotor circuit. The reason for the shaft failure is due to the oscillating electromagnetic torque, which consequently results in the failure of the shaft. This incident invites serious research on the SSR phenomenon in DFIGs and series compensated transmission lines[3].

The SSR phenomena were first discussed in 1937, and it resurfaced in the 1970s after two shaft collapses at the Mohave site received attention[4]. A decade ago, noticed the potential relationship between wind farms and series capacitors. Due to increasing levels of wind power, SSR occurrences have been observed in series-compensated DFIG based wind power plants (WPP) in the south of Texas, the southwest of Minnesota, and the north of China (Hebei province)[5]. Following the incidence, extensive research into the SSR problem among DFIGs and series-compensated power systems was conducted. According to reference [5], DFIGs are more susceptible to SSR in series compensated systems than fixed-speed wind turbine generators and wind generators connected via back-to-back converters.

Several previous research works discuss detailed mathematical modeling of a DFIG-based WPP[3],[6]–[10]. However, the RSC, GSC dynamics have not been considered for the

Curriculum Vitae

PERSONAL INFORMATION	**Neevatika Verma**
	Nationality: Indian Date of Birth: 01.02.1994 Address: Basti, Uttar Pradesh Contact: +919458704732 E-mail: nivetikaverma2311@gmail.com
DESIGNATION	Assistant Professor Government Engineering College Siwan, India
AREA OF INTRESET	Power System Stability, Wind Power System, Battery Energy Storage System
QAULIFICATION	• Ph.D (Pursuing) • M.Tech, Power Electronics & Drives, 2018 • B.Tech, Electrical and Electronics Engineering, 2015
EXPERIANCE	Assistant Professor (2023-Till Date)